MASTER'S THESIS

Master of Science in Advanced Mathematics and Mathematical Engineering

Title: Optimal control over damped oscillations via response curves

Author: Kevin Martímez Añón

Advisor: Antoni Guillamon Grabolosa

Department: Matemàtiques UPC

Academic year: 2019-2020

UNIVERSITAT POLITÈCNICA DE CATALUNYA
BARCELONATECH
Facultat de Matemàtiques i Estadística

Universitat Politècnica de Catalunya
Facultat de Matemàtiques i Estadística

Master in Advanced Mathematics and Mathematical Engineering

Master's thesis

Optimal Control over Damped Oscillations via Response Curves

Kevin Martínez Añón

Supervised by Antoni Guillamon Grabolosa

September, 2020

In the first place, I would like to start by thanking my supervisor, Antoni Guillamon, for having presented me with such a challenging topic that has thrilled and intrigued me so much along the past eight months. Needless to say, without his guidance full of enthusiasm, his endless understanding and his appreciated advice, this Master's Thesis would by no means have ever been possible, or even conceivable.

Secondly, I must show my utter gratitude to my friend and former colleague Román Moreno for having granted me total access to his own Master's Thesis and permission to reproduce his original MATLAB codes without which many of the successful numerical results presented in this paper would have never been achieved. The fruitful and thought-provoking chats in which Román shared with me his bigger experience on the issue were of great help to me when taking the first steps into this topic.

Finally, to my family, my closest friends and my dearest Yohana, I can only say to you: thank you for being so understanding and supportive when my force and motivation were declining; thank you for rejoicing with me and sharing my happiness when the first positive results arrived; and, of course, thank you for lending me your own PCs to run my codes whenever mine needed a little extra help to fulfill its computations. This work is, in some sense, as yours as it is mine.

Abstract

A vast literature has been devoted throughout the years to the construction of both a phase and an amplitude response function that help us study the effects of external stimuli on the dynamics of oscillatory systems. Results trying to reproduce these techniques in the case of damped oscillations have come up recently. Thus, adhering to this recent trend, in this Master's Thesis we complete the study on damped oscillations initiated last year by my colleague Román Moreno in his own Master's Thesis and, based on it, we present a novel optimal control algorithm for the induction of sustained periodic oscillations out of a damped oscillation using a minimum-energy input. The positive results obtained can be seen, from a theoretical point of view, as a deterministic method for the generation of stable structures in systems where they were initially not present; and, from a more practical perspective, they may open the door for therapeutic studies of some neuropathologies when applied to some neuron models in neuroscience.

Keywords

Damped oscillations, strong focus, isochronicity, isochrons, isostables, augmented phase reduction, phase response function, amplitude response function, optimal control, Euler-Lagrange equations, neuron models, Fitzhugh-Nagumo model.

Contents

1. Introduction

Periodic sustained oscillations are represented in dynamical systems by limit cycles. Damped oscillations, on their behalf, find their dynamical counterparts in strong (hyperbolic) and weak (non-hyperbolic) foci. The ubiquitous recurrent appearance of the former in systems of biological interest - and not exclusively system of biological interest - has given rise to an extensive literature covering different techniques to deal with oscillatory regimes in models covering a wide amount of distinct examples. From neural spikes to cardiac rhythms, cell division or the flowering cycle of plants, all these natural phenomena find in the study of periodic oscillations a common step for their complete theoretical understanding.

Among all these many techniques, we will play special attention to **phase reduction**; see, for instance, Winfree in [33], Guckenheimer in [18], Guillamon and Huguet in [19], or Monga *et al.* in [24]. In its classical version, phase reduction is a simplification technique that reduces the dimensionality of a dynamical system around a limit cycle by extending the notion of phase of oscillation to points outside the periodic orbit. The resulting simplified version of the model not only succeeds in reproducing the oscillating dynamics of the original system, but it also enables the study of changes - advancements or delays - in the phase of oscillation due to external stimulus by means of the well-known **Phase Response Curve** (**PRC**); see Malkin in [23], Ermentrout in [11], or Govaerts and Sautois in [17]. Unfortunately, classical phase reduction to a sole dynamically-relevant variable, the **asymptotic phase**, sees its range of applicability confined to a rather scarce number of systems where the time lapse between the moment in which a trajectory is stimulated out of the periodic orbit and the moment in which it is back on it again is very small.

In more recent years, Guillamon and Huguet [19] and Castejón *et al.* [6], with the help of modern techniques in dynamical systems such as the **parameterization method** - see Cabré *et al.* in [5] -, managed to augment the phase reduction on planar systems with the inclusion of a second dynamically relevant variable, the **amplitude**, accounting for the distance of a point to the periodic orbit and, by doing so, they where able to broaden the range of applicability of the phase reduction formalism. Moreover, these authors also defined the so-called **Phase** and **Amplitude Response Functions** (**PRF**/**ARF**), generalizations of the classical PRC for the two new variables of the augmented phase reduction.

Thus, phase reduction techniques make the analysis of high-dimensional systems more tractable and, in doing so, they reveal plenty of room for new applications and theories to arise. Among these new possibilities enabled by the augmented phase reduction, we find the potential to develop control strategies on the main features of oscillations, such as its period, by means of external energy inputs. In this sense, Monga and Moehlis in [25] and Monga *et al.* in [24] presented some **optimal control strategies** with the purpose of inducing deterministic changes, advancement or delay, in the oscillation phase of some rather realistic oscillatory systems using a minimum-energy input whose effect on the dynamics of the system is handled by means of the augmented phase reduction and its response curves. Monga and Moehlis algorithms are based in the posing of a certain **variational problem** that matches the specific requirements of each problem and their resolution via the classical **Euler-Lagrange equations**.

The positive results reported by Monga and Moehlis together with the wide applicability of their procedure were absolutely inspiring and determinant for the proposal of this Master's Thesis. Indeed, it is after the reading of their publications that the main dynamic force driving these investigations appears in the form of the question: "can these ideas be applied to the case of a damped oscillation in order to restore its

lost periodic behaviour?"; and many others derived from it: "is an augmented phase reduction formalism plausible for the reduction of a damped oscillation?", "can a periodic orbit with arbitrary period and radius be induced out of any damped oscillation?", "how does the dynamics of the focus underneath the damped oscillation affect the resolution of the variational problem?", etc. Some of these questions, the fewer, are answered and investigated along the subsequent sections of this Master's Thesis. Some other, the most, unfortunately remain as unsolved interrogations that further studies and research on the topic may tackle.

The structure of this Master's Thesis is as follows. In Section 2 we go back to the problem of phase reduction around limit cycles and present some of the key theoretical results that we will later need to reproduce in the case of damped oscillations, such as the concepts of isochrony, isochrons and isostables. In Section 3 we resume the work with strong foci initiated by Moreno in [26] and complete it with the addition of the entire theory concerning the definition of the ARF associated to a strong focus. Afterwards, when a solid augmented phase reduction is theoretically grounded by merging the work of Moreno and the original additions, a control strategy for the induction of periodic oscillations around strong foci using a minimum-energy input is designed in the same fashion as Monga and Moehlis did in their papers, [25, 24].

Section 4 serves as the perfect bridge in between the theoretical aspects of the Master's Thesis and the presentation of the numerical results. In this sense, in Section 4 we present a brief scheme of the many different numerical tools that have been used along the implementation of the required algorithms. Further details are given about those methodologies whose significance in the resolution of the problem is crucial, or whose handling may be, in the view of the author, novel for a student on the verge of finishing his Master's studies in Mathematics. Finally, in Section 5, the main numerical results of the Master's Thesis are included. The augmented phase reduction and the control algorithm are successfully applied to the case of a strong linear focus and to induce early oscillations in the excitable regime of the Fitzhgh-Nagumo model. In the case of the strong linear focus, given the simplicity of its equations, an exhaustive analysis of the performance of the control algorithm is done aiming to gain experience enough for a better execution in other more complicated non-linear systems.

2. Background and preliminaries

In this preliminary section we are going to review some of the key theoretical results concerning the reduction of the oscillating dynamics of a planar system around a periodic orbit to a phase model that succinctly encapsulates its main features in simpler equations. Although it is not directly related to the main topic of this paper, this brief summary serves as a good starting point for our study as it presents the most important tools that we intend to replicate in subsequent sections for the case of damped oscillations. Any reader well versed about the augmented phase reduction around limit cycles can easily skip this section without losing grip on the rest of the paper.

2.1 Augmented phase reduction for limit cycles

Let us consider an autonomous system of ODEs on the real plane,

$$\dot{\mathbf{x}} = \mathcal{X}(\mathbf{x}), \quad \mathbf{x} \in \mathbb{R}^2, \tag{1}$$

where $\mathcal{X}$ is an analytic vector field with a hyperbolic **periodic orbit** γ of period $T > 0$ inside an open set $\mathcal{U} \subset \mathbb{R}^2$ and parameterized by an oscillation phase $\theta = \frac{2\pi}{T} t$ as

$$\gamma : \theta \in [0, 2\pi) \to \gamma(\theta) \in \mathcal{U} \subset \mathbb{R}^2, \tag{2}$$

so that it verifies $\gamma(\theta + 2\pi) = \gamma(\theta)$. Without loss of generality, we can assume that γ is a stable limit cycle of (1), that is, any trajectory near γ flow towards γ until they ultimately match after an infinite time. Otherwise, we only need to reverse the direction of time of the system to transform any unstable cycle into a stable one. We will denote by ϕ_t the flow associated to system (1).

Definition 2.1 (Points in phase around a limit cycle)**.** Given a planar analytic vector field $\mathcal{X}$ as in (1) with a periodic orbit $\gamma \subset \mathcal{U}$, we say that a point $\mathbf{x} \in \mathcal{U}$ is **in (asymptotic) phase** with a point $\mathbf{p} \in \gamma$ if

$$\lim_{t \to +\infty} |\phi_t(\mathbf{x}) - \phi_t(\mathbf{p})| = 0. \tag{3}$$

Definition 2.2 (Isochronous limit cycle)**.** Given a planar analytic vector field $\mathcal{X}$ with a periodic orbit $\gamma \subset \mathcal{U}$, we say that γ is an **isochronous limit cycle** if any point $\mathbf{x} \in \mathcal{U}$ is in phase with a point on the limit cycle.

Under the assumption of hyperbolicity, Guckenheimer proved in [18] that the stable manifold theorem ensures the isochrony of γ as well as the existence of a unique scalar function,

$$\vartheta : \mathbf{x} \in \mathcal{U} \subset \mathbb{R}^2 \to \vartheta(\mathbf{x}) = \theta \in [0, 2\pi), \tag{4}$$

verifying, for all $\mathbf{x} \in \mathcal{U}$,

$$\lim_{t \to +\infty} \left|\phi_t(\mathbf{x}) - \gamma\left(\tfrac{2\pi}{T}\, t + \vartheta(\mathbf{x})\right)\right| = 0. \tag{5}$$

Function ϑ is commonly known as the **phase function** of the limit cycle and it maps each point in a neighborhood of the limit cycle to its associated value of the **asymptotic phase** which corresponds to the value of the oscillation phase that parameterizes the point $\mathbf{p} = \gamma(\theta)$ it is in phase with. The level curves Θ_θ of the phase function - that is, the sets of points sharing the same asymptotic phase - are called **isochrons** and they correspond to the phase sets described by Winfree in his seminal paper [33].

Thus, phase function ϑ and isochrons extend the notion of oscillation to points in a neighborhood of the limit cycle and are the key tools in the construction of the **Classical Phase Reduction** (**CPR**) that captures the approximate dynamics around the limit cycle in the simplified lineal model

$$\dot{\theta} = \omega, \tag{6}$$

where $\omega = \frac{2\pi}{T}$ is the frequency of the oscillation. Nonetheless, this CPR-dynamics is just a coarsed-grained approximation whose range of applicability is compromised to very strong assumptions such as a great power of attraction of the limit cycle or a slow frequency of possible external perturbations.

In a recent paper, Guillamon and Huguet [19] cleverly used the parameterization method by Cabré, Fontich and de la Llave [5] to compute a local analytic change of variables $(x, y) = K(\theta, \sigma)$ that conjugates system (1) with a refined and augmented version of the CPR-dynamics in (6) given by the system

$$\begin{cases} \dot{\theta} = \omega, \\ \dot{\sigma} = F(\theta, \sigma), \end{cases} \tag{7}$$

where $F(\theta,\sigma)$ is an analytic function such that $F(\theta,0)=0$ and σ is a transversal variable to the limit cycle that we call **amplitude** or **isostable variable**. System (7) is the **Augmented Phase Reduction** (**APR**) of the dynamics around the limit cycle. This idea is encapsulated in the following theorem which, under hyperbolicity conditions on the limit cycle, proves the viability of such reduction of the dynamics and, additionally, establishes a relation between $K(\theta,\sigma)$ and the existence of a second vector field $\mathcal{Y}$ bearing some kind of Lie-symmetry with respect to $\mathcal{X}$.

Theorem 2.3 (Guillamon and Huguet, [19])**.** *Given a planar analytic vector field $\mathcal{X}$ as in (1) with a hyperbolic limit cycle γ of period T and non-trivial Floquet multiplier $\lambda<0$ parameterized by the phase θ according to (2), the following statements are equivalent:*

(i) Limit cycle γ is isochronous and its isochrons are analytic curves.

(ii) There exists an analytical vector field $\mathcal{Y}$ defined in a neighborhood of the limit cycle, transversal to $\mathcal{X}$ and satisfying,

$$[\mathcal{X},\mathcal{Y}]=\frac{2\pi\lambda}{T}\,\mathcal{Y}. \tag{8}$$

(iii) There exists an analytic change of variables $K:[0,2\pi)\times\mathbb{R}\to\mathbb{R}^2$ such that

$$K_*\big(\tfrac{2\pi}{T}\,\tfrac{\partial}{\partial\theta}+\tfrac{2\pi\lambda}{T}\sigma\,\tfrac{\partial}{\partial\sigma}\big)(\theta,\sigma)\big)\;=\mathcal{X}\big(K(\theta,\sigma)\big), \tag{9}$$

in an open set $\mathcal{N}\subset[0,2\pi)\times\mathbb{R}$ containing the fiber $[0,2\pi)\times\{0\}$. In other words, we can say that vector field $\mathcal{X}$ is conjugated to $\frac{2\pi}{T}\,\frac{\partial}{\partial\theta}+\frac{2\pi\lambda}{T}\sigma\,\frac{\partial}{\partial\sigma}$ via the change of variables $(x,y)=K(\theta,\sigma)$.

Moreover, we have that $\mathcal{Y}\circ K=\frac{\partial}{\partial\sigma}K$, that is,

$$K(\theta,\sigma)=\phi_\sigma^{\mathcal{Y}}\big(\gamma(\theta)\big), \tag{10}$$

where $\phi_\sigma^{\mathcal{Y}}$ represents the flow associated to vector field $\mathcal{Y}$.

Remark 2.4. Expression (10) provides a parameterization of the isochron Θ_{θ_0}, for some $\theta_0\in[0,2\pi)$, in terms of σ given by the map $K(\theta_0,\cdot):\sigma\in\mathbb{R}\to K(\theta_0,\sigma)\in\mathbb{R}^2$. Hence, it follows that isochrons associated to each point on the limit cycle coincide with the orbits of vector field $\mathcal{Y}$ through the limit cycle.

Now, if we compare (9) with the general APR-dynamics given in (7), we can easily see that in the case of a hyperbolic limit cycle $F(\theta,\sigma)=\frac{\lambda\sigma}{T}$ is independent of the phase variable θ. Indeed, it follows from (7) that there exists a unique scalar function,

$$\varsigma:\mathbf{x}\in\mathcal{U}\subset\mathbb{R}^2\to\varsigma(\mathbf{x})=\sigma\in\mathbb{R}, \tag{11}$$

such that

$$\varsigma\big(\phi_t(\mathbf{x})\big)=\varsigma(\mathbf{x})\,e^{\frac{\lambda t}{T}}, \tag{12}$$

for all $\mathbf{x}$ in a small neighborhood $\mathcal{U}$ of the limit cycle. In analogy with (4), ς is referred to as the **amplitude function** of the limit cycle and associates each point surrounding it to its respective value of the amplitude variable σ which, as it is shown in (10), measures the distance to the limit cycle in terms of the integration time along the orbits of vector field $\mathcal{Y}$.

Finally, the level curves Σ_σ of the amplitude function are called **isostables** and, as in the case of the isochrons, it can be seen that they coincide with the orbits of a third vector field that also shares some Lie-symmetry with respecto to $\mathcal{X}$. This is shown in the following result proved by Castejón *et al.* in [6].

Theorem 2.5 (Castejón *et al.*, [6])**.** *Given a planar analytic vector field $\mathcal{X}$ with a hyperbolic limit cycle γ of period T and non-trivial Floquet multiplier $\lambda < 0$ parameterized by the phase θ according to (2), there exists a planar analytic vector field $\mathcal{Z}$ defined in a neighborhood of γ and Lie-commuting with $\mathcal{X}$, that is,*

$$[\mathcal{X}, \mathcal{Z}] = [\mathcal{Z}, \mathcal{X}] = 0. \tag{13}$$

Moreover, we have that $\mathcal{Z} \circ K = \frac{\partial}{\partial \theta}$, or equivalently,

$$K(\theta, \sigma) = \phi_\theta^{\mathcal{Z}}\left(K^{-1}(0, \sigma)\right), \tag{14}$$

where $\phi_\theta^{\mathcal{Z}}$ represents the flow associated to vector field $\mathcal{Z}$ and K is the analytic change of variables introduced in Theorem 2.3.

Remark 2.6. So as we noted in Remark 2.4, expression (14) provides a parameterization of the isostable Σ_{σ_0}, for some $\sigma_0 \in \mathbb{R} \setminus \{0\}$, in terms of the phase θ given by $K(\cdot, \sigma_0) : \theta \in [0, 2\pi) \to K(\theta, \sigma_0) \in \mathbb{R}^2$. Thus, we can conclude that isostables coincide with the orbits of vector field $\mathcal{Z}$ around the limit cycle.

2.2 Phase-amplitude response functions for limit cycles

One of the main applications of the Augmented Phase Reduction is the study and control of the effect that a small external perturbation may produce on the dynamics of a system on a neighborhood of the limit cycle. In this sense, let us consider the following planar perturbed system of ODEs,

$$\dot{\mathbf{x}} = \mathcal{X}(\mathbf{x}) + U(t, \mathbf{x}), \quad \mathbf{x} \in \mathbb{R}^2, \tag{15}$$

where $\mathcal{X}$ is a planar analytic vector field as in (1) with a hyperbolic periodic orbit γ of period $T > 0$ inside an open set $\mathcal{U} \in \mathbb{R}^2$ and parameterized by a phase θ according to (2), and $U(t, \mathbf{x})$ represents a small time-dependent perturbation of modulus $u(t, \mathbf{x}) = |U(t, \mathbf{x})|$.

It is worth noting that both the phase and the amplitude functions can be expressed in terms of the inverse of parameterization $K(\theta, \sigma)$ given in Theorem 2.3 as

$$\vartheta(\mathbf{x}) = \pi_1 \circ K^{-1}(\mathbf{x}) \quad \text{and} \quad \varsigma(\mathbf{x}) = \pi_2 \circ K^{-1}(\mathbf{x}), \tag{16}$$

being $\pi_1 : [0, 2\pi) \times \mathbb{R} \to [0, 2\pi)$ and $\pi_2 : [0, 2\pi) \times \mathbb{R} \to \mathbb{R}$ the natural projections onto the first and second components of $[0, 2\pi) \times \mathbb{R}$. Thus, if we now apply $K^{-1}(x, y)$ on system (15) in order to conjugate it to the APR-dynamics we obtain,

$$\begin{cases} \dot{\theta} = \nabla\vartheta(\mathbf{x})^T \cdot \big(\mathcal{X}(\mathbf{x}) + U(t, \mathbf{x})\big) = \omega + \nabla\vartheta(\mathbf{x})^T \cdot U(t, \mathbf{x}), \\ \dot{\sigma} = \nabla\varsigma(\mathbf{x})^T \cdot \big(\mathcal{X}(\mathbf{x}) + U(t, \mathbf{x})\big) = \frac{\lambda}{T}\sigma + \nabla\varsigma(\mathbf{x})^T \cdot U(t, \mathbf{x}), \end{cases} \tag{17}$$

where, as in (9), $\omega = \frac{2\pi}{T}$ represents the frequency of the oscillation and $\lambda < 0$, the non-trivial Floquet multiplier of the limit cycle. As we can see, the evolution of the phase-amplitude variables is modified

by the effect of the perturbation $U(t, \mathbf{x})$ as it forces the trajectories of the original system (9) to follow the orbits of the perturbed system (17). This allows us to introduce the so-called **phase-resetting** as the difference between the asymptotic phase of a point $\mathbf{x}$, $\vartheta(\mathbf{x}) = \theta$, and the new phase $\theta'(t)$ displaced by action of the perturbation,

$$\Delta\theta(t) = \theta'(t) - \theta. \tag{18}$$

Analogously, we introduce the **amplitude resetting** as the difference between the original amplitude of a point, $\varsigma(\mathbf{x})$, and its altered amplitude $\sigma'(t)$ after perturbation,

$$\Delta\sigma(t) = \sigma'(t) - \sigma. \tag{19}$$

In order to predict, control and analyze those changes in the phase and amplitude of points close to a isochronous limit cycle, and in accordance with (17), we introduce the **phase-amplitude response curves**:

Definition 2.7 (Phase response curve for a limit cycle)**.** Given a planar system of ODEs as in (1) with an isochronous limit cycle γ, we define the **Phase Response**, or **Resetting**, **Function** (**PRF**) as the infinitesimal rate of change of the asymptotic phase of a point $\mathbf{x}$ on a neighborhood of γ in the direction of a given small perturbation $U(t, \mathbf{x})$ of modulus $u(t, \mathbf{x})$, that is,

$$\mathrm{PRF}(t, \mathbf{x}) = D_{U(t,\mathbf{x})}\vartheta(\mathbf{x}) = \frac{1}{u(t, \mathbf{x})} \nabla\vartheta(\mathbf{x})^T \cdot U(t, \mathbf{x}), \tag{20}$$

where $\vartheta(\mathbf{x})$ is the phase function from the APR formalism around the limit cycle defined in (4).

Definition 2.8 (Amplitude response curve for a limit cycle)**.** Given a planar system of ODEs as in (1) with an isochronous limit cycle γ, we define the **Amplitude Response**, or **Resetting**, **Function** (**ARF**) as the infinitesimal rate of change of the amplitude of a point $\mathbf{x}$ on a neighborhood of γ in the direction of a given small perturbation $U(t, \mathbf{x})$ of modulus $u(t, \mathbf{x})$, that is,

$$\mathrm{ARF}(t, x) = D_{U(t,\mathbf{x})}\varsigma(\mathbf{x}) = \frac{1}{u(t, \mathbf{x})} \nabla\varsigma(\mathbf{x})^T \cdot U(t, \mathbf{x}), \tag{21}$$

where $\varsigma(\mathbf{x})$ is the amplitude function from the APR formalism around the limit cycle defined in (11).

Remark 2.9. It is worth noting that the fiber $\mathrm{PRC}(t, \theta) = \mathrm{PRF}(t, K(\theta, 0))$ for all $\theta \in [0, 2\pi)$ corresponds to the classical **Phase Response Curve** (**PRC**) of the CPR formalism - see, for instance, [11, 17, 23, 24].

Remark 2.10. In the context of mathematical neuroscience, one is commonly concerned in studying the implications of external stimuli on the voltage variable - usually considered in the abscissa direction - for it is the most easily modified parameter in real-life models. In such cases, the perturbations considered will have a fixed direction and, consequently, the phase-amplitude response functions will lose their dependence on time, namely, $\mathrm{PRF} = \mathrm{PRF}(\mathbf{x})$ and $\mathrm{ARF} = \mathrm{ARF}(\mathbf{x})$.

In terms of the recently introduced PRF and ARF, the perturbed APR system (17) reads,

$$\begin{cases} \dot{\theta} = \omega + \mathrm{PRF}(t, \mathbf{x})\, u(t, \mathbf{x}), \\ \dot{\sigma} = \frac{\lambda}{T}\, \sigma + \mathrm{ARF}(t, \mathbf{x})\, u(t, \mathbf{x}). \end{cases} \tag{22}$$

Thus, the phase-amplitude response functions are key tools in the study of perturbations over the dynamics around an isochronous limit cycle. In this sense, explicit local expressions for $\nabla\vartheta$ and $\nabla\varsigma$ in terms of the geometrical relation between vector fields $\mathcal{X}$, $\mathcal{Y}$ and $\mathcal{Z}$ are given in [6, 19]. These are

$$\nabla\vartheta(\mathbf{x}) = \omega\, \frac{\mathcal{Y}^{\perp}(\mathbf{x})}{\mathcal{Y}^{\perp}(\mathbf{x})^{T} \cdot \mathcal{X}(\mathbf{x})}, \tag{23}$$

and

$$\nabla\varsigma(\mathbf{x}) = \frac{\lambda\sigma}{T}\, \frac{\mathcal{Z}^{\perp}(\mathbf{x})}{\mathcal{Z}^{\perp}(\mathbf{x})^{T} \cdot \mathcal{X}(\mathbf{x})}, \tag{24}$$

where $\cdot$ denotes the usual dot-product of vectors on the plane and $^{\perp}$ the orthogonal vector field according to such dot-product. Clearly, if we now plug (23) and (24) into (20) and (21) we obtain local expressions for the PRF and the ARF respectively whose limited range of applicability depends on the domain of definition of the parameterization $K(\theta, \sigma)$ in Theorem 2.3.

In order to extended these formulas to a wider region and, in doing so, gaining more information about the effects of perturbations on the dynamics of the system, Guillamon and Huguet designed a methodology for the extension of the PRF based on the classical **adjoint method** for the computation of the PRC along the limit cycle - see, for instance, the work of Ermentrout and Kopell in [12]. Indeed, their novel approach on the problem using the parameterization method allowed them to substitute the usual periodic conditions of the adjoint equation for some Cauchy conditions of the form (23) and extend the adjoint problem out of the periodic orbit onto a region around it. Thus, one simply needs to solve the **adjoint equation for the PRF** backwards in time starting at a point close to the limit cycle up to the extended area. The following result corresponds to this new adjoint method and is proved in [19].

Theorem 2.11 (Guillamon and Huguet, [19]). *Given a planar analytic vector field $\mathcal{X}$ as in (1) with an isochronous periodic orbit γ of period T and non-trivial Floquet multiplier $\lambda < 0$ parameterized by a phase θ according to (2) and a neighbothood $\mathcal{U}$ of the limit cycle where formula (23) holds true, the gradient $\nabla\vartheta$ satisfies the following Cauchy problem along the orbits of $\mathcal{X}$ through any $\mathbf{x} \in \mathcal{U}$,*

$$\begin{cases} \frac{d}{dt} \nabla\vartheta\big(\phi_t(\mathbf{x})\big) = -D\mathcal{X}\big(\phi_t(\mathbf{x})\big)^{T}\, \nabla\vartheta\big(\phi_t(\mathbf{x})\big), \\ \nabla\vartheta\big(\phi_0(\mathbf{x})\big) = \omega\, \frac{\mathcal{Y}^{\perp}(\phi_0(\mathbf{x}))}{\mathcal{Y}^{\perp}(\phi_0(\mathbf{x}))^{T} \cdot \mathcal{X}(\phi_0(\mathbf{x}))}, \end{cases} \tag{25}$$

where $\phi_t(\mathbf{x})$ represents the flow associated to vector field $\mathcal{X}$.

In a later paper, Castejón, Guillamon and Huguet completed this result by proving the existance of an analogous **adjoint equation for the ARF** that we present in the following. This theorem is proved in [6].

Theorem 2.12 (Castejón *et al.*, [6]). *Given a planar analytic vector field $\mathcal{X}$ as in (1) with an isochronous periodic orbit γ of period T and non-trivial Floquet multiplier $\lambda < 0$ parameterized by a phase θ according*

to (2) *and a neighborhood* $\mathcal{U}$ *of the limit cycle where formula* (23) *holds true, the gradient* $\nabla\varsigma$ *satisfies the following Cauchy problem along the orbits of* $\mathcal{X}$ *through any* $\mathbf{x} \in \mathcal{U}$,

$$\begin{cases} \frac{d}{dt}\nabla\varsigma(\phi_t(\mathbf{x})) = \left(\frac{\lambda}{T}\, Id - D\mathcal{X}(\phi_t(\mathbf{x}))^T\right) \nabla\varsigma(\phi_t(\mathbf{x})), \\ \nabla\varsigma(\phi_0(\mathbf{x})) = \frac{\lambda}{T}\varsigma(\mathbf{x})\, \frac{\mathcal{Z}^\perp(\phi_0(\mathbf{x}))}{\mathcal{Z}^\perp(\phi_0(\mathbf{x}))^T \cdot \mathcal{X}(\phi_0(\mathbf{x}))}, \end{cases} \tag{26}$$

where $\phi_t(\mathbf{x})$ *represents the flow associated to vector field* $\mathcal{X}$.

3. Theoretical results

In this section we are going to present the main theoretical results concerning the development of an Augmented Phase Reduction (APR) formalism and its consequent response functions in the case of a system with a strong focus in the fashion of that presented for systems with limit cycles in Section 2. We also propose a novel optimal control strategy based on such APR approximation with the objective of inducing a periodic oscillation around the strong focus by means of a minimum energy input.

3.1 Augmented phase reduction for strong foci

Let us consider an autonomous system of ODEs on the real plane,

$$\dot{\mathbf{x}} = \mathcal{X}(\mathbf{x}), \quad \mathbf{x} \in \mathbb{R}^2, \tag{27}$$

where $\mathcal{X}$ is an analytic vector field with an isolated **critical point** at the origin $\mathcal{O} \in \mathbb{R}^2$ of the form

$$\mathcal{X} = \big(\alpha x - \beta y + f_1(x,y)\big)\frac{\partial}{\partial x} + \big(\beta x + \alpha y + f_2(x,y)\big)\frac{\partial}{\partial y}, \tag{28}$$

with $\beta \neq 0$ and $f_{1,2}(x,y)$ analytic functions of order at least 2 in a neighborhood of $\mathcal{O}$, that is, $f_i(\mathcal{O}) = 0$ and $Df_i(\mathcal{O}) = 0$ for $i \in \{1,2\}$. This isolated critical point is a **strong focus** if $\alpha \neq 0$ and either a **center** or a **weak focus** if $\alpha = 0$. Moreover, we will say that a strong focus is **stable**, or **attracting**, if $\alpha < 0$, and **unstable**, or **repelling**, if $\alpha > 0$. Along this section we will be assuming that the foci at issue are stable since the study of their repelling counterback is analogous by simply changing the direction of time. We will denote by ϕ_t the flow associated to vector field (28).

Definition 3.1 (Isochron for a center or focus)**.** Given a planar analytic vector field with an isolated critical point with complex-conjugated eigenvalues at the origin $\mathcal{O} \in \mathbb{R}^2$ and a neighborhood $\mathcal{U}$ of the origin, an **isochron**, or **isochronous section**, for such a critical point is a transversal section $\Theta \subset \mathcal{U}$ parameterized in $[0,\infty)$ verifying $\Theta(0) = \mathcal{O}$, $[\Theta'(0)] \in \mathbb{PR}^2$ and such that there exists a constant $T \in \mathbb{R}^+$ satisfying

(i) $\phi_T(\mathbf{x}) \in \Theta$, for all $\mathbf{x} \in \Theta$; but,

(ii) $\phi_t(\mathbf{x}) \notin \Theta$, for any $\mathbf{x} \in \Theta$ and any $0 < t < T$.

Remark 3.2. Constant $T \in \mathbb{R}^+$ in the previous definition is commonly known as the **natural period** of the critical point at issue.

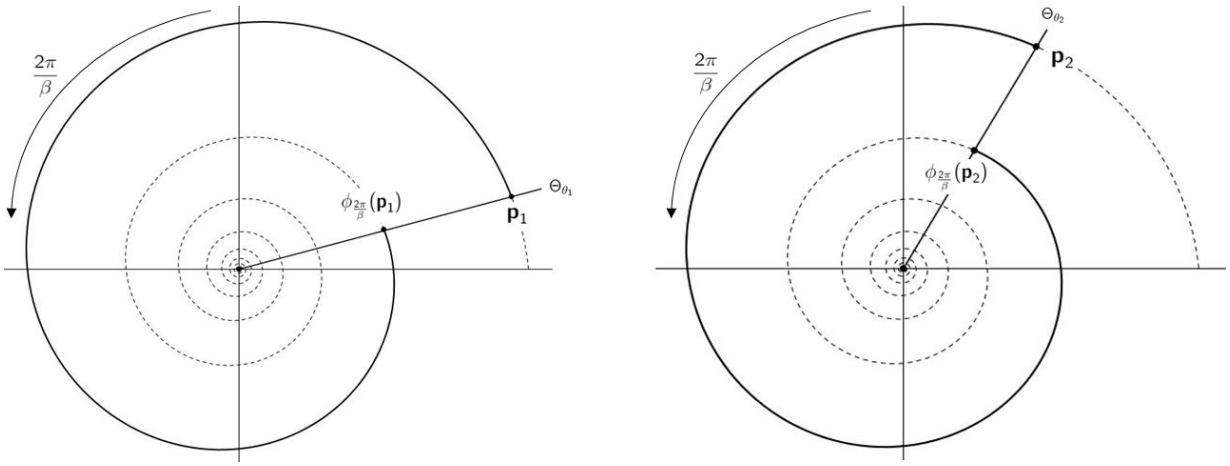

Figure 1: Scheme of the behaviour of orbits around a strong linear focus for two different rays through the origin. In both cases, the flow comes back to $\tilde{\Theta}_\theta$ in a fixed time $\frac{2\pi}{\beta}$. Therefore, the focus is isochronous.

Definition 3.3 (Isochronous center or focus)**.** An isolated critical point with complex-conjugated eigenvalues in a planar analytic vector field is said to be **isochronous** if it admits at least one isochron.

By the way of illustration, we will examine the isochrony of the stable strong linear focus obtained when taking $f_1, f_2 \equiv 0$ and $\alpha < 0$ in vector field (28), that is,

$$\tilde{\mathcal{X}} = (\alpha x - \beta y)\frac{\partial}{\partial x} + (\beta x + \alpha y)\frac{\partial}{\partial y}, \tag{29}$$

with $\alpha < 0$ and $\beta \neq 0$. The flow associated to this vector field is given by

$$\tilde{\phi}_t(\mathbf{x}) = k(\mathbf{x})e^{-|\alpha|t}\begin{pmatrix}\cos(\beta t + \omega(\mathbf{x}))\\ \sin(\beta t + \omega(\mathbf{x}))\end{pmatrix}, \tag{30}$$

for some $k(\mathbf{x}) \in \mathbb{R}^+$ and $\omega(\mathbf{x}) \in [0, 2\pi)$, and so, the critical point at $\mathcal{O}$ is an isochronous strong focus with natural period $T = \frac{2\pi}{\beta}$ and its infinitely many isochrons given by the sets

$$\tilde{\Theta}_\theta = \{(\sigma\cos\theta, \sigma\sin\theta) \,|\, \sigma \in (0, +\infty)\}, \tag{31}$$

for every $\theta \in [0, 2\pi)$. Indeed, given $\mathbf{x} \in \tilde{\Theta}_{\theta_0}$ for some $\theta_0 \in [0, 2\pi)$, it is obvious in the view of (30) that $\phi_{\frac{2\pi}{\beta}}(\mathbf{x}) \in \tilde{\Theta}_{\theta_0}$, and never before. Figure 1 portrays an scheme of this situation.

A general characterization of isochronous critical points with complex-conjugated eigenvalues in planar vector fields has been studied by several authors in the recent years, see [3, 15] and some references therein. In order to present such characterizations, an essential step is to consider the dynamics of vector field (28) in polar coordinates, that is,

$$\rho_*(\mathcal{X}) = S(\sigma, \theta)\frac{\partial}{\partial\theta} + \sigma R(\sigma, \theta)\frac{\partial}{\partial\sigma}, \tag{32}$$

where R and S are analytic functions in a neighborhood of $\rho(\mathcal{O})$, ρ represents the usual change to polar coordinates - namely, $\theta = \arctan\left(\frac{y}{x}\right)$ and $\sigma = \sqrt{x^2 + y^2}$ - and ρ_* denotes the pushforward of ρ.

The following theorem proved by Giné and Grau in [15] offers the two most common methods used to study the isochronicity of centers and foci. These are, on one hand, finding a linearization for system (27), and, on the other hand, exploiting some certain Lie-simmetry of $\mathcal{X}$ with respect to a second vector field.

Theorem 3.4 (Giné and Grau, [15]). *Given a planar analytic vector field $\mathcal{X}$ in the conditions of (28) with a critical point with complex-conjugated eigenvalues at the origin, the following statements are equivalent:*

(i) The critical point at $\mathcal{O}$ is isochronous.

(ii) There exists a local analytic change of variables around the origin, $\tilde{\mathbf{x}} = \varphi(\mathbf{x})$, with $D\varphi(\mathcal{O}) = Id$ and such that the angular velocity of the dynamics of the transformed system in polar coordinates is independent of the radius, that is, expression (32) actually reads

$$\rho_*\varphi_*\mathcal{X} = S(\theta)\,\frac{\partial}{\partial\theta} + \sigma R(\sigma,\theta)\,\frac{\partial}{\partial\sigma}. \tag{33}$$

(iii) There exists a planar analytic vector field $\mathcal{Y}$ defined in a neighborhood of the origin with a star-node at $\mathcal{O}$, that is, a vector field of the form

$$\mathcal{Y} = \big(x + g_1(x,y)\big)\,\frac{\partial}{\partial x} + \big(y + g_2(x,y)\big)\,\frac{\partial}{\partial y}, \tag{34}$$

with $g_{1,2}(x,y)$ analytic functions of order greater or equal than 2, such that

$$[\mathcal{X},\mathcal{Y}] = \mu(x,y)\,\mathcal{Y}, \tag{35}$$

for some smooth scalar function $\mu(x,y)$ verifying $\mu(\mathcal{O}) = 0$.

Remark 3.5. Whenever two planar vector fields $\mathcal{X}$ and $\mathcal{Y}$ satisfy condition (35), we say that vector field $\mathcal{Y}$ is **normalized** by vector field $\mathcal{X}$.

In this same spirit, the following two results by Algaba and Reyes, [3], explore useful further properties of vector field $\mathcal{Y}$ and relate it to the isochrons of the critical point at the origin.

Corollary 3.6 (Algaba and Reyes, [3]). *Given a planar analytic vector field $\mathcal{X}$ in the conditions of (28) with a critical point with complex-conjugated eigenvalues at the origin, the critical point at $\mathcal{O}$ is isocronous if and only if there exists a planar analytic vector field $\mathcal{Y}$ with a star-node at $\mathcal{O}$ normalized by $\mathcal{X}$. Furthermore, every orbit of $\mathcal{Y}$ in a certain neighborhood of the origin coincides with an isochron of the critical point.*

Corollary 3.7 (Algaba and Reyes, [3]). *Given a planar analytic vector field $\mathcal{X}$ in the conditions of (28) with a critical point with complex-conjugated eigenvalues at the origin, the critical point at $\mathcal{O}$ is isocronous if and only if it admits not one, but infinitely many isochrons. If, moreover, this critical point is a focus - weak or strong -, those isochrons are disjoint two by two, they completely cover up a certain neighborhood of the origin and, given any $[\nu] \in \mathbb{PR}^2$, there is only one of them that arrives to $\mathcal{O}$ in the direction of ν.*

At this point we are in position of moving on to the particular study of systems with a strong focus. This means that from now on, and until the end of this section, we will be considering at all time a vector field $\mathcal{X}$ in the conditions of (28) with the extra assumption that $\alpha \neq 0$ - actually, $\alpha < 0$. Under this circumstances, the following classical normal form result due to Poincaré, [28], states that any system with a strong focus at the origin is locally conjugated to the linear system given by (29) through a local analytical change of variables. For a modern approach on the proof of the theorem, see [8, 26].

Theorem 3.8 (Poincaré, [28]). *Given a real planar analytic vector field of the form* $\mathcal{X} = (\alpha x - \beta y + o(2))\frac{\partial}{\partial x} + (\beta x + \alpha y + o(2))\frac{\partial}{\partial y}$, *with* $\alpha, \beta \neq 0$, *there exists a real local analytic change of variables,* $\tilde{\mathbf{x}} = \psi(\mathbf{x})$, *with* $D\psi(\mathcal{O}) = Id$, *that transforms* $\mathcal{X}$ *into* $\tilde{\mathcal{X}} = (\alpha\tilde{x} - \beta\tilde{y})\frac{\partial}{\partial \tilde{x}} + (\beta\tilde{x} + \alpha\tilde{y})\frac{\partial}{\partial \tilde{y}}$.

This theorem can be used to proof that any general strong focus is isochronous. Thus, given a planar analytic vector field $\mathcal{X}$ with a strong focus at the origin, we can take $\psi(x, y)$ in Theorem 3.8 to be the change of variables $\varphi(x, y)$ in Theorem 3.4 and then, the dynamics of the transformed vector field $\tilde{\mathcal{X}}$ in polar coordinates will read

$$\rho_*\tilde{\mathcal{X}} = \rho_*\varphi_*\mathcal{X} = \beta\,\frac{\partial}{\partial\theta} + \sigma\alpha\,\frac{\partial}{\partial\sigma}; \tag{36}$$

so, given that the angular velocity of this dynamics is constant and equal to β, we know by Theorem 3.4 that the strong focus in $\mathcal{X}$ is isochronous. Consequently, it is possible to construct an **Augmented Phase Reduction** (**APR**) that encapsulates the dynamics around any general strong focus. In fact, polar coordinates (θ, σ) in (36) happen to be the natural phase-amplitude variables of such formalism and the analytic change of variables $L(x, y) = \rho \circ \varphi(x, y)$ is the conjugation map between system (27) and the APR-dynamics given by (36), namely,

$$L^{-1}\big((\beta\,\tfrac{\partial}{\partial\theta} + \sigma\alpha\,\tfrac{\partial}{\partial\sigma})(\theta, \sigma)\big) = \mathcal{X}(L^{-1}(\theta, \sigma)). \tag{37}$$

Remark 3.9. Note that the change of variables $(x, y) = L^{-1}(\theta, \sigma)$ plays, in the realm of strong foci, the same role as parameterization $K(\theta, \sigma)$ plays in the case of limit cycles, [6, 19].

According to conjugation (37), given a neighborhood $\mathcal{U}$ of the origin, we can consider the **phase function** $\vartheta(\mathbf{x})$ as the unique function

$$\vartheta : \mathbf{x} \in \mathcal{U} \subset \mathbb{R}^2 \to \vartheta(\mathbf{x}) \in [0, 2\pi), \tag{38}$$

verifying

$$\vartheta\big(\phi_{\frac{2\pi}{\beta}}(\mathbf{x})\big) = \vartheta(\mathbf{x}), \qquad \text{but} \qquad \vartheta\big(\phi_t(\mathbf{x})\big) \neq \vartheta(\mathbf{x}), \tag{39}$$

for all $\mathbf{x} \in \mathcal{U}$ and all $0 < t < \frac{2\pi}{\beta}$. The phase function associates each point in $\mathcal{U}$ to its corresponding value of the **asymptotic phase** θ and, therefore, it can be written in terms of the change of variables $L(x, y)$ as $\vartheta(\mathbf{x}) = \pi_1 \circ L(\mathbf{x})$, where $\pi_1 : [0, 2\pi) \times \mathbb{R} \to [0, 2\pi)$ represents the usual projection onto the first component of $[0, 2\pi) \times \mathbb{R}$. Moreover, we know by Corollary 3.7 that isochrons of an isochronous focus are disjoint two by two and they cover up a neighborhood of the focus at issue. Consequently, if $\mathcal{U}$ is small enough, for any $\mathbf{x} \in \mathcal{U}$ there will exist a unique isochron Θ such that $\mathbf{x} \in \Theta$ and then, the asymptotic phase associated to

$\mathbf{x}$ will correspond to the polar angular coordinate defining the direction $[\nu] \in \mathbb{PR}^2$ with which Θ hits the origin. Hence, isochrons can be identified with the level curves of the phase function, that is,

$$\Theta_\theta = \{\mathbf{x} \,|\, \vartheta(\mathbf{x}) = \theta\}, \qquad \text{for some } \theta \in [0, 2\pi). \tag{40}$$

Definition 3.10 (Points in phase around a strong focus)**.** Given a planar analytic vector field $\mathcal{X}$ with an strong focus at the origin, we say that two points in a neighborhood of the origin are **in phase** if they share the same asymptotic phase or, in other words, if they belong to the same isochron.

In a similar way, we can introduce the **amplitude function** $\varsigma(\mathbf{x})$ as the unique function

$$\varsigma : \mathbf{x} \in \mathcal{U} \subset \mathbb{R}^2 \to \varsigma(\mathbf{x}) \in \mathbb{R}, \tag{41}$$

such that

$$\varsigma(\phi_t(\mathbf{x})) = \varsigma(\mathbf{x})\, e^{-|\alpha| t}, \tag{42}$$

for all $\mathbf{x} \in \mathcal{U}$ and all $t \in \mathbb{R}$. In the view of the APR-dynamics given by (37), it is clear that the amplitude function associates each point in $\mathcal{U}$ with its corresponding value of the **amplitude** variable σ and, consequently, that it can be written as $\varsigma(\mathbf{x}) = \pi_2 \circ L(\mathbf{x})$, where $\pi_2 : [0, 2\pi) \times \mathbb{R} \to \mathbb{R}$ is now the projection onto the second component of $[0, 2\pi) \times \mathbb{R}$. In this case, the amplitude of a point $\mathbf{x} \in \mathcal{U}$ directly corresponds to the radial distance of point $\varphi(\mathbf{x})$ to the origin $\varphi(\mathcal{O})$ in the linear framework displayed by vector field $\tilde{\mathcal{X}} = \varphi_* \mathcal{X}$. Finally, in analogy to isochrons, we introduce the **isostables** or **isostable curves** associated to a strong focus as the level curves of the amplitude function, that is,

$$\Sigma_\sigma = \{\mathbf{x} \in \mathbb{R}^2 \,|\, \varsigma(\mathbf{x}) = \sigma\}, \qquad \text{for some } \sigma \in \mathbb{R}^+. \tag{43}$$

The following theorem explores the main properties of isostables and relates them to the existence of a third vector field $\mathcal{Z}$ bearing a relation of Lie-commutativity with respect to $\mathcal{X}$. In this sense, this result mimics the thesis of Corollaries 3.6 and 3.7 for the case of isostable curves around a strong focus.

Theorem 3.11. *Given a planar analytic vector field $\mathcal{X}$ in the conditions of (28) with a strong focus at the origin - i.e., $\alpha < 0$ -, there exists a planar analytic vector field $\mathcal{Z}$ defined in a neighborhood of the origin with a linear center at $\mathcal{O}$, that is, a vector field of the form*

$$\mathcal{Z} = \big(-y + h_1(x, y)\big)\, \frac{\partial}{\partial x} + \big(x + h_2(x, y)\big)\, \frac{\partial}{\partial y}, \tag{44}$$

with $h_{1,2}(x, y)$ analytic functions of order greater or equal than 2, satisfying $[\mathcal{X}, \mathcal{Z}] = 0$ and such that every orbit of $\mathcal{Z}$ coincides with an isostable of the strong focus at $\mathcal{O}$. Moreover, those isostables are closed curves around $\mathcal{O}$, disjoint two to two and they completely cover up a neighborhood of the origin.

Proof. In virtue of Theorem 3.8, we know that there exists a real local analytic change of variables $\tilde{\mathbf{x}} = \psi(\mathbf{x})$, with $D\psi(\mathcal{O}) = Id$, that transforms $\mathcal{X}$ into

$$\tilde{\mathcal{X}} = \psi_* \mathcal{X} = \big(\alpha\tilde{x} - \beta\tilde{y}\big)\, \frac{\partial}{\partial \tilde{x}} + \big(\beta\tilde{x} + \alpha\tilde{y}\big)\, \frac{\partial}{\partial \tilde{y}}. \tag{45}$$

Thus, if we consider vector field $\tilde{\mathcal{Z}} = -\tilde{y}\frac{\partial}{\partial \tilde{x}} + \tilde{x}\frac{\partial}{\partial \tilde{y}}$, we have

$$\left[\tilde{\mathcal{X}}, \tilde{\mathcal{Z}}\right] = \left[\left(\alpha\tilde{x} - \beta\tilde{y}\right)\frac{\partial}{\partial \tilde{x}} + \left(\beta\tilde{x} + \alpha\tilde{y}\right)\frac{\partial}{\partial \tilde{y}},\ -\tilde{y}\frac{\partial}{\partial \tilde{x}} + \tilde{x}\frac{\partial}{\partial \tilde{y}}\right] = 0. \tag{46}$$

Now, we define $\mathcal{Z} = \psi_*^{-1}\tilde{\mathcal{Z}}$. Hence, given that $D\psi(\mathcal{O}) = Id$, it is clear that $\mathcal{Z}$ will possess a linear center at $\mathcal{O}$ and so, that it can be written in the form of (44) in a certain neighborhood of the origin. Moreover, since the pushforward of a diffeomorphism is bracket-commuting, we have that

$$[\mathcal{X}, \mathcal{Z}] = \left[\psi_*^{-1}(\psi_*\mathcal{X}), \psi_*^{-1}\tilde{\mathcal{Z}}\right] = \psi_*^{-1}\left[\tilde{\mathcal{X}}, \tilde{\mathcal{Z}}\right] = 0. \tag{47}$$

To prove that the orbits of $\mathcal{Z}$ coincide with the isostables of the strong focus at $\mathcal{O}$, we shall first recall that the flow of vector field $\tilde{\mathcal{Z}}$ is given by

$$\phi_t^{\tilde{\mathcal{Z}}}(\tilde{\mathbf{x}}) = k(\tilde{\mathbf{x}})\begin{pmatrix}\cos(t + \omega(\tilde{\mathbf{x}}))\\ \sin(t + \omega(\tilde{\mathbf{x}}))\end{pmatrix}, \tag{48}$$

for some $k(\tilde{\mathbf{x}}) \in \mathbb{R}^+$ and some $\omega(\tilde{\mathbf{x}}) \in [0, 2\pi)$, and, accordingly, its orbits correspond to the sets

$$\tilde{\Sigma}_\sigma = \{(\sigma\cos\theta, \sigma\sin\theta)\,|\,\theta \in [0, 2\pi)\}, \tag{49}$$

for all $\sigma \in \mathbb{R}^+$. By definition, the orbits of $\mathcal{Z}$ in a neighborhood $\mathcal{U}$ of the origin are then given by

$$\Sigma_\sigma = \psi^{-1}(\tilde{\Sigma}_\sigma), \tag{50}$$

for all $0 < \sigma < \sigma_{max}$, where $\sigma_{max} = \sigma_{max}(\mathcal{U})$ represents the maximum radius of $\tilde{\Sigma}_\sigma$ such that its image completely fits inside $\mathcal{U}$ and, naturally, depends on the size of $\mathcal{U}$. Thus, given $0 < \sigma < \sigma_{max}$ fixed,

$$\varsigma(\Sigma_\sigma) = \pi_2 \circ L(\Sigma_\sigma) = \pi_2 \circ \rho(\tilde{\Sigma}_\sigma) \equiv \sigma, \tag{51}$$

that is, Σ_σ is the isostable associated to the constant amplitude of σ. Finally, the properties of isostables stated at the end of Theorem 3.11 are easily derived by conjugation from the properties of orbits $\tilde{\Sigma}_\sigma$ in (49) and the fact that they coincide with the orbits of an analytic vector field.

□

3.2 Phase-amplitude response functions for strong foci

Let us consider a planar perturbed system of ODEs,

$$\dot{\mathbf{x}} = \mathcal{X}(\mathbf{x}) + U(t, \mathbf{x}), \quad \mathbf{x} \in \mathbb{R}^2, \tag{52}$$

where $\mathcal{X}$ is a planar analytic vector field as in (28) with a strong focus at the origin $\mathcal{O} \in \mathbb{R}^2$, and $U(t, \mathbf{x})$ represents a small time-dependent perturbation of modulus $u(t, \mathbf{x}) = |U(t, \mathbf{x})|$. Our goal in this subsection is to study how this small pertubation affects the original dynamics of the system around the origin.

In the absence of pertubation - i.e., $U(t, \mathbf{x}) \equiv 0$ -, we know that there exists a local analytic change of variables $L(\mathbf{x}) = (\vartheta(\mathbf{x}), \varsigma(\mathbf{x}))$ that conjugates system (52) to the APR-dynamics given by the system

$$\begin{cases} \dot{\theta} = \nabla\vartheta(\mathbf{x})^T \cdot \mathcal{X}(\mathbf{x}) = \beta, \\ \dot{\sigma} = \nabla\varsigma(\mathbf{x})^T \cdot \mathcal{X}(\mathbf{x}) = \alpha\sigma, \end{cases} \tag{53}$$

with $\mathbf{x} = L^{-1}(\theta, \sigma)$. If $U(t, \mathbf{x}) \not\equiv 0$, on the other hand, the evolution of the APR-dynamics is naturally modified and given up to a first order by

$$\begin{cases} \dot{\theta} = \nabla\vartheta(\mathbf{x})^T \cdot \big(\mathcal{X}(\mathbf{x}) + U(t, \mathbf{x})\big) = \beta + \nabla\vartheta(\mathbf{x})^T \cdot U(t, \mathbf{x}), \\ \dot{\sigma} = \nabla\varsigma(\mathbf{x})^T \cdot \big(\mathcal{X}(\mathbf{x}) + U(t, \mathbf{x})\big) = \alpha\sigma + \nabla\varsigma(\mathbf{x})^T \cdot U(t, \mathbf{x}). \end{cases} \tag{54}$$

As we can see, the action of the perturbation $U(t, \mathbf{x})$ alters the value of the phase-amplitude variables of the trajectories of the original system (53) forcing them to follow the orbits of system (54). Hence, we can introduce the **phase resetting** as the difference between the asymptotic phase of a point $\mathbf{x}$ in the original configuration, $\vartheta(\mathbf{x}) = \theta$, and the new phase $\theta'(t)$ induced by the perturbation,

$$\Delta\theta(t) = \theta'(t) - \theta. \tag{55}$$

In a similar way, we define the **amplitude resetting** as the difference between the original amplitude of a point $\mathbf{x}$, $\varsigma(\mathbf{x}) = \sigma$, and the amplitude $\sigma'(t)$ after perturbation,

$$\Delta\sigma(t) = \sigma'(t) - \sigma. \tag{56}$$

So as we did in the case of limit cycles, we now introduce, in accordance with (54), the corresponding **phase-amplitude response curves** associated to a strong focus:

Definition 3.12 (Phase response curve for a strong focus)**.** Given a planar system of ODEs as in (27) with a strong focus at the origin, the **Phase Response**, or **Resetting**, **Function** (**PRF**) is defined as the infinitesimal rate of change of the asymptotic phase of a point $\mathbf{x}$ in a neighborhood of $\mathcal{O}$ in the direction of a given small perturbation $U(t, \mathbf{x})$ of modulus $u(t, \mathbf{x})$, that is,

$$\mathrm{PRF}(t, \mathbf{x}) = D_{U(t,\mathbf{x})}\vartheta(\mathbf{x}) = \frac{1}{u(t, \mathbf{x})} \nabla\vartheta(\mathbf{x})^T \cdot U(t, \mathbf{x}), \tag{57}$$

where $\vartheta(\mathbf{x})$ is the phase function associated to the APR formalism of the strong focus defined in (38).

Definition 3.13 (Amplitude response curve for a strong focus)**.** Given a planar system of ODEs as in (27) with a strong focus at the origin, the **Amplitude Response**, or **Resetting**, **Function** (**ARF**) is defined as the infinitesimal rate of change of the amplitude of a point $\mathbf{x}$ in a neighborhood of $\mathcal{O}$ in the direction of a given small perturbation $U(t, \mathbf{x})$ of modulus $u(t, \mathbf{x})$, that is,

$$\mathrm{ARF}(t, \mathbf{x}) = D_{U(t,\mathbf{x})}\varsigma(\mathbf{x}) = \frac{1}{u(t, \mathbf{x})} \nabla\varsigma(\mathbf{x})^T \cdot U(t, \mathbf{x}), \tag{58}$$

where $\varsigma(\mathbf{x})$ is the amplitude function associated to the APR formalism of the strong focus defined in (41).

Remark 3.14. So as we commented in Remark 2.10, it is common in neuroscience that the stimuli at issue have the fixed direction of the voltage variable for it is the most easily modified parameter in real-life neuronal experiments. Consequently, the phase-amplitude response functions lose their dependence on time, namely, $\mathrm{PRF} = \mathrm{PRF}(\mathbf{x})$ and $\mathrm{ARF} = \mathrm{ARF}(\mathbf{x})$.

In terms of the PRF and the ARF, the equations of the perturbed APR-dynamics read

$$\begin{cases} \dot{\theta} \;=\; \beta + \mathrm{PRF}(t,\mathbf{x})\, u(t,\mathbf{x}), \\ \dot{\sigma} \;=\; \alpha\sigma + \mathrm{ARF}(t,\mathbf{x})\, u(t,\mathbf{x}). \end{cases} \tag{59}$$

Our main goal now is to give explicit analytical expressions for the phase-amplitude response functions similar to those found in (23) and (24) for limit cycles since, as we can see in (59), it is them who determine the effects of small perturbations on the dynamics of system (52). The main theoretical results regarding the definition of a PRF in the surroundings of a strong focus, which we include here for the sake of completeness, are given by Moreno in [26] while the theory concerning the ARF is, to the best of our knowledge, original of this paper.

We will begin by studying an explicit formula for the PRF, that is, an explicit formula for $\nabla\vartheta$ as it is this gradient, together with the direction of the perturbation, what fully determines the PRF. First, recall that the isochrons of a strong focus correspond, on one hand, with the level curves of ϑ and, on the other hand, with the orbits of a vector field $\mathcal{Y}$ with a star-node at $\mathcal{O}$ and normalizing $\mathcal{X}$ on account of Corollaries 3.6 and 3.7. Hence, we can write

$$\nabla\vartheta(\mathbf{x})^{T} \cdot \mathcal{Y}(\mathbf{x}) = 0, \tag{60}$$

for all $\mathbf{x}$ in a neighborhood $\mathcal{U}$ of the origin, or, equivalently,

$$\nabla\vartheta(\mathbf{x}) = C(\mathbf{x})\, \mathcal{Y}^{\perp}(\mathbf{x}), \tag{61}$$

for all $\mathbf{x} \in \mathcal{U}$ and some normalization constant $C(\mathbf{x}) \in \mathbb{R}$. In order to compute the normalization constant, let us consider the derivative of the phase function along the orbits of vector field $\mathcal{X}$, that is,

$$\frac{d}{dt}\vartheta(\phi_t(\mathbf{x})) = \nabla\vartheta(\phi_t(\mathbf{x}))^{T} \cdot \frac{d}{dt}\phi_t(\mathbf{x}) = \nabla\vartheta\big(\phi_t(\mathbf{x})\big)^{T} \cdot \mathcal{X}\big(\phi_t(\mathbf{x})\big) = \beta, \tag{62}$$

where the last equal is obtained according to the APR-dynamics (53) that states $\frac{d}{dt}\vartheta\big(\phi_t(\mathbf{x})\big) = \beta$. Thus, plugging (61) into the penultimate term of (62), we are led to

$$C(\mathbf{x}) = \beta\, \frac{1}{\mathcal{Y}^{\perp}(\mathbf{x})^{T} \cdot \mathcal{X}(\mathbf{x})}, \tag{63}$$

and so, going back to (61), we finally get, for any $\mathbf{x} \in \mathcal{U}$,

$$\nabla\vartheta(\mathbf{x}) = \beta\, \frac{\mathcal{Y}^{\perp}(\mathbf{x})}{\mathcal{Y}^{\perp}(\mathbf{x})^{T} \cdot \mathcal{X}(\mathbf{x})}. \tag{64}$$

Remark 3.15. It is worth noting that a local form for vector field $\mathcal{Y}$ can be computed as the pushforward $\mathcal{Y} = \psi_*\tilde{\mathcal{Y}}$, where ψ is the analytic change of variables from Theorem 3.8 and $\tilde{\mathcal{Y}}$ is the canonical planar linear vector field with a star-node at the origin given by

$$\tilde{\mathcal{Y}} = \tilde{x}\,\frac{\partial}{\partial\tilde{x}} + \tilde{y}\,\frac{\partial}{\partial\tilde{y}}. \tag{65}$$

Under such circumstances, vector field $\mathcal{Y}$ is not only a normalizer of vector field $\mathcal{X}$, but a commutator, that is, $\mu(x,y) \equiv 0$ in (35). Indeed,

$$\big[\mathcal{X},\mathcal{Y}\big] = \psi_*^{-1}\big[\tilde{\mathcal{X}},\tilde{\mathcal{Y}}\big] = \psi_*^{-1}\big[(\alpha\tilde{x}-\beta\tilde{y})\,\tfrac{\partial}{\partial\tilde{x}} + (\beta\tilde{x}+\alpha\tilde{y})\,\tfrac{\partial}{\partial\tilde{y}}, \tilde{x}\,\tfrac{\partial}{\partial\tilde{x}} + \tilde{y}\,\tfrac{\partial}{\partial\tilde{y}}\big] = 0. \tag{66}$$

Expression (64) is a purely local formula that allows us to compute the PRF associated to a strong focus in terms of known information in a small neighborhood of the focus that depends on the domain of definition of $\psi(\mathbf{x})$. In order to extend this definition to a broader region, the following theorem provides an **adjoint equation for the PRF** analogous to (25) that we can solve backwards in time to get the PRF in distant points from the strong focus. The proof we present for such result is based on the scheme of the proof of Theorem 2.11 by Guillamon and Huguet in [19].

Theorem 3.16 (Adjoint equation for the PRF of a strong focus)**.** *Given a planar analytic vector field $\mathcal{X}$ as in (28) with a strong focus at the origin and a neighborhood $\mathcal{U}$ of the origin where formula (64) holds true, the gradient $\nabla\vartheta$ satisfies the following Cauchy problem along the orbits of $\mathcal{X}$ through any $\mathbf{x}\in\mathcal{U}$,*

$$\begin{cases} \frac{d}{dt}\nabla\vartheta\big(\phi_t(\mathbf{x})\big) = -D\mathcal{X}\big(\phi_t(\mathbf{x})\big)^T\,\nabla\vartheta\big(\phi_t(\mathbf{x})\big), \\ \nabla\vartheta\big(\phi_0(\mathbf{x})\big) = \beta\,\frac{\mathcal{Y}^\perp(\phi_0(\mathbf{x}))}{\mathcal{Y}^\perp(\phi_0(\mathbf{x}))^T\cdot\mathcal{X}(\phi_0(\mathbf{x}))}. \end{cases} \tag{67}$$

Proof. Along this proof, we will denote $\mathbf{x}_t = \phi_t(\mathbf{x})$ and write $\mathcal{Y}^\perp(\mathbf{x}) = J\mathcal{Y}(\mathbf{x})$, with

$$J = \begin{pmatrix} 0 & -1 \\ 1 & 0 \end{pmatrix}. \tag{68}$$

Thus, given $\mathbf{x}=\mathbf{x}_0\in\mathcal{U}$, from expression (64), we have

$$\nabla\vartheta(\mathbf{x}_t) = \beta\,\frac{J\mathcal{Y}(\mathbf{x}_t)}{\mathcal{Y}^\perp(\mathbf{x}_t)^T\cdot\mathcal{X}(\mathbf{x}_t)}, \tag{69}$$

for all $t>0$, and so, taking time derivatives in (69), we are led to

$$\begin{aligned} \frac{d}{dt}\nabla\vartheta(\mathbf{x}_t) =& \beta\,\frac{J\,D\mathcal{Y}(\mathbf{x}_t)\mathcal{X}(\mathbf{x}_t)}{\mathcal{Y}^\perp(\mathbf{x}_t)^T\cdot\mathcal{X}(\mathbf{x}_t)} \\ & - \beta\,\frac{J\mathcal{Y}(\mathbf{x}_t)\Big((J\,D\mathcal{Y}(\mathbf{x}_t)\mathcal{X}(\mathbf{x}_t))^T\cdot\mathcal{X}(\mathbf{x}_t) + (J\mathcal{Y}(\mathbf{x}_t))^T\cdot D\mathcal{X}(\mathbf{x}_t)\mathcal{X}(\mathbf{x}_t)\Big)}{\big(\mathcal{Y}^\perp(\mathbf{x}_t)^T\cdot\mathcal{X}(\mathbf{x}_t)\big)^2}. \end{aligned} \tag{70}$$

Now, we use the Lie-commutation of vector fields $\mathcal{X}$ and $\mathcal{Y}$ given in (66) - i.e., $D\mathcal{Y}\,\mathcal{X} = D\mathcal{X}\,\mathcal{Y}$ -, to exchange all the derivatives of $\mathcal{Y}$ in (70) by derivatives of $\mathcal{X}$. Hence, we get

$$\begin{aligned} \frac{d}{dt}\nabla\vartheta(\mathbf{x}_t) =& \underbrace{\beta\,\frac{J\,D\mathcal{X}(\mathbf{x}_t)\mathcal{Y}(\mathbf{x}_t)}{\mathcal{Y}^\perp(\mathbf{x}_t)^T\cdot\mathcal{X}(\mathbf{x}_t)}}_{A} \\ & \underbrace{- \beta\,\frac{J\mathcal{Y}(\mathbf{x}_t)\Big((J\,D\mathcal{X}(\mathbf{x}_t)\mathcal{Y}(\mathbf{x}_t))^T\cdot\mathcal{X}(\mathbf{x}_t) + (J\mathcal{Y}(\mathbf{x}_t))^T\cdot D\mathcal{X}(\mathbf{x}_t)\mathcal{X}(\mathbf{x}_t)\Big)}{\big(\mathcal{Y}^\perp(\mathbf{x}_t)^T\cdot\mathcal{X}(\mathbf{x}_t)\big)^2}}_{B}. \end{aligned} \tag{71}$$

In order to simplify A, we first notice that,

$$J\,D\mathcal{X}(\mathbf{x}_t) + D\mathcal{X}(\mathbf{x}_t)^T J = \tau(\mathbf{x}_t)J, \tag{72}$$

where $\tau(\mathbf{x}_t) = tr(D\mathcal{X}(\mathbf{x}_t))$ represents the trace of $D\mathcal{X}(\mathbf{x}_t)$, and therefore,

$$A = \beta \frac{(\tau(\mathbf{x}_t)Id - D\mathcal{X}(\mathbf{x}_t)^T)J\mathcal{Y}(\mathbf{x}_t)}{\mathcal{Y}^\perp(\mathbf{x}_t)^T \cdot \mathcal{X}(\mathbf{x}_t)} = (\tau(\mathbf{x}_t)Id - D\mathcal{X}(\mathbf{x}_t)^T)\,\nabla\vartheta(\mathbf{x}_t). \tag{73}$$

To simplify B, on the other hand, we first use the immediate relation

$$(J\mathcal{Y}(\mathbf{x}_t))^T \cdot D\mathcal{X}(\mathbf{x}_t)\mathcal{X}(\mathbf{x}_t) = \left(D\mathcal{X}(\mathbf{x}_t)^T J\mathcal{Y}(\mathbf{x}_t)\right)^T \cdot \mathcal{X}(\mathbf{x}_t), \tag{74}$$

and then, expression (72) once again to obtain

$$B = \beta \frac{\tau(\mathbf{x}_t)J\mathcal{Y}(\mathbf{x}_t)\ (\mathcal{Y}^\perp(\mathbf{x}_t)^T \cdot \mathcal{X}(\mathbf{x}_t))}{(\mathcal{Y}^\perp(\mathbf{x}_t)^T \cdot \mathcal{X}(\mathbf{x}_t))^2} = \beta \frac{\tau(\mathbf{x}_t)\,J\mathcal{Y}(\mathbf{x}_t)}{\mathcal{Y}^\perp(\mathbf{x}_t)^T \cdot \mathcal{X}(\mathbf{x}_t)} = \tau(\mathbf{x}_t)\,\nabla\vartheta(\mathbf{x}_t). \tag{75}$$

Thus, plugging (73) and (75) back in (71) and cancelling out the opposite terms, we finally get

$$\frac{d}{dt}\nabla\vartheta(\mathbf{x}_t) = -D\mathcal{X}(\mathbf{x}_t)^T\,\nabla\vartheta(\mathbf{x}_t), \tag{76}$$

as we wanted to proof.

□

With respect to the ARF, the scheme of the explanation is entirely analogous. First, we use Theorem 3.11 together with the definition of the isostables as level sets of ς to write

$$\nabla\varsigma(\mathbf{x}) = D(\mathbf{x})\,\mathcal{Z}^\perp(\mathbf{x}), \tag{77}$$

for all $\mathbf{x}$ in a neighborhood $\mathcal{U}$ of the origin and some normalization constant $D(\mathbf{x}) \in \mathbb{R}$. Then, in order to compute a local expression for $D(\mathbf{x})$, we use the APR-dynamics (53) - in particular, $\dot{\sigma} = \alpha\sigma$ - to evaluate the time derivative of the amplitude function along the orbits of vector field $\mathcal{X}$. Thus, we get

$$\frac{d}{dt}\varsigma(\phi_t(\mathbf{x})) = \nabla\varsigma(\phi_t(\mathbf{x}))^T \cdot \frac{d}{dt}\phi_t(\mathbf{x}) = \nabla\varsigma(\phi_t(\mathbf{x}))^T \cdot \mathcal{X}(\phi_t(\mathbf{x})) = \alpha\sigma, \tag{78}$$

for all $\mathbf{x} \in \mathcal{U}$, and so, plugging (77) in the penultimate term of (78), after some reordering we are lead to

$$D(\mathbf{x}) = \alpha\varsigma(\mathbf{x})\,\frac{1}{\mathcal{Z}^\perp(\mathbf{x})^T \cdot \mathcal{X}(\mathbf{x})}. \tag{79}$$

Finally, substituting (79) back in (77) we are led to the respective local expression for $\nabla\varsigma$ in terms of vector fields $\mathcal{X}$ and $\mathcal{Z}$, namely,

$$\nabla\varsigma(\mathbf{x}) = \alpha\varsigma(\mathbf{x})\,\frac{\mathcal{Z}^\perp(\mathbf{x})}{\mathcal{Z}^\perp(\mathbf{x})^T \cdot \mathcal{X}(\mathbf{x})}. \tag{80}$$

Remark 3.17. Recall from the proof of Theorem 3.11 that vector field $\mathcal{Z}$ is defined as the pushforward $\mathcal{Z} = \psi_*^{-1}\tilde{\mathcal{Z}}$, where ψ is the analytic change of variables from Theorem 3.8 and $\tilde{\mathcal{Z}}$ is the canonical planar linear vector field with a center at the origin given by

$$\tilde{\mathcal{Z}} = -\tilde{y}\,\frac{\partial}{\partial\tilde{x}} + \tilde{x}\,\frac{\partial}{\partial\tilde{y}}. \tag{81}$$

Furthermore, we also know as part of the thesis of Theorem 3.11 that vector fields $\mathcal{X}$ and $\mathcal{Z}$ are, actually, commutators, that is,

$$\big[\mathcal{X},\mathcal{Z}\big] = \psi_*^{-1}\big[\tilde{\mathcal{X}},\tilde{\mathcal{Z}}\big] = \psi_*\big[(\alpha\tilde{x}-\beta\tilde{y})\,\tfrac{\partial}{\partial\tilde{x}} + (\beta\tilde{x}+\alpha\tilde{y})\,\tfrac{\partial}{\partial\tilde{y}}, -\tilde{y}\,\tfrac{\partial}{\partial\tilde{x}} + \tilde{x}\,\tfrac{\partial}{\partial\tilde{y}}\big] = 0. \tag{82}$$

The extension of the ARF to regions far from the domain of accuracy of the local expression (80) is done, like in the previous cases, by means of an **adjoint equation for the ARF** that we can integrate backwards in time starting at points on such region. The proof we present for the following result is done based on the scheme of the proof of Theorem 2.12 by Castejón *et al.* in [6].

Theorem 3.18 (Adjoint equation for the ARF of a strong focus)**.** *Given a planar analytic vector field $\mathcal{X}$ as in (28) with a strong focus at the origin and a neighborhood $\mathcal{U}$ of the origin where formula (80) holds true, the gradient $\nabla\varsigma$ satisfies the following Cauchy problem along the orbits of $\mathcal{X}$ through any $\mathbf{x}\in\mathcal{U}$,*

$$\begin{cases} \frac{d}{dt}\nabla\varsigma\big(\phi_t(\mathbf{x})\big) = \big(\alpha Id - D\mathcal{X}\big(\phi_t(\mathbf{x})\big)^T\big)\,\nabla\varsigma\big(\phi_t(\mathbf{x})\big), \\ \nabla\varsigma\big(\phi_0(\mathbf{x})\big) = \alpha\varsigma(\mathbf{x})\,\frac{\mathcal{Z}^\perp(\phi_0(\mathbf{x}))}{\mathcal{Z}^\perp(\phi_0(\mathbf{x}))^T\cdot\mathcal{X}(\phi_0(\mathbf{x}))}. \end{cases} \tag{83}$$

Proof. As in the case of the PRF, we will denote $\mathbf{x}_t = \phi_t(\mathbf{x})$ and write $\mathcal{Z}^\perp(\mathbf{x}) = J\mathcal{Z}(\mathbf{x})$, with J given by (68). Thus, given any $\mathbf{x}=\mathbf{x}_0\in\mathcal{U}$, we have by (80),

$$\nabla\varsigma(\mathbf{x}_t) = \alpha\varsigma(\mathbf{x}_t)\,\frac{J\mathcal{Z}(\mathbf{x}_t)}{\mathcal{Z}^\perp(\mathbf{x}_t)^T\cdot\mathcal{X}(\mathbf{x}_t)}, \tag{84}$$

for all $t>0$, and so, taking time derivatives in (84), we get

$$\begin{aligned} \frac{d}{dt}\nabla\varsigma(\mathbf{x}_t) =& \alpha\,\frac{d\varsigma}{dt}(\mathbf{x}_t)\,\frac{J\mathcal{Z}(\mathbf{x}_t)}{\mathcal{Z}^\perp(\mathbf{x}_t)^T\cdot\mathcal{X}(\mathbf{x}_t)} + \alpha\varsigma(\mathbf{x}_t)\,\frac{J\,D\mathcal{Z}(\mathbf{x}_t)\mathcal{X}(\mathbf{x}_t)}{\mathcal{Z}^\perp(\mathbf{x}_t)^T\cdot\mathcal{X}(\mathbf{x}_t)} \\ & - \alpha\varsigma(\mathbf{x}_t)\,\frac{J\mathcal{Z}(\mathbf{x}_t)\Big(\big(J\,D\mathcal{Z}(\mathbf{x}_t)\mathcal{X}(\mathbf{x}_t)\big)^T\cdot\mathcal{X}(\mathbf{x}_t) + \big(J\mathcal{Z}(\mathbf{x}_t)\big)^T\cdot D\mathcal{X}(\mathbf{x}_t)\mathcal{X}(\mathbf{x}_t)\Big)}{\big(\mathcal{Z}^\perp(\mathbf{x}_t)^T\cdot\mathcal{X}(\mathbf{x}_t)\big)^2}. \end{aligned} \tag{85}$$

Now, we use the Lie-commutation of vector fields $\mathcal{X}$ and $\mathcal{Z}$ given in (82) - i.e., $D\mathcal{Z}\,\mathcal{X} = D\mathcal{X}\,\mathcal{Z}$ -, to exchange all the derivatives of $\mathcal{Z}$ in (85) by derivatives of $\mathcal{X}$. Hence, we have

$$\begin{aligned} \frac{d}{dt}\nabla\varsigma(\mathbf{x}_t) =& \underbrace{\alpha\,\frac{d\varsigma}{dt}(\mathbf{x}_t)\,\frac{J\mathcal{Z}(\mathbf{x}_t)}{\mathcal{Z}^\perp(\mathbf{x}_t)^T\cdot\mathcal{X}(\mathbf{x}_t)}}_{A} + \underbrace{\alpha\varsigma(\mathbf{x}_t)\,\frac{J\,D\mathcal{X}(\mathbf{x}_t)\mathcal{Z}(\mathbf{x}_t)}{\mathcal{Z}^\perp(\mathbf{x}_t)^T\cdot\mathcal{X}(\mathbf{x}_t)}}_{B} \\ & \underbrace{- \alpha\varsigma(\mathbf{x}_t)\,\frac{J\mathcal{Z}(\mathbf{x}_t)\Big(\big(J\,D\mathcal{X}(\mathbf{x}_t)\mathcal{Z}(\mathbf{x}_t)\big)^T\cdot\mathcal{X}(\mathbf{x}_t) + \big(J\mathcal{Z}(\mathbf{x}_t)\big)^T\cdot D\mathcal{X}(\mathbf{x}_t)\mathcal{X}(\mathbf{x}_t)\Big)}{\big(\mathcal{Z}^\perp(\mathbf{x}_t)^T\cdot\mathcal{X}(\mathbf{x}_t)\big)^2}}_{C}. \end{aligned} \tag{86}$$

The simplification of term A is rather simple. Indeed, using the APR-dynamics (53), we get

$$A = \alpha^2\varsigma(\mathbf{x}_t)\,\frac{J\mathcal{Z}(\mathbf{x}_t)}{\mathcal{Z}^\perp(\mathbf{x}_t)^T\cdot\mathcal{X}(\mathbf{x}_t)} = \alpha\,\nabla\varsigma(\mathbf{x}_t). \tag{87}$$

In order to simplify B, we simply need to recall expression (72) from the proof of Theorem 3.16 and so, we obtain

$$B = \alpha\varsigma(\mathbf{x}_t)\,\frac{\left(\tau(\mathbf{x}_t)Id - D\mathcal{X}(\mathbf{x}_t)^T\right)J\mathcal{Z}(\mathbf{x}_t)}{\mathcal{Z}^{\perp}(\mathbf{x}_t)^T\cdot\mathcal{X}(\mathbf{x}_t)} = \left(\tau(\mathbf{x}_t)Id - D\mathcal{X}(\mathbf{x}_t)^T\right)\nabla\varsigma(\mathbf{x}_t), \tag{88}$$

where $\tau(\mathbf{x}_t) = tr\big(D\mathcal{X}(\mathbf{x}_t)\big)$ denotes the trace of $D\mathcal{X}(\mathbf{x}_t)$.

In the same spirit, to work C out, we use the immediate relation

$$\big(J\mathcal{Z}(\mathbf{x}_t)\big)^T\cdot D\mathcal{X}(\mathbf{x}_t)\mathcal{X}(\mathbf{x}_t) = \big(D\mathcal{X}(\mathbf{x}_t)^T J\mathcal{Z}(\mathbf{x}_t)\big)^T\cdot\mathcal{X}(\mathbf{x}_t), \tag{89}$$

together with (72), and we get

$$C = \alpha\varsigma(\mathbf{x}_t)\,\frac{\tau(\mathbf{x}_t)J\mathcal{Z}(\mathbf{x}_t)\big(J\mathcal{Z}(\mathbf{x}_t)^T\cdot\mathcal{X}(\mathbf{x}_t)\big)^2}{\big(\mathcal{Z}^{\perp}(\mathbf{x}_t)^T\cdot\mathcal{X}(\mathbf{x})\big)^2} = \alpha\varsigma(\mathbf{x}_t)\,\frac{\tau(\mathbf{x}_t)\,J\mathcal{Z}(\mathbf{x}_t)}{\mathcal{Z}^{\perp}(\mathbf{x}_t)^T\cdot\mathcal{X}(\mathbf{x})} = \tau(\mathbf{x}_t)\,\nabla\varsigma(\mathbf{x}_t). \tag{90}$$

Finally, plugging (87), (88) and (90) in (86) and cancelling out the opposite terms, we are led to

$$\frac{d}{dt}\nabla\varsigma(\mathbf{x}_t) = \left(\alpha\,Id - D\mathcal{X}(\mathbf{x}_t)^T\right)\nabla\varsigma(\mathbf{x}_t), \tag{91}$$

as we wanted to proof.

□

3.3 APR-based optimal control over damped oscillations

In this subsection we are going to present an optimal control algorithm based on the APR formalism that we have developed so far with the objective of inducing a periodic oscillation around a strong focus. In this sense, imagine that we start at a point $\mathbf{x}$ near a strong focus on a planar analytic vector field $\mathcal{X}$. Without any external control input, the trajectory of $\mathbf{x}$, in accordance with (53), will spiralize around the strong focus as its amplitude continously decreases. Thus, the purpose of our algorithm is to devise a control input $U(t,\mathbf{x})$ that forces the trajectory of $\mathbf{x}$ to follow a periodic orbit $\gamma(t)$ around the focus and get back to $\mathbf{x}$ after a given period $T_1\in\mathbb{R}$. What is more, this periodic orbit should be achieved using a minimum energy input and staying close to a fixed amplitude σ_1 that shall correspond to the mean amplitude of the induced orbit. An scheme of this situation is portrayed in Figure 2.

For the purposes of this study, motivated by the application of these techniques to the realm of mathematical neuroscience, we will assume that the external control input that we are searching for is of the form $U(t) = \big(u(t),0\big)^T$, with no dependence on $\mathbf{x}$ and a fixed direction along the x-axis. Hence, the APR-dynamics describing the evolution of the controlled system can be approximated by

$$\begin{cases} \dot{\theta} &= \beta + \mathrm{PRF}_x(\theta,\sigma)\,u(t), \\ \dot{\sigma} &= \alpha\sigma + \mathrm{ARF}_x(\theta,\sigma)\,u(t), \end{cases} \tag{92}$$

where PRF_x and ARF_x stand, respectively, for the phase and amplitude response curves to stimuli in the direction of the x-axis. In the following, as no room for confusion is left, we will do away with this subscript

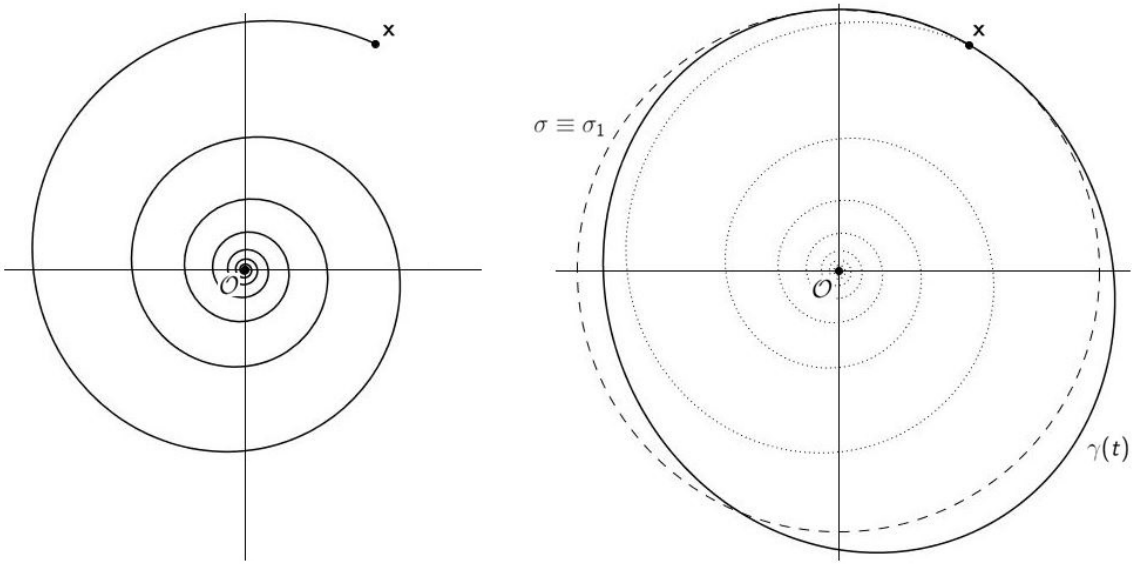

Figure 2: Scheme of the pretended action of the control algorithm. On the left, the uncontrolled orbits spiralizes towards $\mathcal{O}$. On the right, the induced periodic orbit gets back to $\mathbf{x}$ in time $t = T_1$.

notation and write them as PRF and ARF.

Without loss of generality, we shall assume that our initial condition is a zero-phase point, that is, $\mathbf{x} = L^{-1}(0, \sigma_1)$ - if not, a mere translation of the APR-variables moves it there. Thus, our control strategy consists in finding, among all the possible stimuli $U(t)$ which produce on system (92) a periodic orbit satisfying the boundary conditions

$$\theta(0) = 0, \quad \theta(T_1) = 2\pi, \quad \sigma(0) = \sigma_1, \text{ and } \sigma(T_1) = \sigma_1, \tag{93}$$

the one which minimizes the **cost function**,

$$\mathcal{G}[u] = \int_0^{T_1} \Big(p_1 u(t)^2 + p_2(\sigma - \sigma_1)^2 + \lambda_1\big(\dot\theta - \beta - \mathrm{PRF}(\theta,\sigma)u(t)\big) + \lambda_2\big(\dot\sigma - \alpha\sigma - \mathrm{ARF}(\theta,\sigma)u(t)\big)\Big)\, dt. \tag{94}$$

The first term in $\mathcal{G}[u]$ accounts for our requirement that the control stimulus $U(t)$ uses a minimum energy input. The second term ensures that the amplitude of the resulting periodic orbit is at any time close to σ_1 for if it got too far away, the validity of the APR-dynamics (92) may be compromised. In this sense, coefficients $p_1, p_2 \geq 0$ avail us the possibility of weighting energy minimization and amplitude minimization differently depending on their relative importance for the problem at issue. Finally, the last two terms in (94) secure that the dynamics of $\theta(t)$ and $\sigma(t)$ obey equations (92), being $\lambda_1 = \lambda_1(t)$ and $\lambda_2 = \lambda_2(t)$ the respective two Lagrange multipliers associated to such restrictions.

Written in those terms, our search for the optimal control input $U(t)$ constitutes a variational problem whose **Lagrangian** $\mathcal{L} = \mathcal{L}(\theta, \dot\theta, \sigma, \dot\sigma, \lambda_1, \lambda_2, u)$ is given by the integrand of the cost function (94), that is,

$$\mathcal{L} = p_1 u^2 + p_2(\sigma - \sigma_1)^2 + \lambda_1\big(\dot\theta - \beta - \mathrm{PRF}(\theta,\sigma)u\big) + \lambda_2\big(\dot\sigma - \alpha\sigma - \mathrm{ARF}(\theta,\sigma)u\big). \tag{95}$$

Therefore, the **Euler-Lagrange equations** associated to such variational problem [13, 16],

$$\frac{\partial}{\partial q}\mathcal{L} = \frac{d}{dt}\left(\frac{\partial}{\partial \dot{q}}\mathcal{L}\right), \qquad \text{with } q = \lambda_1,\ \lambda_2,\ \theta,\ \sigma \text{ and } u, \tag{96}$$

yield the following system of ODEs,

$$\begin{cases} \dot{\theta} &= \beta + \mathrm{PRF}(\theta,\sigma)\, u(t), \\ \dot{\sigma} &= \alpha\sigma + \mathrm{ARF}(\theta,\sigma)\, u(t), \\ \dot{\lambda}_1 &= -u(t)\big(\lambda_1 \frac{\partial}{\partial\theta}\mathrm{PRF}(\theta,\sigma) + \lambda_2 \frac{\partial}{\partial\theta}\mathrm{ARF}(\theta,\sigma)\big), \\ \dot{\lambda}_2 &= 2p_2(\sigma-\sigma_1) - \alpha\lambda_2 - u(t)\big(\lambda_1 \frac{\partial}{\partial\sigma}\mathrm{PRF}(\theta,\sigma) + \lambda_2 \frac{\partial}{\partial\sigma}\mathrm{ARF}(\theta,\sigma)\big), \end{cases} \tag{97}$$

together with the expression

$$u(t) = \frac{\lambda_1(t)\mathrm{PRF}(\theta,\sigma) + \lambda_2(t)\mathrm{ARF}(\theta,\sigma)}{2p_1}, \tag{98}$$

for the control input that we are searching for. System (97) shall be solved as a two point boundary value problem with boundary conditions given by (93) and then, plugging the respective solution into (98), obtain the full shape of the control input $u(t)$. In these sense, the first of this conditions makes sure that the period of the induced orbit is T_1, while the second one ensures that it is, actually, a closed orbit.

Once we have computed a proper input $U(t)$, it can be applied to the full system $\dot{\mathbf{x}} = \mathcal{X}(\mathbf{x}) + U(t)$ in order to get the desired periodic orbit $\gamma(t)$ around the strong focus at the origin. At this point, it is important to bear in mind two different quantities that help us measure the performance of our control input. On one hand, we can compute the **total energy** consumed by the external input as

$$E = \int_0^{T_1} u(t)^2 dt, \tag{99}$$

with $u(t)$ given by (98). On the other hand, as suggested in [24, 25], we can define the **control error** as the normalized distance between the final an initial positions of the induced orbit after one period, that is,

$$\epsilon = \frac{||\gamma(T_1) - \gamma(0)||}{\max\left(||\gamma(t)||\right)}, \tag{100}$$

where $||\cdot||$ represents the standard Euclidean norm on the plane and $\max\left(||\gamma(t)||\right)$ stands, consequently, for the maximum distance from any point of the induced orbit to the strong focus. In a perfect situation, this control error shall be zero since we are forcing the induced orbit to close up after a period in (93). Nonetheless, we must take into account that $U(t)$ is computed according to the reduced APR-system (92), not the full original system, and so, ϵ constitutes a good measure of the total amount of numerical errors assumed along the resolution of the problem.

4. Methodology and implementation

In this section we are going to present a brief scheme of the different steps that a numerical implementation of the previous ideas needs to follow in order to apply the techniques presented in Section 3 to different

systems characterized by the existence strong linear foci and damped oscillations. This summary will be supplemented in the hereunder subsections with detailed information about all such methodology that, in opinion of the author, deserve detailed explanations. All the algorithms used in this work are implemented using the MATLAB R2020a software [1][1].

The first step in our computations is the numerical implementation of the local diffeomorphism $\varphi(x, y)$ from Theorem 3.8. It is worth noting that the proof of this result - see [26] for further detail - relies on the composition of three different changes of variables, being the last of them a normal form transformation that can only be numerically reproduced up to a finite order. As a consequence of the **invariance error** derived from the discordances between the numerically attainable change of variables, $\tilde{\mathbf{x}} = \hat{\varphi}(\mathbf{x})$, and the analytical one predicted by the theory, $\tilde{\mathbf{x}} = \varphi(\mathbf{x})$, the range of validity of the explicit formulas derived from $L(x, y)$ is confined to a small **fundamental domain** around the strong focus where such error is bounded. These features will be treated in Subsection 4.1 below.

Thus, we can compute numerical approximations for the isochrons, isostables and phase-amplitude response functions associated to the strong focus within the fundamental domain by making use of the explicit formulas developed for such purpose along Section 3 on the phase-amplitude plane and then translate them back to the original phase space via the approximate diffeomorphism $\hat{\varphi}(x, y)$. Afterwards, integration of the system's equations backwards in time together with the two adjoint equations (67) and (83) allows us to extend these numerical expressions to a wider region. A systematic method to perform the extension of isochrons, isostables and phase-amplitude response functions in such a way that the resulting data are suitable for further operations is explained in Subsection 4.2.

Next, once we know information about the PRF and ARF associated to the strong focus in a sufficiently wide region of the plane, we are in position of carrying out the resolution of the Euler-Lagrange equations. As we know, system (97) shall be solved as a two point boundary problem satisfying boundary conditions of the form (93). Our choice for the resolution of such system is a **shooting method** based on a Newton-Raphson iteration that, given a proper initial, guess converges to an orbit matching the imposed requirements on its both edges. A general explanation of shooting methods followed by the particular method used in our case are included in Subsection 4.3 hereunder.

Finally, Subsection 4.4 regarding classical **parametric continuation methods** is included at the end of the current section. This ubiquitous techniques play a role of great significance in the realm of computational methods for dynamical systems as they are the basic tools behind the numerical computation of bifurcation diagrams. In our work, parametric continuation finds another application of great importance as it can be used to do exhaustive analysis of the performance of the control algorithm for a wide range of different values of crucial parameters of the problem. Moreover, strategies based on parametric continuation were found to be rather successful when looking for solutions of the Euler-Lagrange equations in cases for which a good initial guess for the shooting method is troublesome. Parametric continuation enables us to trace back accurate initial guesses from cases for which the convergence of the method is easier.

[1] All codes are available at: https://web.mat.upc.edu/antoni.guillamon/Code/OptimalControlDampedOscillations .

4.1 Invariance error and fundamental domain

As we have already commented, diffeomorphism $\varphi(x, y)$ in Theorem 3.8 is build by the composition of three different changes of variables. The first one is just the technical translation of the fixed point to the origin that we assumed without loss of generality at the beginning of Section 3; the second one is a Jordan transformation that takes the linear part of vector field $\mathcal{X}$ to its canonical Jordan form (28); and, finally, a normal form transformation that gets rid of the higher order terms in vector field $\mathcal{X}$. This means that, apart from certain academic examples for which an explicit analytical expression for $\varphi(x, y)$ is known, we will have to work with an approximate $\hat{\varphi}(x, y)$ that reproduces its intrinsic normal form transformation up to a given finite order and, in turn, an approximate conjugation $\hat{L}(x, y) = \rho \circ \hat{\varphi}(x, y)$.

Definition 4.1 (Invariance error)**.** Given a planar analytic vector field $\mathcal{X}$ in the conditions of (28) with a strong focus at the origin and a numerical approximation $(\theta, \sigma) = \hat{L}(x, y)$ to the analytic APR-conjugation $(\theta, \sigma) = L(x, y)$, we define the **invariance error** as the discrepancy emerging in the invariance equation (37) when considering $\hat{L}(x, y)$ instead of $L(x, y)$, that is,

$$\epsilon_{inv}(\theta, \sigma) = ||\hat{L}_*^{-1}((\beta \frac{\partial}{\partial \theta} + \alpha\sigma \frac{\partial}{\partial \sigma})(\theta, \sigma)) - \mathcal{X}(\hat{L}^{-1}(\theta, \sigma))||, \tag{101}$$

for every pair $(\theta, \sigma) \in [0, 2\pi) \times \mathbb{R}^+$ and being $|| \cdot ||$ is the usual Euclidean norm on the plane $\mathbb{R}^2$.

Clearly, a correct analysis and handling of this invariance error is a crucial task in the treatment of our numerical implementation. For that purpose, we will introduce the so-called **fundamental domain** $\mathcal{U}_{fd}$ as the biggest open set containing the strong focus for which the invariance error is smaller than a given tolerance - in our computations, $tol = 10^{-9}$. Inside the fundamental domain we will accept that $\hat{L}(x, y) \equiv L(x, y)$ and, therefore, all the several formulas derived along Section 3 that make explicit use of $L(x, y)$ will be assumed to hold true therein. Hence, the fundamental domain can be written as

$$\mathcal{U}_{fd} = \hat{L}(\theta, \sigma), \qquad \text{for all } \theta \in [0, 2\pi) \text{ and all } \sigma < \sigma_{fd}, \tag{102}$$

where the **radius of the fundamental domain** $\sigma_{fd} = \sigma_{fd}(tol)$ is given by

$$\sigma_{fd} = \sup \left\{ \sigma \in \mathbb{R}^+ \,|\, \epsilon_{inv}(\theta, \sigma) < tol, \text{ for all } \theta \in [0, 2\pi) \right\}. \tag{103}$$

In practice, the radius of the fundamental domain, and, in turn, the fundamental domain itself, is determined by sequentially evaluating the invariance error (101) along isostables of increasing amplitude until it eventualy matches the tolerance of the problem. The amplitude associated to that latter isostable is the radius of the fundamental domain. The MATLAB handle functions employed along this paper for the numerical computations of approxiamtion $\hat{\varphi}(x, y)$ and the corresponding fundamental domain are borrowed from the work by Moreno in [26] and reproduced with his permission.

4.2 Isochron and isostable computation and PRF/ARF extension

One of the core computations that we need to be performed in the computational part of this work is that of the isochrons, isostables and phase-amplitude response functions. Indeed, this step of crucial importance

is the basis for a correct performance of the control strategy designed at the end of Section 3. In particular, an accurate resolution of the Euler-Lagrange equations requires an exhaustive computation of the PRF and ARF on a fine grid along a rather wide region around the strong focus at issue.

Computations of the isochrons, isostables and phase-amplitude response curves begins within the fundamental domain. Remember that inside the fundamental domain we are assuming that $\hat{L}(x,y) \equiv L(x,y)$ and so, that the main explicit formulas derived in Section 3 still hold true when applied using the approximate conjugation. Thus, by definition of isochron, and in accordance with expression (102), it is easy to see that a parameterization of the isochrons of the strong focus within the fundamental domain in terms of the amplitude variable σ is given by the map,

$$\hat{L}^{-1}(\theta_0,\cdot) : \sigma \in (0,\sigma_{fd}) \subset \mathbb{R}^+ \to \hat{L}^{-1}(\theta_0,\sigma) \in \mathcal{U}_{fd} \subset \mathbb{R}^2, \tag{104}$$

for each $\theta_0 \in [0,2\pi)$. Converseley, a parameterization of the isochrons of the strong focus within the fundamental domain in terms of the asymptotic phase θ is given by

$$\hat{L}^{-1}(\cdot,\sigma_0) : \theta \in [0,2\pi) \to \hat{L}^{-1}(\theta,\sigma_0) \in \mathcal{U}_{fd} \subset \mathbb{R}^2, \tag{105}$$

for each amplitude $0 < \sigma < \sigma_{fd}$. Notice that this two parameterizations are equivalent to the ones given in Remarks 2.4 and 2.6 for the isochrons and isostables associated to an isochronous limit cycle.

According to the phase-amplitude response function, they both can be evaluated on the same points within the fundamental domain where isochrons and isostables were already computed by means of the local formulas (64) and (80), respectively. Recall that vector fields $\mathcal{Y}$ and $\mathcal{Z}$ shall be computed as the pushforward of the linear vector fields $\tilde{\mathcal{Y}}$ in (65) and $\tilde{\mathcal{Z}}$ in (81).

Once we have information about the isochrons, isostables and phase-amplitude functions of the problem computed inside the fundamental domain, we are in position of extending it to a wider domain $\mathcal{U} \supset \mathcal{U}_{fd}$. This globalization is of great importance for future computations because of two main reasons: on one hand, we must bear in mind that the strong focus is an actual singularity of the dynamics and so, one can easily foresee computational complications on the closest neighborhoods - in particular, as we will see in Section 5, PRFs will generically have a singularity when σ goes to 0 -; on the other hand, the shooting strategy chosen for the subsequent resolution of the Euler-Lagrange equations requires a wide region of action in other to test different candidates to optimal orbit in sequencial iterations without any of them going beyond the limits of our knowledge about the phase-amplitude response functions.

The extension of isochrons, isostables and phase-response functions is an easy task in itself. Isochrons and isostables are globalized by integrating the equations of the system backwards in time up to a given point in $\mathcal{U} \setminus \mathcal{U}_{fd}$, the PRF and ARF by integrating the adjoint equations (67) and (83) backwards in time up to the same point in $\mathcal{U} \setminus \mathcal{U}_{fd}$. In our case, all these computations are done using the classical MATLAB ODE-solver *ode45* with default absolute and relative tolerances of 10^{-13}.

The more intricate question about this globalization of information from the fundamental domain outwards is the choice of the correct initial conditions that yield a suitable display of the final data that we can harness for subsequent computations. In our case, this next operation is a 2D interpolation performed using the MATLAB interpolator *griddedInterpolant* for which an array of data along a $N \times M$ grid is required. This means that along each extended isochron, for instance, we need to recover the same amount

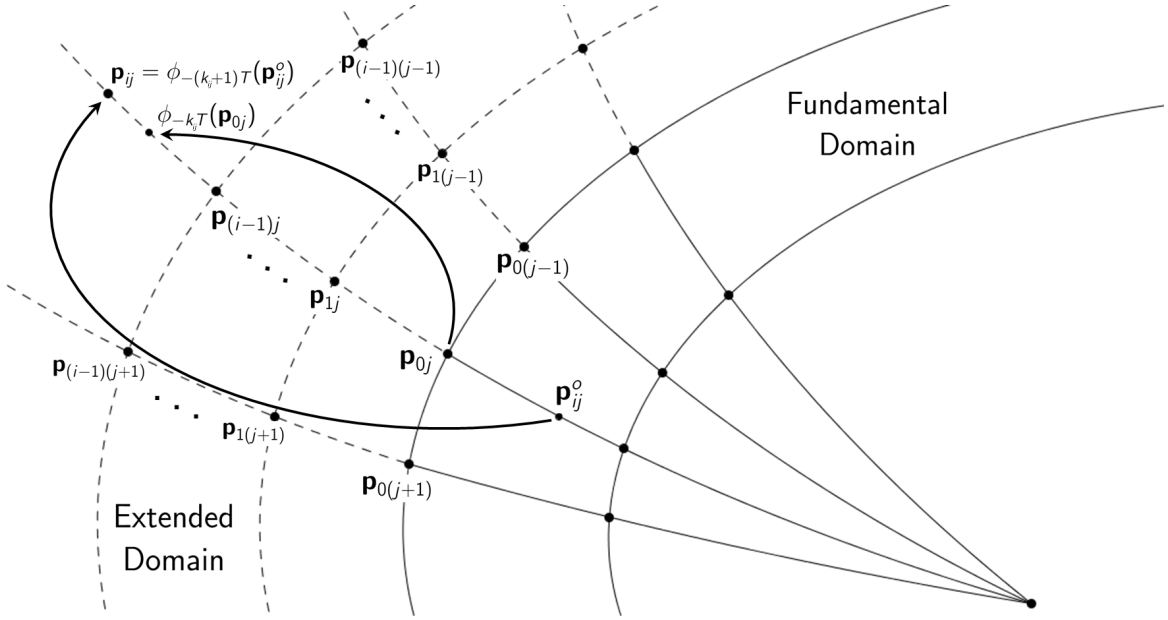

Figure 3: Scheme of the globalization method employed to extend information outside the fundamental domain. First, integer k_{ij} in (106) is computed by taking $\mathbf{p}_{0j}$ as close as possible to $\mathbf{p}_{ij}$ without exceeding it. Then, extension is completed by integrating backwards in time from $\mathbf{p}^o_{ij} \in \mathcal{U}_{fd}$ for a time $-(k+1)T$.

of extended points. Our method to overcome this difficulty is explained in the following.

Imagine we have computed a grid of $N_{fd} \times M_{fd}$ of points on the isochrons and isostables associated to the strong focus at issue within a fundamental domain of radius σ_{fd} such that the last row of data corresponds to the isostable $\Sigma_{\sigma_{fd}}$, and we want to extend them to a $N_{ex} \times M_{ex}$ grid out of the fundamental domain up to a maximum amplitude σ_{max}. The first step is to perform a 2D interpolation of the known data so that we have information about isochrons, isostables and phase-amplitude response functions for any point in $\mathcal{U}_{fd}$ within some assumable error margins. Afterwards, for each $i \in \{1, \dots, N_{ex}\}$ and each $j \in \{1, \dots, M_{ex}\}$, we compute the number k_{ij} of iterations of the inverse time-T map required to get as close as possible to the point $\mathbf{p}_{ij} = L^{-1}(j\Delta\theta, \sigma_{fd} + i\Delta\sigma)$, without exceeding it, from the point $\mathbf{p}_{0j} = \hat{L}^{-1}(\theta_0, \sigma_{fd}) \in \mathcal{U}_{fd}$ as

$$k_{ij} = \left\lfloor \frac{-1}{\alpha T} \log\left(1 + \frac{i\Delta\sigma}{\sigma_{fd}}\right) \right\rfloor, \tag{106}$$

where $\Delta\theta = \frac{2\pi}{M_{ex}}$, $\Delta\sigma = \frac{\sigma_{max} - \sigma_{fd}}{N_{ex}}$ and $\lfloor \cdot \rfloor$ denotes the integer part plus 1 of the real number inside. Then, we would only need to consider

$$\sigma^o_{ij} = (\sigma_{fd} + \Delta\sigma)\, e^{(k+1)\alpha T} < \sigma_{fd}, \tag{107}$$

as the initial point of a backwards integration up to time $-(k+1)T$ in order to get all the information in $\mathbf{p}^o_{ij} = \hat{L}(j\Delta\theta, \sigma^o_{fd}) \in \mathcal{U}_{fd}$ extended to the point $\mathbf{p}_{ij} = L^{-1}(j\Delta\theta, \sigma_{fd} + i\Delta\sigma) \notin \mathcal{U}_{fd}$. In the end, this method yields an extension of the information on the original $N_{fd} \times M_{fd}$ grid of points in the fundamental domain to the points on a $N_{ex} \times M_{ex}$ grid outside it that we can interpolate to get information about isochrons, isostables and the phase-amplitude response functions in a neighborhood $\mathcal{U} \supset \mathcal{U}_{fd}$ of the strong focus at issue. Figure 3 portrays a simple and visual scheme of the ideas behind this methodology.

4.3 Shooting method for a two point boundary problem

Another of the key steps in the correct performance of our control strategy is the resolution of the Euler-Lagrange equations (97) associated to the variational problem of inducing a periodic orbit around the strong focus with a minimum-energy input. As we know, these equations shall be solved as a two point boundary problem satisfying the boundary conditions given in (93) and so, this subsection is devoted to the **shooting methods** usually employed to solve them. First, we will give a brief description of a general shooting method and afterwards we will move into our particular problem in hand.

Let us consider an n-dimensional ODE system given by

$$\dot{\mathbf{y}} = \mathcal{F}(t, \mathbf{y}), \qquad \text{with } \mathbf{y} \in \mathbb{R}^n \text{ and } t \in [0, a], \tag{108}$$

for some analytical vector field $\mathcal{F}$ in $\mathbb{R}^n$ and some integration time $a > 0$, subject to the linear boundary conditions given by

$$B_0\, \mathbf{y}(0) + B_a\, \mathbf{y}(a) = \mathbf{b}, \tag{109}$$

where $B_0, B_a \in \mathcal{M}_{n\times n}(\mathbb{R})$, $\mathbf{b} \in \mathbb{R}^n$ and $\mathbf{y}(a)$ represents the solution to system (108) starting at $\mathbf{c} = \mathbf{y}(0)$ after a time $a > 0$. In order to solve such problem, we integrate system (108) for some initial condition $\mathbf{c} \in \mathbb{R}^n$ and use the corresponding solution $\mathbf{y}(t)$ to evaluate the **shooting function**,

$$g : \mathbf{c} \in \mathbb{R}^n \to g(\mathbf{c}) \in \mathbb{R}^n, \tag{110}$$

given by

$$g(\mathbf{c}) = B_0\, \mathbf{c} + B_a\, \mathbf{y}(a) - \mathbf{b}. \tag{111}$$

If $\mathbf{c}$ is a correct initial guess; then, $g(\mathbf{c}) = \mathbf{0}$ and we would have found an orbit of system (108) fulfilling the boundary conditions in (109) as we wanted to. If $\mathbf{c}$ is not a correct initial guess; then, $g(\mathbf{c}) \neq \mathbf{0}$ can be used to refine the initial condition for a subsequent computation by means of a **Newton-Raphson iteration** as long as the Jacobian of the shooting function $J_g(\mathbf{c})$ is non-singular. Thus, given $\mathbf{c}^m$ the initial guess for the m-th iteration of our shooting method and $g(\mathbf{c}^m)$ its corresponding value for the shooting function, we will choose the initial condition for the following iterate of the method to be

$$\mathbf{c}^{(m+1)} = \mathbf{c}^m - J_g(\mathbf{c}^m)^{-1}\, g(\mathbf{c}), \tag{112}$$

where, for each $i \in \{1, \dots, n\}$, the i-th column of the Jacobian of the shooting function g, $J_g^{(i)}(\mathbf{c})$, is numerically computed as the divided difference

$$J_g^{(i)}(\mathbf{c}) = \frac{g^+(\mathbf{c}) - g^-(\mathbf{c})}{2\delta}, \tag{113}$$

with

$$g^+(\mathbf{c}) = g(\mathbf{c}^m + \delta \mathbf{e}_i) \quad \text{and} \quad g^-(\mathbf{c}) = g(\mathbf{c}^m - \delta \mathbf{e}_i), \tag{114}$$

for some small $\delta > 0$ and being $\mathbf{e}_i \in \mathbb{R}^n$ the column vector with a 1 at the i-th position and 0s elsewhere.

Now, let us move onto the particular problem of solving the Euler-Lagrange equations (97) in our control algorithm as a two point boundary problem satisfying conditions (93). First, note that we can rewrite such conditions, namely, $\theta(0) = 0$, $\theta(T) = 2\pi$, $\sigma(0) = \sigma_0$ and $\sigma(T) = \sigma_0$, in the form of (109) as

$$\underbrace{\begin{pmatrix} 1 & 0 & 0 & 0 \\ 0 & 1 & 0 & 0 \\ 0 & 0 & 0 & 0 \\ 0 & 0 & 0 & 0 \end{pmatrix}}_{B_T \in \mathcal{M}_{4\times 4}(\mathbb{R})} \underbrace{\begin{pmatrix} \theta(0) \\ \sigma(0) \\ \lambda_1(0) \\ \lambda_2(0) \end{pmatrix}}_{\mathbf{c}\in\mathbb{R}^4} + \underbrace{\begin{pmatrix} 0 & 0 & 0 & 0 \\ 0 & 0 & 0 & 0 \\ 1 & 0 & 0 & 0 \\ 0 & 1 & 0 & 0 \end{pmatrix}}_{B_T \in \mathcal{M}_{4\times 4}(\mathbb{R})} \underbrace{\begin{pmatrix} \theta(T) \\ \sigma(T) \\ \lambda_1(T) \\ \lambda_2(T) \end{pmatrix}}_{\mathbf{y}(T)\in\mathbb{R}^4} = \underbrace{\begin{pmatrix} 0 \\ \sigma_0 \\ 2\pi \\ \sigma_0 \end{pmatrix}}_{\mathbf{b}\in\mathbb{R}^4}, \tag{115}$$

with time $a = T$, and, therefore, the shooting function associated to this prticular problem reads

$$g(\mathbf{c}) = \begin{pmatrix} 1 & 0 & 0 & 0 \\ 0 & 1 & 0 & 0 \\ 0 & 0 & 0 & 0 \\ 0 & 0 & 0 & 0 \end{pmatrix} \begin{pmatrix} \theta(0) \\ \sigma(0) \\ \lambda_1(0) \\ \lambda_2(0) \end{pmatrix} + \begin{pmatrix} 0 & 0 & 0 & 0 \\ 0 & 0 & 0 & 0 \\ 1 & 0 & 0 & 0 \\ 0 & 1 & 0 & 0 \end{pmatrix} \begin{pmatrix} \theta(T) \\ \sigma(T) \\ \lambda_1(T) \\ \lambda_2(T) \end{pmatrix} - \begin{pmatrix} 0 \\ \sigma_0 \\ 2\pi \\ \sigma_0 \end{pmatrix}. \tag{116}$$

Nonetheless, since the values of $\theta(0)$ and $\sigma(0)$ are already fixed by the boundary conditions, the value of function $g(\mathbf{c})$ is only influenced by our initial choice of the Lagrange multipliers $\lambda_1(0)$ and $\lambda_2(0)$. Hence, we can reduce the dimensions of the problem by considering $\hat{\mathbf{c}} = (\lambda_1(0), \lambda_2(0)) \in \mathbb{R}^2$ so that the new shooting function of the method at the m-th iteration is

$$\hat{g}(\hat{\mathbf{c}}^m) = \begin{pmatrix} \theta(T) - 2\pi \\ \sigma(T) - \sigma_0 \end{pmatrix}, \tag{117}$$

and its Jacobian matrix,

$$J_g(\hat{\mathbf{c}}) = \begin{pmatrix} \dfrac{\partial\theta}{\partial\mathbf{c}_1} & \dfrac{\partial\theta}{\partial\mathbf{c}_2} \\ \dfrac{\partial\sigma}{\partial\mathbf{c}_1} & \dfrac{\partial\sigma}{\partial\mathbf{c}_2} \end{pmatrix}, \tag{118}$$

where we are denoting $\mathbf{c}_1 = \lambda_1(0)$ and $\mathbf{c}_2 = \lambda_2(0)$. All the intermediate ODE integration required for the resolution of this shooting method is performed, as in the previous subsection, using the MATLAB ODE integrator *ode45* with absolute and relative tolerances of 10^{-13}. Also, it is worth recalling for practical applications of this strategy that the convergence of the Newton-Raphson iteration will be compromised whenever the determinant of the Jacobian matrix (118) gets too close to 0.

4.4 Parametric continuation methods

In this subsection we will give a brief description of some classical **parametric continuation methods** that we have explicitly used along the buildout of the several algorithms required for the practical implementation of the theoretical results presented in Section 3. Numerical continuation is a key methodology with ubiquitous applications in many fields of mathematics and, particularly, in Dynamical Systems where it serves as a fundamental tool in bifurcation analysis. In our case, however, numerical continuation also proofs to be very useful for the testing of the performance of our control strategy for different values of the parameters of a model as well as a good strategy for finding the correct initial guess for the shooting

method we previously described in those cases in which its convergence may be compromised.

Generally speaking, parametric continuation methods pretend to give approximate solutions for a system of non-linear equation depending on one or more parameters starting from a solution known for some value of the parameters. Thus, let us consider a non-linear system of equations of the form

$$G(\mathbf{u}, \boldsymbol{\lambda}) = 0, \quad \mathbf{u} \in \mathbb{R}^n, \tag{119}$$

where $\boldsymbol{\lambda} \in \mathbb{R}^m$ is a set of parameters and $G : \mathbb{R}^n \times \mathbb{R}^k \to \mathbb{R}^n$ is a smooth function, and imagine that we know a tuple $(\mathbf{u}_0, \boldsymbol{\lambda}_0)$ for which $G(\mathbf{u}_0, \lambda_0) = 0$; then, the objective of a parametric continuation method is to find a curve $\Gamma(\boldsymbol{\lambda}) = (\mathbf{u}(\boldsymbol{\lambda}), \boldsymbol{\lambda}) \in \mathbb{R}^n \times \mathbb{R}^k$ such that $G(\mathbf{u}(\boldsymbol{\lambda}), \boldsymbol{\lambda}) = 0$ for all $\lambda \in \Omega$, for some $\Omega \subset \mathbb{R}^k$ open and connected. For the sake of simplicity, along our explanation we will assume $k = 1$, that is, $\lambda \in \mathbb{R}$ and $\Omega = \mathcal{I} \subset \mathbb{R}$ an open interval. Further details on continuation methods can be found in [7, 21, 30].

Definition 4.2 (Regular and singular solutions)**.** Given $G : \mathbb{R}^n \times \mathbb{R} \to \mathbb{R}^n$ a smooth function, we say that a solution $(\mathbf{u}, \lambda) \in \mathbb{R}^n \times \mathbb{R}$ is a **regular solution** of the non-linear system $G(\mathbf{u}, \lambda) = 0$ if and only if $J_G(\mathbf{u}, \lambda)$ has maximal rank, that is, $Rank(J_G(\mathbf{u}, \lambda)) = n$. Conversely, we will say that $(\mathbf{u}, \lambda)$ is a **singular solution** of the system if $Rank(J_G(\mathbf{u}, \lambda)) < n$.

In this brief explanation of continuation methods we will stick to the study of regular points. Singular points in a solution curve $\Gamma(\lambda)$ are associated to **bifurcation points** in which the uniqueness of solution of $G(\mathbf{u}, \lambda) = 0$ no longer hold and, hence, different branches of the curve $\Gamma(\lambda)$ emerge. These points are, undoubtedly, of great significance for the performance of bifurcation analysis and the study in changes on the dynamics of a system. More on singular solutions can be found in the already mentioned references.

According to regular solutions, it is worth noting that there are only two possibilities that the rank of $J_G(\mathbf{u}, \lambda)$ is maximal: either $J_G(\mathbf{u}, \lambda)$ is non-singular; or $\dim(N(G_{\mathbf{u}}(\mathbf{u}, \lambda)) = 1$ and $G_\lambda(\mathbf{u}, \lambda) \notin R(G_{\mathbf{u}}(\mathbf{u}, \lambda))$, where $N(G_{\mathbf{u}}(\mathbf{u}, \lambda))$ is the nullspace of $G_{\mathbf{u}}(\mathbf{u}, \lambda)$, $R(G_{\mathbf{u}}(\mathbf{u}, \lambda))$ is the range of $G_{\mathbf{u}}(\mathbf{u}, \lambda)$ and the subindeces represent partial differentiation so thatm for instance, $G_{\mathbf{u}}(\mathbf{u}, \lambda)$ denotes the jacobian matrix of G with respect to $\mathbf{u}$. In the former case, we will say that $(\mathbf{u}, \lambda)$ is a **simple regular solution**; in the latter, that it is a **simple limit point** or **simple fold**. Figure 4 pictures sketches for the case of a simple regular point, a simple fold and a bifurcation point.

Thus, if our initial point $(\mathbf{u}_0, \lambda_0)$ happens to be a simple regular point, a straightforward plausible procedure to find neighboring points of the solution curve is to use $\mathbf{u}_0$ as the initial guess of a Newton-Raphson iteration for the resolution of system

$$G(\mathbf{u}, \lambda_0 + \Delta\lambda) = 0, \tag{120}$$

for some small step $\Delta\lambda$. Indeed, if $\mathbf{u}^m$ represents the approximate solution for system $G(\mathbf{u}, \lambda_0 + \Delta\lambda) = 0$ after m steps of the Newton-Raphson algorithm, the next iteration of the method can be computed as

$$\mathbf{u}^{m+1} = \mathbf{u}^m + G_{\mathbf{u}}^{-1}(\mathbf{u}^m, \lambda_0 + \Delta\lambda)\, \mathbf{u}^m, \tag{121}$$

as long as the initial guess $(\mathbf{u}_0, \lambda_0)$ is a simple regular point, and hence, $G_{\mathbf{u}}(\mathbf{u}^m, \lambda^m)$ invertible, and $|\Delta\lambda|$ small enough. Once this iterations reach convergence to a point $\mathbf{u}_1(\lambda_1)$, with $\lambda_1 = \lambda_0 + \Delta\lambda$, the solution

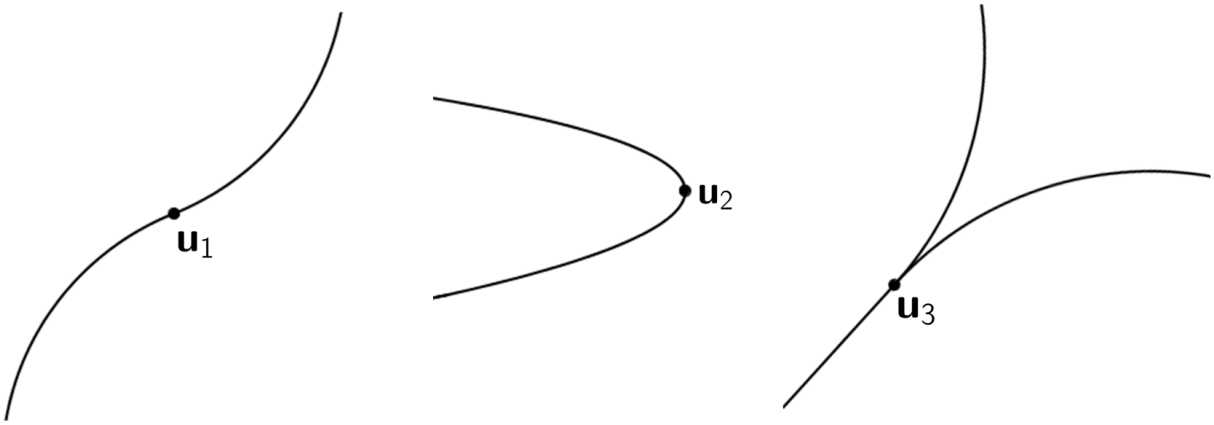

Figure 4: From left to the right, graphic examples of a simple regular point $\mathbf{u}_1$, a simple fold $\mathbf{u}_2$, and a bifurcation point, $\mathbf{u}_3$ on three solution curves.

$(\mathbf{u}_1(\lambda_1), \lambda_1)$ can be used as the new initial guess and so forth until a discretization $\{(\mathbf{u}(\lambda_i), \lambda_i) \,|\, \lambda_i \in \mathcal{I} \subset \mathbb{R}\}$ of the solution curve $\Gamma(\lambda) = (\mathbf{u}(\lambda), \lambda)$ is attained.

This procedure is commonly known as the **natural continuation method** for it provides points on the solution curve parameterized by the **continuation parameter** λ - the naturally occurring parameter of the problem. Natural continuation was used in our numerical computation to explore how the variation of the period of the induced oscillation affects the performance of our control algorithm.

Unfortunately, natural continuation fails when the region of the solution curve that we are studying presents one or more simple folds. If our initial solution $(\mathbf{u}, \lambda)$ is in the vicinity of a simple fold, $\det(G_{\mathbf{u}}(\mathbf{u}, \lambda))$ will be close to 0 and, at best, the Newton-Raphson iteration would have a slow and costly convergence. At worst, $\Delta\lambda$ would displace the initial guess of the iteration too far from the 'folding' solution curve for the problem $G(\mathbf{u}, \lambda + \Delta\lambda) = 0$ to even have a solution that we can find.

Keller proposed an alternative strategy to overcome these difficulties that dropped the parameterization of the solution curve in terms of the continuation parameter λ and instead uses a the arclength parameterization of the solution curve seen as a curve in $\mathbb{R}^{n+1}$, [7, 21]. This novel procedure is consequently referred to as the **pseudo-arclength continuation** and, as we will see, allows us to compute the solution curve in any of the two possible types of regular points.

More specifically, let $s \in \mathbb{R}$ represent the arclength parameter of the solution curve $\Gamma(s) = (\mathbf{u}(s), \lambda(s)) \in \mathbb{R}^{n+1}$. Then, if $(\mathbf{u}_0, \lambda_0) = (\mathbf{u}(s_0), \lambda(s_0))$ are a known solution for system (119) and $(\mathbf{u}_0', \lambda_0')$ is the unit vector tangent to the solution curve at $(\mathbf{u}_0, \lambda_0)$, the pseudo-arclength continuation method consists in the resolution of the following system of $(n+1)$ non-linear equations,

$$\begin{cases} G(\mathbf{u}, \lambda) = 0, \\ (\mathbf{u}_1 - \mathbf{u}_0, \lambda - \lambda_0)^T \cdot (\mathbf{u}_0', \lambda_0') = \Delta s, \end{cases} \tag{122}$$

for some small step Δs. The former n of these equations correspond to the system of n non-linear equations that we are pretending to solve. The latter of them is just a normalization condition which implies

that we are taking a step of length Δs along the tangent direction $(\mathbf{u}_0', \lambda_0')$ to the solution curve at $(\mathbf{u}_0, \lambda_0)$.

In order to solve system (122), it is convenient to rewrite it as $F(\mathbf{u}, \lambda) = (G(\mathbf{u}, \lambda), N(\mathbf{u}, \lambda, \Delta s)) = 0$, where $N(\mathbf{u}, \lambda, \Delta s)$ represents the normalization condition and is given by

$$N(\mathbf{u}, \lambda, \Delta s) = (\mathbf{u} - \mathbf{u}_0)^T \mathbf{u}_0' + (\lambda - \lambda_0)\lambda_0' - \Delta s. \tag{123}$$

Thus, we can take $(\mathbf{u}_1^0, \lambda_1^0) = (\mathbf{u}_0, \lambda_0) + \Delta s\,(\mathbf{u}_0', \lambda_0')$ and then, the subsequent iterations of the Newton-Raphson method will be computed as

$$(\mathbf{u}_1^{m+1}, \lambda_1^{m+1}) = (\mathbf{u}_1^m, \lambda_1^m) + (\Delta\mathbf{u}_1^m, \Delta\lambda_1^m), \tag{124}$$

where the corrections $\Delta\mathbf{u}_1^m$ and $\Delta\lambda_1^m$ are obtained from the resolution of

$$\begin{pmatrix} G_{\mathbf{u}}(\mathbf{u}_1^m, \lambda_1^m) & G_\lambda(\mathbf{u}_1^m, \lambda_1^m) \\ (\mathbf{u}_0')^T & \lambda_0' \end{pmatrix} \begin{pmatrix} \Delta\mathbf{u}_1^m \\ \Delta\lambda_1^m \end{pmatrix} = \begin{pmatrix} G(\mathbf{u}_1^m, \lambda_1^m) \\ N(\mathbf{u}_1^m, \lambda_1^m, \Delta s) \end{pmatrix}. \tag{125}$$

The convergence of sequence (124) is ensured by the following theorem proved by Keller in [21]:

Theorem 4.3 (Keller,[21]). *Given $G : \mathbb{R}^n \times \mathbb{R} \to \mathbb{R}^n$ a smooth function, the Jacobian matrix of the the function $F(\mathbf{u}, \lambda) = (G(\mathbf{u}, \lambda), N(\mathbf{u}, \lambda, \Delta s))$, where $N(\mathbf{u}, \lambda, \Delta s))$ is the normalization condition in (123), is non-singular for any regular solution of the system $G(\mathbf{u}, \lambda) = 0$.*

Once the convergence of sequence (124) to a point $(\mathbf{u}_1, \lambda_1)$ has been reached, the unit tangent vector to the solution curve at that point $(\mathbf{u}_1', \lambda_1')$ is computed as the solution to the linear system,

$$\begin{pmatrix} G_{\mathbf{u}}(\mathbf{u}_1, \lambda_1) & G_\lambda(\mathbf{u}_1, \lambda_1) \\ (\mathbf{u}_0')^T & \lambda_0' \end{pmatrix} \begin{pmatrix} \mathbf{u}_1' \\ \lambda_1' \end{pmatrix} = \begin{pmatrix} 0 \\ 1 \end{pmatrix}, \tag{126}$$

where the first n equations are obtained from the derivation of expression (119) with respect to to s and the last one is obtained from the requirement that both $(\mathbf{u}_0', \lambda_0')$ and $(\mathbf{u}_1', \lambda_1')$ point in the same direction. In the end, after normalizing $(\mathbf{u}_1', \lambda_1')$, point $(\mathbf{u}_1, \lambda_1)$ can be used as a new known solution for the method and so forth, until a discretization $\{(\mathbf{u}(s_i)), \lambda(s_i) \,|\, s_i \in \mathcal{I} \subset \mathbb{R}\}$ of the solution curve $\Gamma(s)$ is attained.

Remark 4.4. In practice, it is usual to find situations in which one wants to apply a pseudo-arclength continuation method knowing only an initial point $(\mathbf{u}_0, \lambda_0)$ on the solution curve but not its tangent direction $(\mathbf{u}_0', \lambda_0')$ at such point. In those cases, it is common to assume that $(\mathbf{u}_0, \lambda_0)$ is a simple regular solution away of any possible simple fold so that we can consider the solution curve to be parameterized by λ on a neighborhood of $(\mathbf{u}_0, \lambda_0)$, that is, $(\mathbf{u}(\lambda), \lambda)$, and then,

$$(\mathbf{u}_0', \lambda_0') = \frac{(\mathbf{u}_0', 1)}{||(\mathbf{u}_0', 1)||}, \tag{127}$$

where $\mathbf{u}_0'$ can be obtained, as in (126), by solving the linear system that we get from deriving expression (119) with respect to λ, namely,

$$G_{\mathbf{u}}(\mathbf{u}_0, \lambda_0)\,\mathbf{u}_0' = -G_\lambda(\mathbf{u}_0, \lambda_0). \tag{128}$$

5. Numerical results

In this section, we apply our APR-based algorithm to two representative examples in order to test its validity and performance. In this sense, we will first study the simplest possible case, the Strong Linear Focus (SLF), for it is a canonical example for which the simplicity of computations enables the study of many features of the problem. Finally, we will apply our algorithm to the more realistic Fitzhugh-Nagumo model (FNM) on its excitable regime where a strong focus dominates the neural dynamics in order to induce an early oscillatory state. The most relevant results are presented and discussed in the following.

All algorithms used to compute the results presented in this section were implemented using the MATLAB R2020a software [1][2]. The vast majority of these algorithms are original of the author, while some of them are borrowed from the work by Moreno in [26] and reproduced here with his permission.

5.1 Strong linear focus

We will begin by applying our control algorithm to the canonical example of the **Strong Linear Focus** (**SLF**). This simple model in which we have explicit analytic expressions for the phase-amplitude response functions defined in the whole $\mathbb{R}^2 \setminus \{\mathcal{O}\}$ will allow us to study the performance of our control strategy in different scenarios and even push it to its limits. In fact, any conclusion or property that we can infer on this canonical model may be used to postulate new hypothesis about the performance of the algorithm in later more complicated models.

The planar Strong Linear Focus model is given by the system,

$$\begin{cases} \dot{x} = \alpha x - \beta y, \\ \dot{y} = \beta x + \alpha y, \end{cases} \tag{129}$$

with $\alpha < 0$ and $\beta \neq 0$. This linear system was already studied in Section 3 when we introduced the concept of isochronous focus. The SLF model possesses a strong focus at the origin that captures the whole dynamics of the system. Indeed, attending to its associated flow given by (30), it is easy to see that the trajectory of any point on $\mathbb{R}^2 \setminus \{\mathcal{O}\}$ will spiralize inwards around the origin (see Figure 5).

The dynamics of system (129) in polar coordinates is given by

$$\rho_* \tilde{\mathcal{X}} = \beta \frac{\partial}{\partial \theta} + \alpha\sigma \frac{\partial}{\partial \sigma}, \tag{130}$$

where, as in the previous sections, ρ represents the usual change to polar coordinates. Hence, it is obvious that the change of variables $\varphi(x, y)$ in Theorem 3.4 corresponds, in the case of the SLF, to the identity - that is, $\varphi(x, y) = id(x, y)$ - and so, the conjugation to the APR-dynamics is simply given by

$$L(x, y) = \rho \circ \varphi(x, y) = \rho(x, y). \tag{131}$$

This means that the phase function (38) for the Strong Linear Focus is

$$\vartheta(x, y) = \arctan\left(\frac{y}{x}\right), \tag{132}$$

[2] All codes are available at: https://web.mat.upc.edu/antoni.guillamon/Code/OptimalControlDampedOscillations .

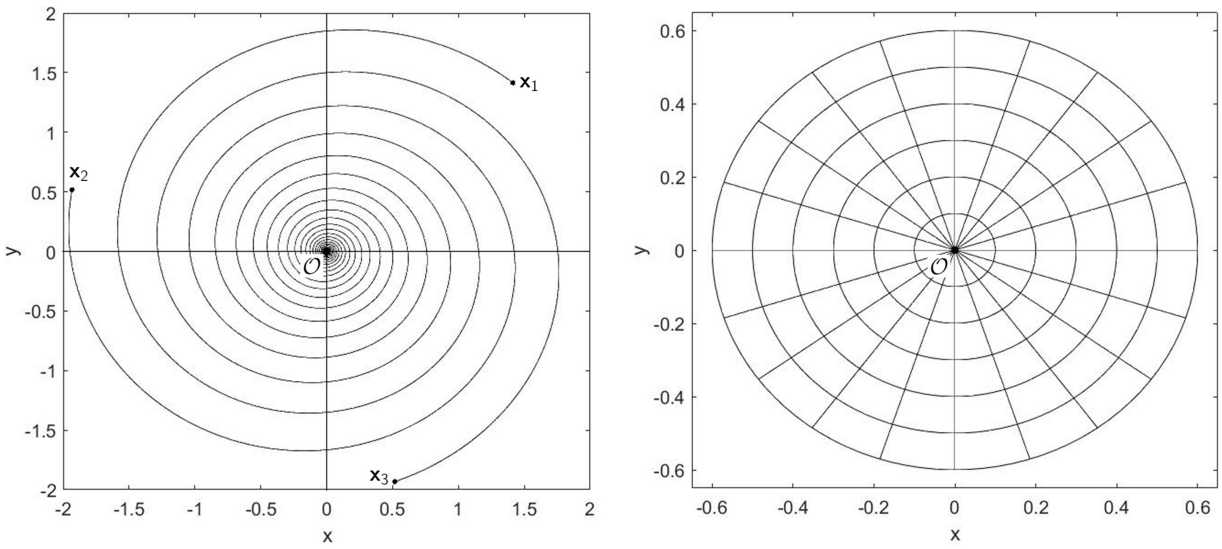

Figure 5: On the left, trajectories of three different points $\mathbf{x}_i \in \mathbb{R}^2$, for $i \in \{1, 2, 3\}$, spiraling inwards around the SLF. On the right, some isochrons (radial sets) and isostables (concentric circles) of the SLF.

while the amplitude function (41) is

$$\varsigma(x, y) = \sqrt{x^2 + y^2}. \tag{133}$$

As a consequence, the isochrons of the strong focus at $\mathcal{O}$ correspond, as we know, to the radial sets,

$$\Theta_\theta = \left\{ (\sigma \cos\theta, \sigma \sin\theta) \,|\, \sigma \in \mathbb{R}^+ \right\}, \tag{134}$$

for any slope $\theta \in [0, 2\pi)$. The isostables, for their part, are defined as the level curves of function (133) and, therefore, consist in the concentric circles around $\mathcal{O}$ given by

$$\Sigma_\sigma = \left\{ (\sigma \cos\theta, \sigma \sin\theta) \,|\, \theta \in [0, 2\pi) \right\}, \tag{135}$$

for any radius $\sigma \in \mathbb{R}^+$. Representative isochrons and isostables of the SLF are portrayed in Figure 5.

Now that we know explicit expressions for the phase and amplitude functions, we are able to derive respective explicit formulas for the PRF and the ARF. This analysis will provide us two main benefits. On the one hand, it is an exercise of didactical significance that allows us to put in practice the theoretical formalism regarding the phase-amplitude response functions for strong foci that we developed in section 3. On the other hand, solutions to this problem shall give us an intuition of how should the PRF and ARF for more complicated systems be like, at least close to the focus where things should behave "close to linear".

Let us consider an external stimulus of the form $U(t) = \big(u(t), 0\big)^T$ perturbing the first coordinate of system (129), that is,

$$\begin{cases} \dot{x} = \alpha x - \beta y + u(t), \\ \dot{y} = \beta x + \alpha y, \end{cases} \tag{136}$$

where $u(t)$ is, at any time, small enough for our APR-formalism to hold true. The reason why we have chosen such an stimulus is our neuroscientifical motivation since, as we commented in Remarks 2.10 and

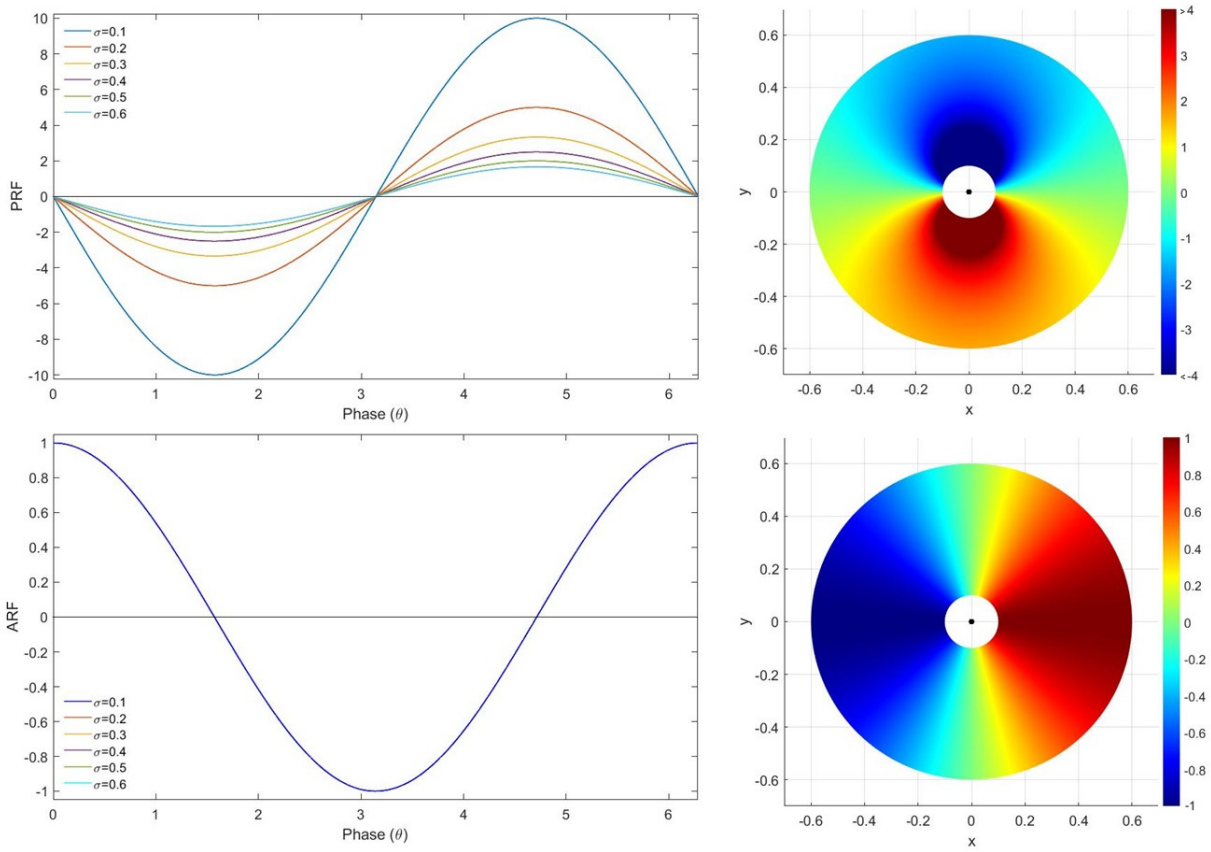

Figure 6: On left, sections of the PRF (up) and the ARF (down) for the six isostables on Figure 5. On the right, color maps depicting the PRF (up) and ARF (down) around the SLF. The darker areas correspond to those regions on the plane that are more sensitive to changes in phase and amplitude respectively.

3.14, it is common in mathematical neuroscience to represent the voltage variable along the x-direction and it is voltage the most significant and exposed to external inputs variable in a neuron model.

Thus, we begin by studying the PRF of the strong linear focus. Form (132) it is obvious that the gradient of the phase function is given by

$$\nabla\vartheta(x,y) = \left(-\frac{y}{x^2+y^2}, \frac{x}{x^2+y^2}\right)^T; \tag{137}$$

and, therefore, using $U(t) = (u(t), 0)^T$ in definition (57), the PRF of the strong linear focus is

$$\text{PRF}(x,y) = -\frac{y}{x^2+y^2}. \tag{138}$$

In a similar way, from (133) we know that the gradient of the amplitude function is

$$\nabla\varsigma(x,y) = \left(\frac{x}{\sqrt{x^2+y^2}}, \frac{y}{\sqrt{x^2+y^2}}\right)^T, \tag{139}$$

so that, according to definition (58), the ARF of the strong linear focus is given by

$$\mathrm{ARF}(x,y) = \frac{x}{\sqrt{x^2+y^2}}. \tag{140}$$

Nonetheless, in order to get a much better insight of both response functions, it is convenient to use phase-amplitude variables (θ,σ) instead of regular variables (x,y) in their definition. Thus, we have

$$\mathrm{PRF}(\theta,\sigma) = \mathrm{PRF}\big(L^{-1}(\theta,\sigma)\big) = -\frac{\sin\theta}{\sigma}, \tag{141}$$

for the phase response function, and

$$\mathrm{ARF}(\theta,\sigma) = \mathrm{ARF}\big(L^{-1}(\theta,\sigma)\big) = \cos\theta, \tag{142}$$

for the amplitude response function. As we can see, the sections of the PRF along different isostables of the focus, that is, sections of the PRF for different fixed values of σ, are sine-curves whose magnitude grows fast as we approach the the focus and rapidly fade away when σ increases. On the contrary, the sections of the ARF are cosine-curves of constant amplitude. Sections of the PRF and the ARF for the strong linear focus can be seen on Figure 6. As we mentioned before, this is the behaviour that we shall expect to be found for the PRF and ARF in other models when one is close to the strong focus at issue.

Once we know explicit expressions for the phase-amplitude functions and have a glimpse of their behaviour around $\mathcal{O}$, we are in position of applying our control strategy in order to induce periodic oscillations around the strong linear focus. Without loss of generality, we will assume that we start at a point $\mathbf{x}_0$ with $\theta_0 = 0$ and $\sigma = \sigma_0$, and we will search for an induced orbit of period T_{PO} and a mean amplitude around $\mathcal{O}$ of $\bar{\sigma} = \sigma_0$. Thus, considering $p_1 = p_2 = 1$, the Euler-Lagrange equations (97) of the problem read

$$\begin{cases} \dot\theta = \beta - \frac{\sin\theta}{\sigma}\,u(t), \\ \dot\sigma = \alpha\sigma + \cos\theta\,u(t), \\ \dot\lambda_1 = \left(\lambda_1\frac{\cos\theta}{\sigma} + \lambda_2\sin\theta\right)\,u(t), \\ \dot\lambda = 2\,(\sigma-\sigma_0) - \alpha\lambda_2 - \lambda_1\frac{\sin\theta}{\sigma^2}\,u(t), \end{cases} \tag{143}$$

with a control input $u(t)$ of the form

$$u(t) = \frac{1}{2}\left(-\lambda_1\frac{\sin\theta}{\sigma} + \lambda_2\cos\theta\right), \tag{144}$$

in accordance with (98). As we know, these equations shall be solved as a two-point boundary value problem with boundary conditions given, in this case, by

$$\theta(0) = 0, \quad \theta(T_{PO}) = 2\pi, \quad \sigma(0) = \sigma_0, \quad \text{and} \quad \sigma(T_{PO}) = \sigma_0, \tag{145}$$

so that the cycle closes up in a time equal to T_{PO}. Figure 7 portrays two examples of periodic orbits computed by means of a shooting strategy on system (143) for $\sigma_0 = 0.5$, $T_{PO} = T_{SF}$ - where $T_{SF} = \frac{2\pi}{\beta}$ is the natural period of the strong focus -, $\alpha = -1$, and $\beta = 1$ and 10, respectively.

As we can observe, the two induced orbits shown in Figure 7 are utterly different as so is the nature of the strong focus around which they spin. In the first case, the system's power of attraction, measured

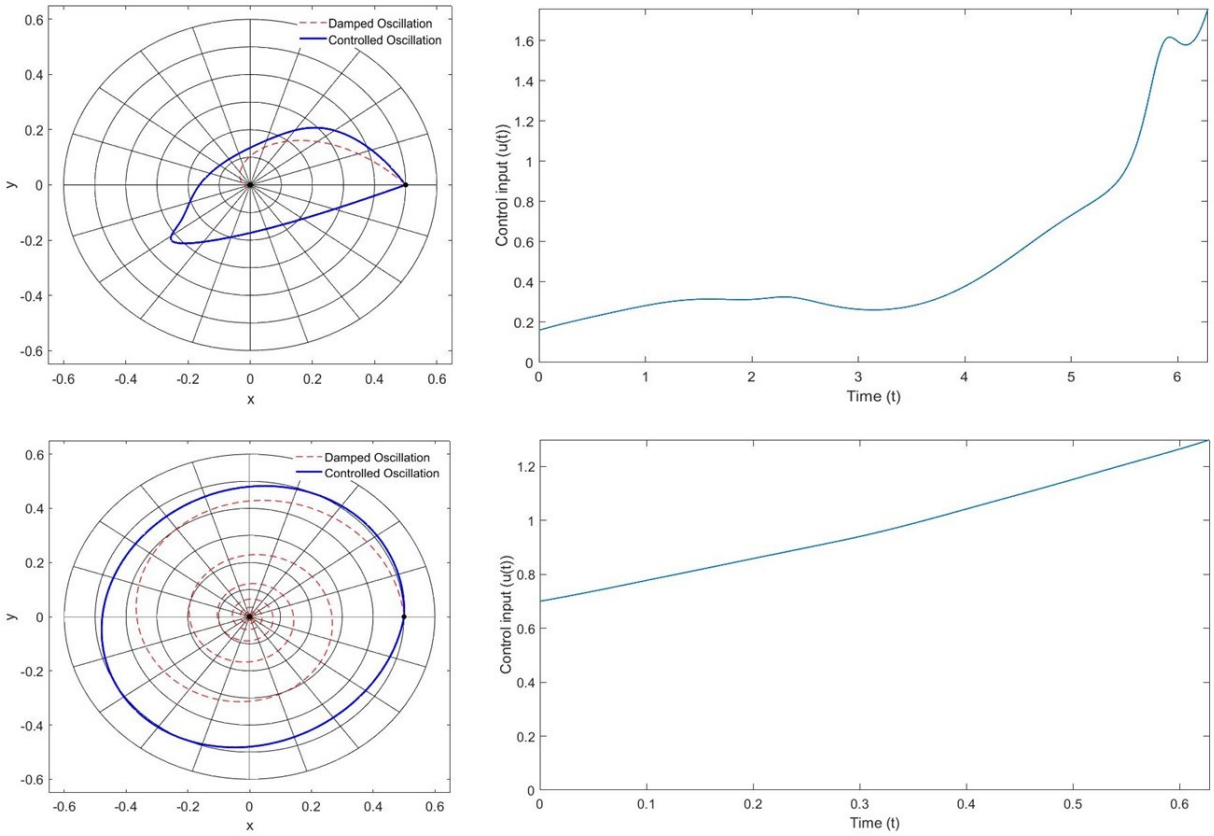

Figure 7: On the left, induced orbits using our control algorithm around the SLF with $\beta = 1$ (up) and $\beta = 10$ (down). On the right, time display of the external control input required for their induction.

by α, and its disposition to spin, measured by β, are balanced and, in consequence, we get a narrow hard-to-induce periodic orbit with a total energy consumption of $E = 2.085$ units. In this sense, our algorithm harnesses the system dynamics to spin with a low energy input in the early stages of the oscillation until it reaches $\theta \approx \pi$ and it starts a rapid escalation up to instantaneous inputs of $1.5 - 1.6$ in order to force the orbit meet the initial point at $t = T_{PO}$. In general, our algorithm fails to keep the induced trajectory close to $\sigma \equiv 0.5$ even though we obtain a successful sustained oscillation (see Figure 14 in Appendix A).

On the other hand, when $\beta = 10 \gg |\alpha|$, the system dynamics is more prone to spinning and, therefore, the resultant orbit is wider, rounder and easier-to-induce. The control input in this case has a soft increasing slope that translates into a total energy consumed of $E = 0.613$ units, way below the energy consumption of the previous case. Moreover, our algorithm is now more effective in minimizing the mean distance of the induced orbit to the isostable $\sigma \equiv 0.5$ (see Figure 14 in Appendix A).

According to the numerical performance of our algorithm, the differences between the two orbits are also clear. In the case $\beta = 10$, we found a wide region of convergence for the shooting method explained in section 4. On the contrary, the convergence was not so straightforward nor fast in the case $\beta = 1$, where we even needed to perform some rudimentary steps of a 2D bisection method - see [4] - in order to

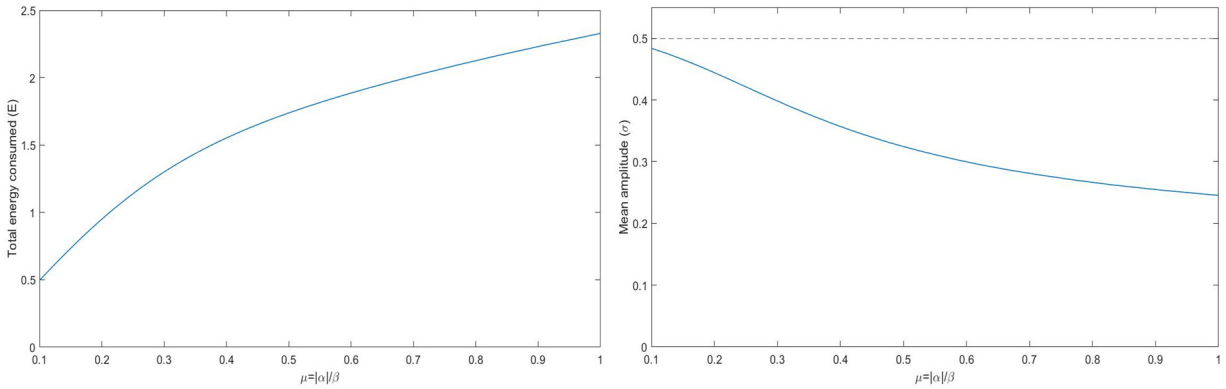

Figure 8: On the left, tracking of the total energy consumed by the induced periodic orbits around strong linear foci with $\mu \in [0.1, 1]$. On the right, tracking of the mean amplitude of such orbits along the same interval for parameter μ. The dashed black line marks the objective isostable $\sigma \equiv 0.5$.

get a more accurate initial seed for our shooting method than our default $c = (0, 0)^T$. For its part, the control error ϵ is not relevant in the SLF model where we have an explicit formula for all the elements involved in system (143). Indeed, ϵ is in both cases bellow the tolerance, $tol = 10^{-13}$, of the shooting method.

These observations suggest that the quotient between α and β, namely,

$$\mu = \frac{|\alpha|}{\beta}, \tag{146}$$

plays a rather significant role in the performance and numerical applicability of our algorithm. Indeed, it is suggested that the closer this μ is to one - that is, the more balanced the attracting and spinning forces of the strong focus are -, the less effective our control would be, the more energy would be required to induce the periodic oscillation and the narrower the convergence zone of our shooting method would happen to be.

In order to validate this hypothesis, we devised a continuation strategy along parameter μ based on Keller's pseudo-arclength continuation explained in Section 4 that allows us to swipe along the interval $[0.1, 1]$ and analyse the resulting periodic oscillations. Thus, Figure 8 shows a tracking of the total energy consumed and the mean amplitude of the induced orbits for an exhaustive analysis of induced orbits with $\sigma_0 = 0.5$, $T_{PO} = T_{SF}$ and $\mu \in [1, 10]$. As we can see, the total energy consumed grows rapidly as μ tends to 1 implying that it gets harder to induce the periodic oscillations as μ goes to 1. Similarly, the mean amplitude of the induce orbits decreases as μ approaches 1 meaning that the ability of our algorithm to keep the induced orbits close to $\sigma \equiv 0.5$ is compromised as μ goes to 1. Figure 15 in Appendix A illustrates this fact in a perhaps more visual way as it portrays some representative resulting periodic orbits and so, we can appreciate how they actually get narrower as μ raises.

It is worth noting that any attempt of extending this parametric continuation far beyond $\mu = 1$ was frustrated as the shooting method rapidly fails to converge as soon as $|\alpha|$ gets bigger than β, that is, $\mu > 1$. From our scarce inquiries in this phenomena, we can sense that the root of this failure in the convergence of the method derives from the fact that the great power of attraction of such foci forces the orbits to pass too close to the origin where the PRF rockets to exorbitant values that end up carrying the solutions of (143) to rather big amplitudes after a time T and, hence, compromises the convergence of our shooting method.

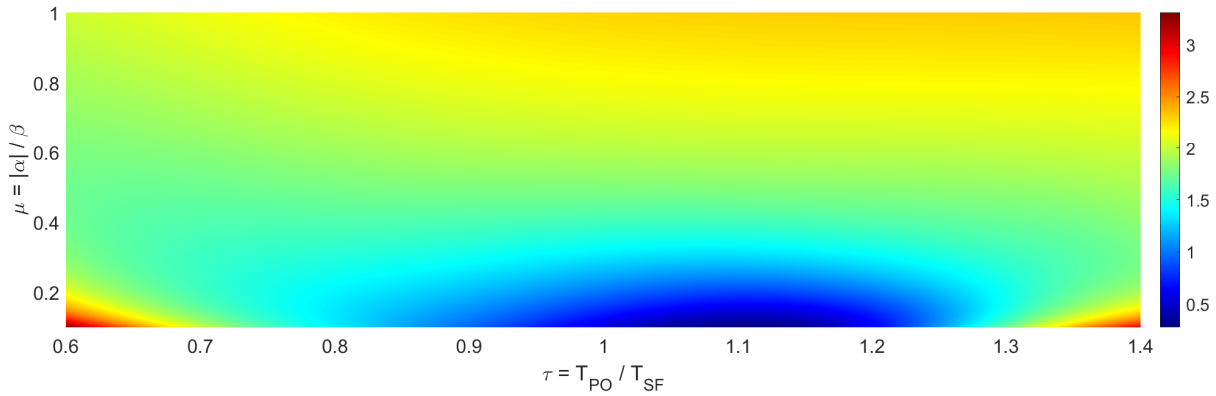

Figure 9: Color map portraying the total energy consumed in the induction of periodic orbits around strong linear foci starting at $(\theta_0, \sigma_0) = (0, 0.5)$ when we vary parameters $\mu \in [0.1, 1]$ and $\tau \in [0.6, 1.4]$.

Figure 16 in Appendix A shows an example of this behaviour on an intermediate iterate of a failing shooting.

Finally, another important ratio to bear in mind is that between the requested period of the induced periodic orbit and the natural period of the strong focus in hand, that is,

$$\tau = \frac{T_{PO}}{T_{SF}}. \tag{147}$$

So far, we have been working with $\tau = 1$ - i.e., $T_{PO} = T_{SF}$ -; nonetheless, the manipulation of this parameter by means of a continuation method allows us to explore the performance of our algorithm when the pretended oscillation advances or delays the original damped oscillation. In this sense, Figure 9 portrays an exhaustive color map showing the total energy consumed for the induction of a periodic oscillations as we vary parameter $\mu \in [0.1, 1]$ and parameter $\tau \in [0.6, 1.4]$.

As we can see, in accordance with what we noticed before, induced orbits for values of μ closer to one are in general more costly than those for lower values of μ regardless the objective period T_{PO}. In this region, as the logic may dictate, the induction of slower orbits, that is, orbits for bigger values of τ, carries a bigger energy consumption. On the other side of the diagram, we find a rather surprising phenomenon for orbits with $\mu \sim 0.1$. Here, in spite of finding a wide central region for which the energy consumption is relatively low, we see that the total energy consumed reaches its minimum not for $\tau = 1$, as we may have thought *a priori*, but for $\tau = 1.1$, that is, our algorithm requires less energy to induce orbits slightly delayed with respect to the natural period of the strong focus. On the extremes of the interval, the energy consumption reaches again utterly high values and, indeed, convergence was not achieved beyond $\tau = 1.4$. Figure 17 in Appendix A offers a comparison of the orbits induced for $\mu = 0.1$ and $\tau = 0.6$, 1, 1.1 and 1.4.

5.2 Fitzhugh-Nagumo model

In the early 1960s, Fitzhugh [14] and Nagumo *et al.* [27] independently developed and analysed a planar simplified version of the 4-dimensional Hodgkin-Huxley system [20] describing the main characteristics of action potential signals through the membrane of neurons. The **Fitzhugh-Nagumo model** (**FN model**), which qualitatively resembles the classical van der Pol oscillator, succeeds in grabbing the main physiological features of nerve membrane encoded in a couple of analytically tractable equations and, therefore,

constitutes one of the most recursively considered models of excitable systems in mathematical neuroscience.

The equations of the Fitzhugh-Nagumo model are

$$\begin{cases} \dot{V} = V(V-a)(1-V) - w + I_{app}, \\ \dot{w} = \varepsilon(V - \gamma w), \end{cases} \tag{148}$$

where V represents the membrane action potential, w is a simplified gating variable accounting for the opening of the ion channels on the neuron membrane that trigger the action potential signaling and I_{app} is an applied electric intensity simulating synaptic currents coming from surrounding neurons. Parameters a, γ and ε are fixed constant that control minor features of the model, whilst I_{app} remains as a free **bifurcation parameter** whose different values will determine great structural changes in the dynamics of system (148) and, in turn, in the physiological properties of the neuron it models. For the first part of this section we will consider the following values for these parameters,

$$a = 0.1, \quad \gamma = 1, \quad \text{and} \quad \varepsilon = 0.1\,. \tag{149}$$

Although it is not a common choice for the parameters of the Fitzhugh-Nagumo model in the specialized literature, it seems to be a natural and easy election for starting the analysis of the Fitzhugh-Nagumo model before moving onto more complicated and realistic cases due to the satisfactory results reported by Moreno in [26] and the rounded shape of the isochrons of the strong focus that we can see in such work that may favour the closure of the induced periodic orbits. Additionaly, as we will see below, this set of parameters also avoids troubelsome dynamical features such as regions of bistability where isochrons and isostables may accumulate near the limit of the basin of attraction of the strong focus yielding exorbitant values for the PRF and the ARF that could spoil the numerical convergence of the shooting method.

Thus, in order to understand the effects that the different variations of the applied current produce on the dynamics of system (148), we perform a bifurcation analysis along the I_{app} parameter with the help of the XPPAUT software [2, 10]. The resulting **bifurcation diagram** is shown in Figure 10 and, as we can see, it can be easily split into three regions characterized by different dynamical features:

- **Excitable regime:** on the leftmost part of the bifurcation diagram a sole attracting fixed point - indeed, a stable strong focus - dominates the entire dynamics of the system. This region is commonly known as the **excitable regime** of the model and corresponds to a physiological state of the neuron in which it rests at electrochemical equilibrium waiting for a synaptic stimulus to activate it. This activation comes on the equations in the form of a **supercritical Hopf bifurcation** at $I_{app} = 0.1057$ after which a stable limit cycle arises while the fixed point switches its stability character to unstable.

- **Oscillatory regime:** in the middle region of the bifurcation diagram in Figure 10 we find a relatively wide region of applied currents for which the dynamics of the model is dominated by an stable limit cycle that encloses an unstable limit cycle within. This periodic oscillation is responsible for the spiking signals observed on the membrane potential of the neurons during synapsis and is known as the **oscillatory regime**. This regime ceases with a second **supercritical Hopf bifurcation** at $I_{app} = 0.5037$ at which the limit cycle and the fixed point collide resulting in the vanishing of the former and a second change of stability of the second.

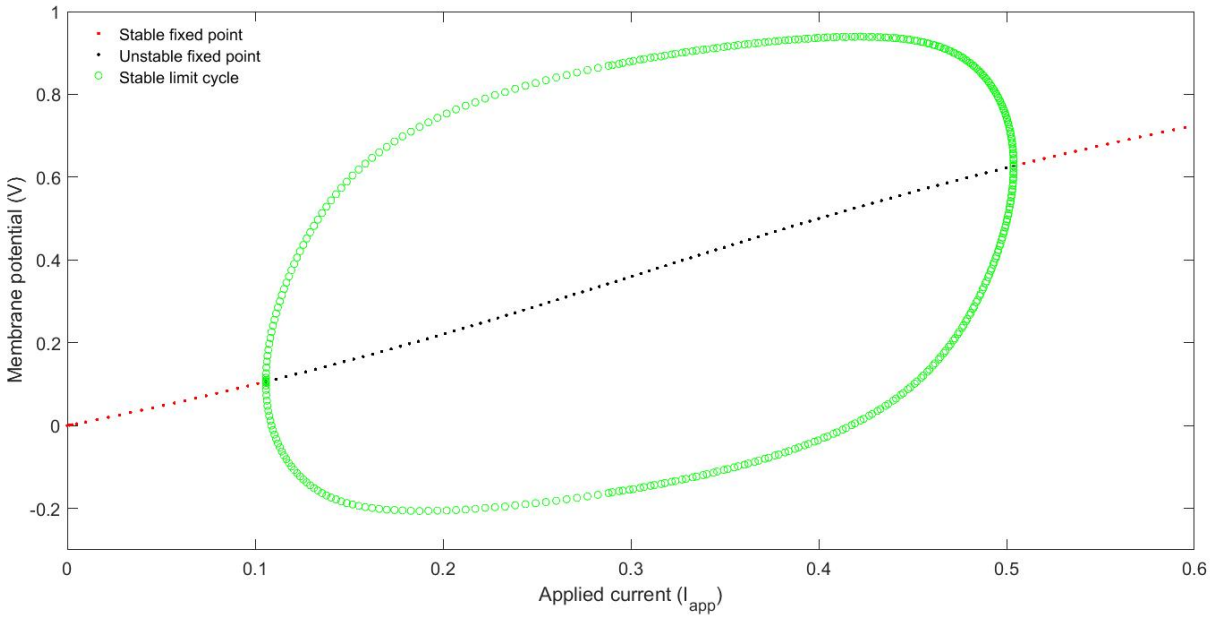

Figure 10: Bifurcation diagram of the Fitzhugh-Nagumo along the I_{app} parameter for $a = 0.1$, $\gamma = 1$ and $\varepsilon = 0.1$. Two supercritical Hopf bifurcations take place at $I_{app} = 0.1057$ and $I_{app} = 0.5037$ when the fixed point and the limit cycle merge together mutually exchanging their stability character.

- **Nerve block:** finally, on the rightmost region of the diagram, a unique stable fixed point acts, once again, as a global attractor of the dynamics of the system. In this situation, the system loses its ability to be excited into a sustained oscillatory state and, therefore, the neuron enters a malfunctioning regime in which no transmision of information is possible. This critical state is known as the **nerve block** and is commonly an irreversible state closely related to the physiological death of the neuron.

In the following, we will consider that our Fitzhugh-Nagumo system is in the excitable regime close to the Hopf bifurcation, which is indeed a rather plausible physiological state for a neuron, and we will use our control algorithm in order to induce an early oscillation in it. This can be interpreted as a way of artificially broadening the oscillatory regime of the neuron and so, enabling it to respond to electrical inputs that are weaker than usual. Hence, along the forthcoming computations, we will consider an applied current of

$$I_{app} = 0.08, \tag{150}$$

so that the dynamics of the system is governed by a stable strong focus $\mathcal{P}$ located at the point $(V, w) = (0.0784, 0.0784)$ with $\alpha = -0.0299$ and $\beta = 0.3067$. This means that we will be working with a strong nonlinear focus with natural period $T_{SF} \simeq 20.5$ and $\mu = 0.0748$ around which, according to the observations made when studying the linear case, the induction of a periodic oscillation by means of our control algorithm should not be demanding. Figure 11 portrays three sample orbits spiraling around the strong focus $\mathcal{P}$.

Unlike in the case of the strong linear focus, we do not have any explicit expression for the APR conjugation $L(x, y)$ and so, as we explained in Section 4, it has to be numerically approximated by a map $\hat{L}(x, y)$ up to a given order. In our case, $\hat{L}(x, y)$ reproduces the action of $L(x, y)$ up to order 8 and yields a fundamental domain of radius $\sigma_{fd} = 0.0285$ for a tolerance of 10^{-9}. Within the fundamental domain,

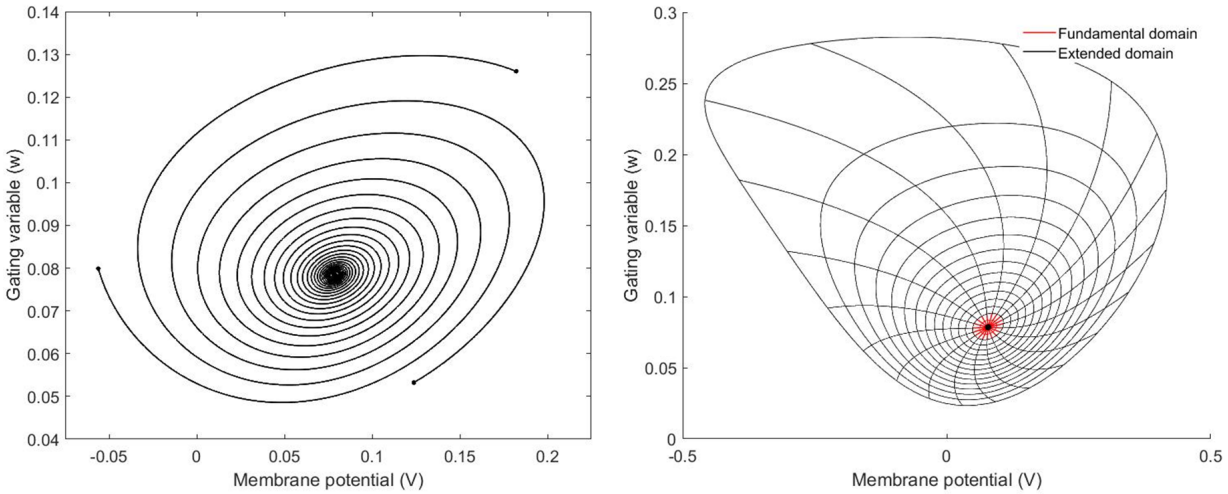

Figure 11: On the left, trajectories of three different points spiraling inwards around the strong focus of the Fitzhugh-Nagumo model for the parametric choice (149) and $I_{app} = 0.08$. On the right, some representative isochrons (radial sets) and isostables (closed curves) of such focus. The region in red is the fundamental domain for $tol = 10^{-9}$ and, in black, its extension up to $\sigma_{max} = 0.2$.

isochrons and isostables are computed via the parametrizations (104) and (105), respectively. Out of the fundamental domain, these isochrons and isostables are extended, as we know, by integrating system (148) backwards in time using the globalization method introduced in Section 4. Figure 11 shows representative isochrons and isostables of the Fitzhugh-Nagumo model for the parametric choice (149) with $I_{app} = 0.08$ both on the fundamental domain and on a extended domain up to $\sigma_{max} = 0.2$.

At this point, it is important to beware the upper part of the isochron-isostable diagram in Figure 11 as isostables seem to distance too much from one another on that region and, consequently, the forthcoming extension of the PRF and ARF may not be accurate enough there. In the following, it would be wise to avoid computations on that region and stick to the region closer to the strong focus for isostables there appear nearer to each other and, additionally, possess a rounder shape, similar to the ones in the SLF model, that shall favour a less demanding closure of induced periodic orbits.

Next, let us consider an external stimulus of the form $U(t) = \big(u(t), 0\big)^T$ that affects the voltage variable V of out Fitzhugh-Nagumo model (148) so that we have

$$\begin{cases} \dot{V} = V(V-a)(1-V) - w + I_{app} + u(t), \\ \dot{w} = \varepsilon(V - \gamma w), \end{cases} \tag{151}$$

where the modulus $u(t)$ is, at any time, small enough for the APR-dynamics around the point $\mathcal{P}$ to hold true. As in the case of the isochrons and isostables, the non-linearity of the equations and the consequent absence of an explicit expression for the APR- conjugation map force us to perform a numerical computation of the phase-amplitude response functions of $\mathcal{P}$.

Thus, as usual, the PRF and ARF are approximated within the fundamental domain by means of the formulas (64) and (80) respectively, where the vector fields $\mathcal{Y}$ and $\mathcal{Z}$ shall be computed in terms of the

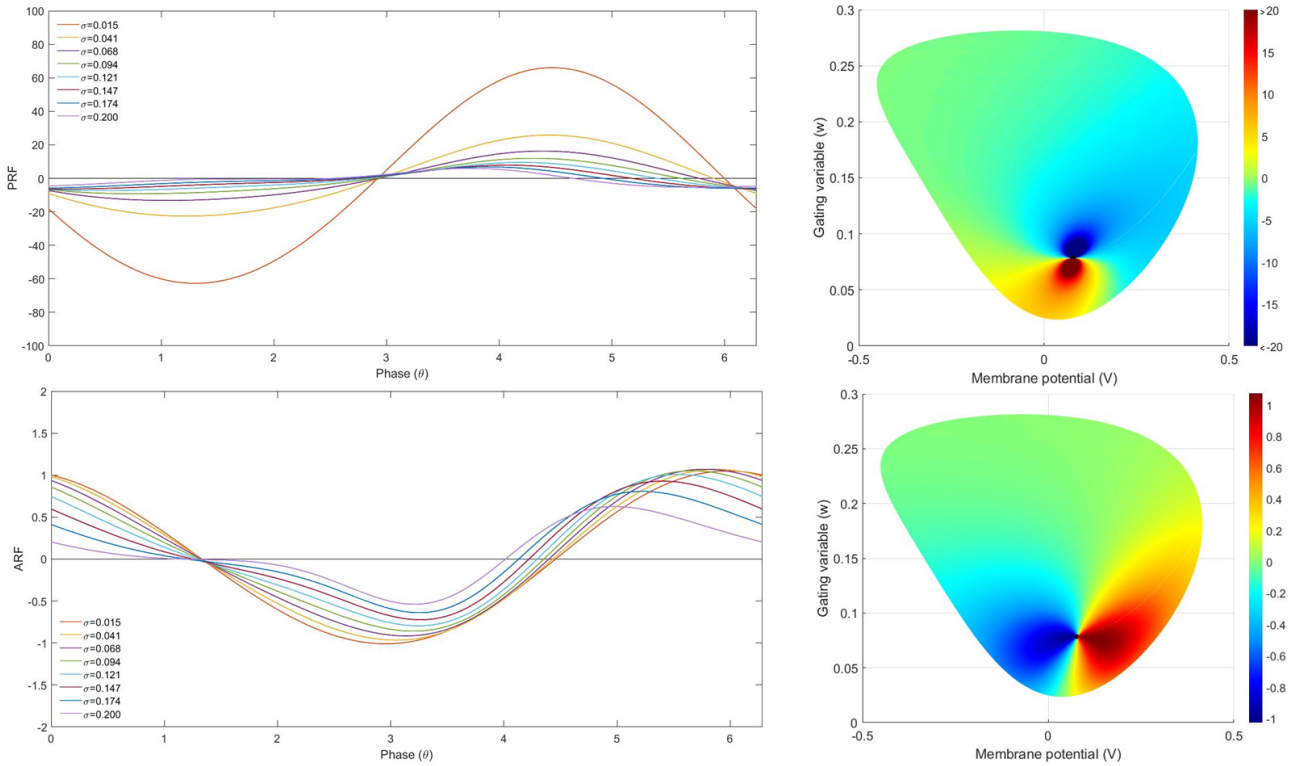

Figure 12: On the left, sections of the PRF (up) and the ARF (down) for eight of the sixteen isostables of the FN model in Figure 11. On the right, color maps depicting the PRF (up) and ARF (down) around the point $\mathcal{P}$. As usual, the darker areas correspond to those regions on the plane that are more sensitive to changes in the phase and amplitude of the orbits, respectively.

pushforward of their linear counterparts $\tilde{\mathcal{Y}}$ and $\tilde{\mathcal{Z}}$ by the approximate diffeomorphism $\hat{\varphi}(x, y)$ in the fashion we commented in Remarks 3.15 and 3.17. Then, once the PRF and ARF are computed for points on the fundamental domain, we extend them to outer regions by integrating their respective adjoint equations (67) and (83) backwards in time following the same scheme as the globalization of isochrons and isostables that we already mentioned. Naturally, it is convenient to perform all these computations at the same time for the sake of sparing computational time and effort. Representative sections of the PRF and the ARF for the strong focus $\mathcal{P}$ are depicted in Figure 12.

The first thing we shall notice is that, so as we expected, the sections of the PRF and ARF that correspond to isostables closer to the strong focus resemble the sinusoidal shape of their linear counterpart, namely, $\mathrm{PRF}(\theta, \sigma) = \sigma^{-1} \sin\theta$ and $\mathrm{ARF}(\theta, \sigma) = \cos\theta$. When the distance to the focus increases, as it is logical, the profile of these functions departs from the linear one. Nevertheless, they still preserve some of the most representative features of the ones presented in Figure 6: on the one hand, the PRF presents a sharp nonlinearity on $\mathcal{P}$ that translates into a relatively wide neighboring region of exorbitant values that one should avoid in numerical computations; on the other hand, the ARF maintains this 'symmetrical' behaviour in which positive and negative values align on both sides of the strong focus. Finally, as we can observe, on the *a priori* troublesome upper region of the diagram both response functions present values very close to 0 and, consequently, external stimuli will have a very low impact on the systems dynamics here.

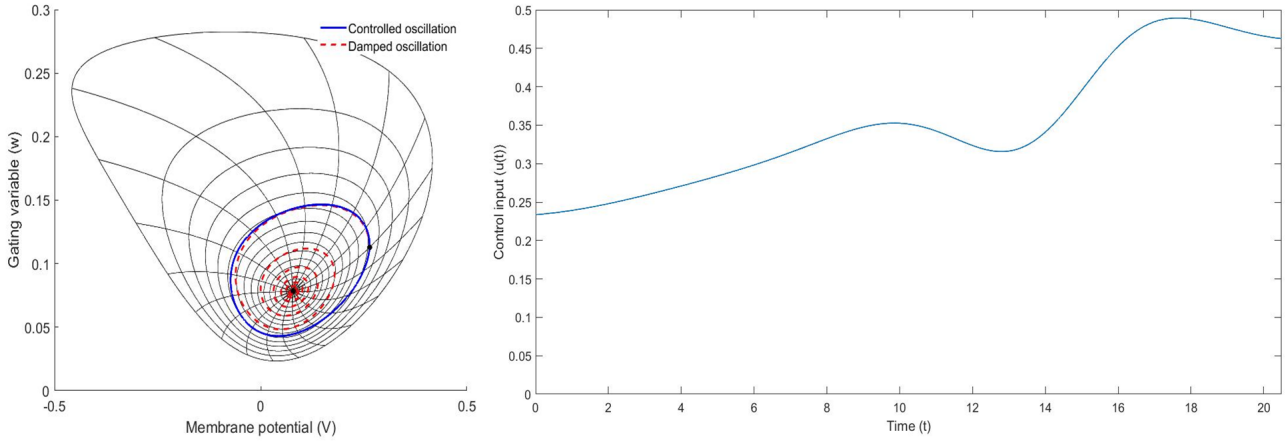

Figure 13: On the left, periodic orbit induced on the Fitzhugh-Nagumo model for the parametric choice (149) with $I_{app} = 0.08$. On the right, time display of the of the external control input inducing it.

Now that we have enough information about the phase-amplitude functions on a sufficiently wide region of the plane around $\mathcal{P}$, we are in position of applying our control algorithm to induce a periodic oscillation around such strong focus. First of all, it is of great significance to point out the fact that, in this new situation, our range of action is confined to the extended domain where we have information about the PRF and the ARF. This means that, if for any reason one of the iterations of the shooting method happen to escape this region, our algorithm will fail to provide a correct answer, or even converge to a solution at all. To overcome problems derived from these situations, we found that a successful strategy is using the tuning parameters p_1 and p_2 in the Euler-Lagrange equations (97) in order to penalize huge energy inputs that may displace the trajectories out of the extended domain. In this sense, positive results were found for $p_1 = 100$ and $p_2 = 1$ with the parameter choice (149) and $I_{app} = 0.08$.

Once this first remark is done, we can pose the problem of periodic orbit induction in the system. We will take a starting point with $\theta_0 = 0$ and $\sigma_0 = 0.15$, and we will seek for an induced orbit of period $T_{PO} = T_{SF} \simeq 20.5$ and mean amplitude around $\mathcal{P}$ of $\bar{\sigma} = \sigma_0 = 0.15$. The corresponding Euler-Lagrange equations for this problem read

$$\begin{cases} \dot{\theta} = \beta + \hat{\mathrm{PRF}}(\theta,\sigma)\, u(t), \\ \dot{\sigma} = \alpha\sigma + \hat{\mathrm{ARF}}(\theta,\sigma)\, u(t), \\ \dot{\lambda}_1 = -\left(\lambda_1 \frac{\partial}{\partial\theta}\hat{\mathrm{PRF}}(\theta,\sigma) + \lambda_2 \frac{\partial}{\partial\theta}\hat{\mathrm{ARF}}(\theta,\sigma)\right) u(t), \\ \dot{\lambda}_2 = 2(\sigma - \sigma_0) - \alpha\lambda_2 - \left(\lambda_1 \frac{\partial}{\partial\sigma}\hat{\mathrm{PRF}}(\theta,\sigma) + \lambda_2 \frac{\partial}{\partial\sigma}\hat{\mathrm{ARF}}(\theta,\sigma)\right) u(t), \end{cases} \tag{152}$$

with the control input $u(t)$ given, for $p_1 = 100$, by

$$u(t) = \frac{1}{200}\left(\lambda_1 \hat{\mathrm{PRF}}(\theta,\sigma) + \lambda_2 \hat{\mathrm{ARF}}(\theta,\sigma)\right), \tag{153}$$

where $\hat{\mathrm{PRF}}(\theta,\sigma)$ and $\hat{ARF}(\theta,\sigma)$ represent the interpolation of the phase-amplitude response functions along the fundamental and extended domains done with the MATLAB 2D-interpolator *griddedInterpolant*. The derivatives with respect to θ and σ were computed numerically by means of a usual divided differences

strategy from the data on the original grid along the extended domain. The boundary conditions imposed on system (152) so that the resulting limit cycle closes up in a time equal to $T_{PO} \simeq 20.5$ are

$$\theta(0) = 0, \quad \theta(T_{PO}) = 2\pi, \quad \sigma(0) = 0.15, \quad \text{and} \quad \sigma(T_{PO}) = 0.15\,. \tag{154}$$

Figure 13 shows the induced periodic orbit in this case computed using our control algorithm. As we can see, this orbit is rather rounded with its amplitude close to the objective $\bar{\sigma} = 0.15$ at any time (see Figure 18 in Appendix A). Indeed, the induced orbit avoid completely the upper region of the extended domain where possible troubles were predicted. According to the energy input, we see that, although we are using an utterly high value for the p_1 parameter, this does not translate into a very low energy input. It is, in fact, similar to the values obtained for the orbits induced around the SLF. The total energy consumption of the process is $E = 2.6251$ units, while the control error is $\epsilon \sim 10^{-10}$.

Finally, it is worth remarking that several attempts to obtain positive results for more realistic sets of parameters in the Fitzhugh-Nagumo model. By way of illustration, we will briefly comment on the issues encountered when working with the rather typical choice in literature given by

$$a = 0.14, \quad \gamma = 3.24, \quad \text{and} \quad \varepsilon = 0.08\,. \tag{155}$$

The main problems encountered with the numerical resolution of the Euler-Lagrange equations are derived from the existence of two short-lived **bistability regimes** on the bifurcation diagram between the excitable and the oscillatory regimes and between this latter and the nerve block. As we can see in Figure 19 in Appendix A, for the parameter choice (155), the excitable regime ends at a double limit cycle bifurcation at $I_{app} = 0.0578$ when two limit cycles of opposite stability character emerge. Along the resulting bistability region, two stable structures, the fixed point and the stable limit cycle, coexist with the unstable limit cycle marking the boundary of their respective basins of attraction. The first bistability regime ends at $I_{app} = 0.0579$ with a subcritical Hopf bifurcation at which the unstable limit cycle and the stable fixed point merge into an unstable fixed point. On the other side of the diagram, the oscillatory regime finishes at $I_{app} = 0.0636$ with a second subcritical Hopf bifurcation at which a new unstable limit cycle appears. This second bistability region persists until a second double limit cycle bifurcation at $I_{app} = 0.0637$ eradicates the two limit cycles making leading to the blocking of the neuron functionality.

This two bifurcation regimes are so narrow that, in practice, they are almost irrelevant. Nonetheless, some of their dynamical features still persists for values of I_{app} that are close to bifurcation as the ones we are interested in for they are those cases in which $\beta \gg \alpha$ and the performance of our algorithm is maximized. In particular, when we are in a bistability regime, isochrons and isostables of both the stable strong foci or the stable limit cycles tend to accumulate around the unstable limit cycle as reported, for instance, by Moreno in [26]. A big accumulation of isochrons and isostables is of great importance for our purposes as it implies that even a slight perturbation on the system may cause great changes in the phase and amplitude of the perturbed points. As we can imagine, this fact may entail numerical issues in the computation of the PRF and ARF and, specially, in the resolution of the Euler-Lagrange equations.

In our attempts, we considered an applied current $I_{app} = 0.055$ so that the system was at the excitable regime on the verge of crossing to an oscillatory state. As we can see on the right panel of Figure 20 in Appendix A, isostables of the model have a rather oblong shape markedly different to the almost round

shape of the isostables in Figure 11. Additionally, both isochrons and isostables tend to accumulate in the lower part of the extended domain as a consequence of the proximity of I_{app} to the bistability regime. As a consequence of this fact, the PRF and ARF take rather big values in the accumulation zone as we can observe in the right panels of Figure 21 in Appendix A. The combined action of these two drawbacks, the narrow shape of the extended domain and the high values of the response functions, has spoiled all our attempts to get a solution for the corresponding Euler-Lagrange equations for they force orbits computed for the intermediate steps of the shooting method exit the extended domain onto a region where no information about the PRF and ARF is known. Different values for the tuning parameters p_1 and p_2 were tested as well as modifications in the period of the induced orbit, the starting point and even a lower I_{app} with similar negative results. Fortunately, the positive results obtained for the parametric choice (149) suggest that the lack of results in this case may correspond to a flaw of our numerical implementation rather than to an intrinsic feature of the theory that impedes the induction of a periodic oscillation for the Fitzhugh-Nagumo model with parameters given by (155). Indeed, we conjecture that, with finer algorithms and a bit more of computational effort, positive results can also be obtained in this case.

6. Conclusions and further horizons

Throughout the pages of this Master's Thesis we have provided a complete and solid theory concerning the Augmented Phase Reduction (APR) formalism to reproduce the dynamics of a system near a damped oscillation by combining the pioneering work initiated by Moreno in [26] with our original results regarding the definition of amplitude response functions (ARF) in this new context. This theoretical background enabled us to pose and solve a control strategy for the induction of sustained periodical oscillations, in a context were originally a damped oscillation may dominate the dynamics of the problem, using a minimum-energy input with many theoretical and practical applications. In fact, this methodology happens to be an optimal way of generating the sustained periodic oscillations that are found to be totally necessary for the proper functioning of many biological models. For example, when applied to models in neuroscience, we have seen that our control strategy can be used to enhance the oscillatory regime of neurons and so allow them to be excited by external stimuli of lower intensity.

Very positive results were found when applying this theory to the practical cases of a strong linear focus, that can be regarded as an easy academical model, and to the more biologically realistic Fitzhugh-Nagumo model of an excitable neuron. From the exhaustive analysis of the former some interesting properties of the control algorithm were observed that we summarize in the forthcoming points:

- The performance of the control algorithm is better the bigger the disposition to spin of the system, measured by β, is with respect to the power of attraction of the strong focus, measured by $|\alpha|$. Indeed, scarce positive solutions were found for cases where $|\alpha| > \beta$.

- The total energy consumed by the control input has strong dependencies on the ratios $\mu = \frac{|\alpha|}{\beta}$ and $\tau = \frac{T_{PO}}{T_{SF}}$, where T_{PO} and T_{SF} are the period of the induced oscillation and the natural period of the damped oscillation respectively. In this sense, it has been observed that the total energy consumed increases when μ gets close to 1 and, in such cases, it is higher when one pretends to delay the period of the oscillation, that is, $\tau > 1$.

- In the same spirit as the previous remark, an interesting and, at first glance, counter-intuitive asymmetry was found in Figure 9 for lower values of μ. Therefore, instead of finding a minimum energy consumption for $\tau = 1$ - in the limit $\mu \to 0$ the optimal periodic orbit will be the orbit of the center and, hence, $E = 0$ for $\tau = 1$ -, we find it displaced at $\tau = 1.1$, that is, it is easier for the algorithm to induce orbits with a period slightly bigger than the natural period of the original damped oscillation.

- The tuning parameters p_1 and p_2 included in the Euler-Lagrange equations (97) proved to be utterly useful for improving the performance of the algorithm in more realistic problems such as the induction of periodic oscillations in the Fitzhugh-Nagumo model.

Concerning possible further applications of our novel control algorithm, it is worth mentioning that, although this Master's Thesis has been oriented to stable foci since, in principle, response functions are traditionally studied around attractors. However, its application to unstable foci seems to be a very promising extension of this work. A relevant stochastic phenomenon that has received great attention in the recent (neuro)biological literature is the so-called **noise-induced stability**: a mechanism in which noise stabilizes - i.e., it creates a stochastic oscillation - a deterministically unstable state. In the context of neuroscience, it has interest in order to generate specific firing patterns; for instance, Ryazanova *et al.* in [29] have studied noise-induced firing patterns in a system of two coupled Fitzhugh-Nagumo subsystems. Moreover, at the crossroad between neuroscience and genetics, interesting applications of these techniques can be found in relation to the generation of circadian rhythms. In [31], it is shown how noise intrinsic to a simple genetic circuit effectively stabilizes a deterministically unstable state, which constitutes a unique mechanism for a genetic timer. It has also been reported and explained through noise-induced oscillations, see [22], that the suprachiasmatic nucleus (SCN) of mutant mice unexpectedly generates stochastic oscillations with periods that overlap the circadian range. In this spirit, the methodology proposed in this thesis brings up a new **control-driven deterministic** mechanism to induce sustained oscillations around unstable equilibria. Furthermore, the control that we impose is optimal in terms of energy, while noise-induced oscillations may not be. In other words, our algorithm provides a better strategy than external noise stimulation in experiments where one seeks at gaining leverage on the sustained oscillations. In contrast, noise-induced stability will be better when explaining the endogenous mechanisms that this induced oscillations may generate.

Finally, from a more practical and therapeutic point of view, we would like to mention that, in a recent paper, Duchet *et al.* [9] proposed an explanation about the benefits of phase-locked deep brain stimulation (phaseDBS) in Parkinson's pacients. This technique constitutes a therapeutic strategy with low side-effects that consists in stimulating the damaged cells with an external stimulus according to the phase of the tremor. In their study, patient data is fitted to a rate model, which reveals that the dynamics is close to a strong focus. Then, phase and amplitude response curves - defined by Duchet *et al.* in an experimental context - serve to provide a satisfactory prediction of how patient tremor will react to phaseDBS. This example suggests promising applications of our method, eventually modifying the constraints of the variational problem used for the definition of system (97) according to the desired evolution of the tremors. Optimal control strategies in this context would lead to low energy stimulations which, in turn, yield a minimization of side-effects inflicted on patients by such treatments.

References

[1] MATLAB R2020a [software], 2020. Available at: https://es.mathworks.com/

[2] XPPAUT 8.0 [software], 2016. Available at: http://www.math.pitt.edu/ bard/xpp/xpp.html

[3] Algaba, A.; and Reyes, M. Characterizing isochronous points and computing isochronous sections. *Journal of Mathematical Analysis and Applications* **355**(2): 564-576, 2009.

[4] Bachrathy, D.; and Stépán, G. Bisection method in higher dimensions and the efficiency number. *Periodica Polytechnica Mechanical Engineering*, **56**(2): 81-86, 2012.

[5] Cabré, X.; Fontich, E.; and de la LLave, R. The parameterization method for invariant manifolds, III. Overview and applications. *Journal of Differential Equations* **218**(2): 444-515, 2005.

[6] Castejón, O.; Guillamón, A.; and Huguet, G. Phase-amplitude response functions fors transient-state stimuli. *The Journal of Mathematical Neuroscience* (*JMN*), **3**(2): 1-26, 2013.

[7] Chan, T.F.C.; and Keller, H.B. Arc-length continuation and multi-grid techniques for elliptic eigenvalue problems. *SIAM Journal on Scientific Computing* **3**(2): 173-194, 1982.

[8] Chow, S. N.; Li, C.; and Wang, D. *Normal forms and bifurcation of planar vector fields*. Cambridge University Press, New York NY, USA, 1994.

[9] Duchet, B.; Weerasinghe, G.; Cagnan, H.; et al. Phase-dependence of response curves to deep brain stimulation and their relationship: from essential tremor patient data to a Wilson–Cowan model. *Journal of Mathematical Neuroscience* **10(4)**, 2020.

[10] Ermentrout, G. B. *Simulating, Analyzing, and Animating Dynamical Systems: A Guide to XPPAUT for Researchers and Students*. SIAM, Philadelphia PA, USA, 2002.

[11] Ermentrout, G. B. Type I membranes, phase resetting curves, and synchrony. *Neural Computation*, **8**(3): 979-1001, 1996.

[12] Ermentrout, G. B.; and Kopell, N. Multiple phase interactions and averaging in systems of copled neural oscillators. *Journal of Mathematical Biology*, **29**: 195-217, 1995.

[13] Elsgoltz, L. *Differential equations and the calculus of variations. 3rd Edition.* Mir Publishers, Paris, France, 1983.

[14] Fitzhugh, R. Impulses and physiological states in theoretical models of nerve membrane. *Biophysical Journal*, **1**(6): 445-466, 1961.

[15] Giné, J.; and Grau, M. Characterization of isochronous foci for planar analytic differential systems. *Proceedings of the Royal Society of Edinburgh* **135**(A): 985-998, 2004.

[16] Goldstein, H.; Poole, C.; and Safko, J. *Classical Mechanics. 3rd Edition*. Addison-Wesley Publishing, Reading MA, USA, 2000.

[17] Govaerts, W.; and Sautois, B. Computation of the phase response curve: A direct numerical approach. *Neural Computation*, **18**: 817-847, 2006.

[18] Guckenheimer, J. Isochrons and phaseless sets. *Journal of Mathematical Biology*, **1**(3): 259-273, 1974/1975.

[19] Guillamon, A.; and Huguet, G. A computational and geometric approach to phase resetting curves and surfaces. *SIAM J. Applied Dynamical Systems*, **8**(3): 1005-1042, 2009.

[20] Hodgkin, A.L.; and Huxley, A.F. A quantitative description of membrane current and its application to conduction and excitation in nerve. *The Journal of Physiology*, **117**(4): 500-544, 1952.

[21] Keller, H.B. *Lectures on numerical methods in bifurcation problems*. Springer-Verlag, Heidelberg, Germany, 1987.

[22] Ko, C.H.; Yamada, Y.; Welsh, D.K.; et al. Emergence of Noise-Induced Oscillations in the Central Circadian Pacemaker. *PLOS Biology* **8**(10): 1-19, 2010.

[23] Malkin, I. *Methods of Poincaré and Liapunov in the theory of nonlinear oscillations*. Gostexizdat, Moscow, Russia, 1949.

[24] Monga, B.; Wilson, D.; Matchen, T.; and Moehlis, J. Phase reduction and phase-based optimal control for biological systems: a tutorial. *Biological Cybernetics* **113**(1): 11-46, 2019

[25] Monga, B.; and Moehlis, J. Optimal phase control of biological oscillators using augmented phase reduction. *Biological Cybernetics* **113**(1): 161-178, 2019.

[26] Moreno, R. Phase response to stimuli: the case of excitable systems. Master's Thesis. Universitat Politècnica de Catalunya, UPC, Barcelona, Spain, 2019.

[27] Nagumo, J.; Arimoto, S.; and Yoshizawa, S. An active pulse transmission line simulating nerve axon. *Proceedings of the IRE*, **50**(10): 2061-2070, 1962.

[28] Poincaré, J. H. *Thèses*. Paris Gauthier-Villiars, Paris, France, 1879.

[29] Ryazanova, L.; Trenikhina, Y.; Zhirin, R.; and Postnov, D. Noise-induced firing patterns in generalized neuron model with subthreshold oscillations. In *Complex Dynamics and Fluctuations in Biomedical Photonics IV*, V.V. Tuchin, Ed., vol. 6436, International Society for Optics and Photonics, SPIE: 190-197, 2007.

[30] Simó, C. On the analytical and numerical approximation of invariant manifolds. *Les Méthodes Modernes de la Mécanique Céleste (Modern Methods in Celestial Mechanics)* **1**: 285-329 (1990).

[31] Turcotte, M.; García-Ojalvo, J.; and Süel, G.M. A genetic timer through noise.induced stabilization of an unstable state. *Proceedings of the National Academy of Sciences* **105**(41): 15732-15737, 2008

[32] van der Pol, B.; and van der Mark, J. The heartbeat considered as a relaxation oscillator and an electrical model of the heart. *The London, Edinburgh, and Dublin Philosophical Magazine and Journal of Science*, **6**(38): 763-775, 1928.

[33] Winfree, A. T. Patterns of phase compromise in biological cycles. *Journal of Mathematical Biology*, **1**: 73-95, 1974/1975.

A. Auxiliary Figures

In this section we include some useful figures that may offer further information about the numerical results presented in section 5 and help in their analysis and discussion.

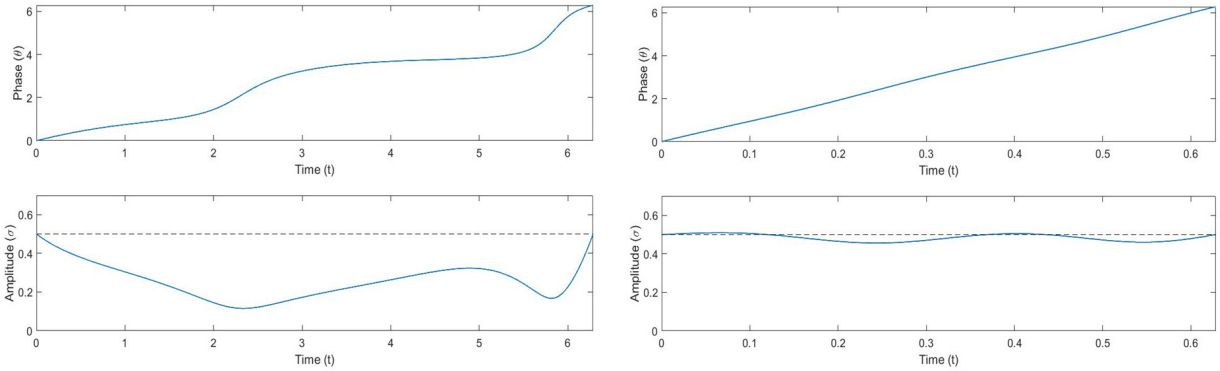

Figure 14: Time tracking of the phase and amplitude for the two induced oscillations in Figure 7. On the left, data referring to the case $\beta = 1$. On the right, $\beta = 10$. The dashed line marks the isostable $\sigma \equiv 0.5$.

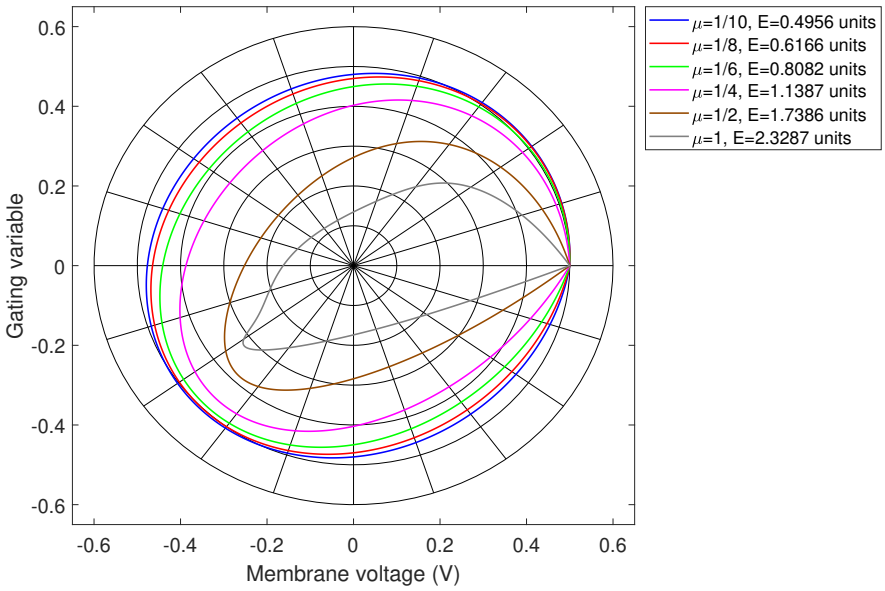

Figure 15: Periodic orbits with $T_{PO} = T_{SF}$ induced using our control algorithm around strong linear foci with several representative values of parameter μ in the interval $[0.1, 1]$ and starting at $(\theta_0, \sigma_0) = (0, 0.5)$.

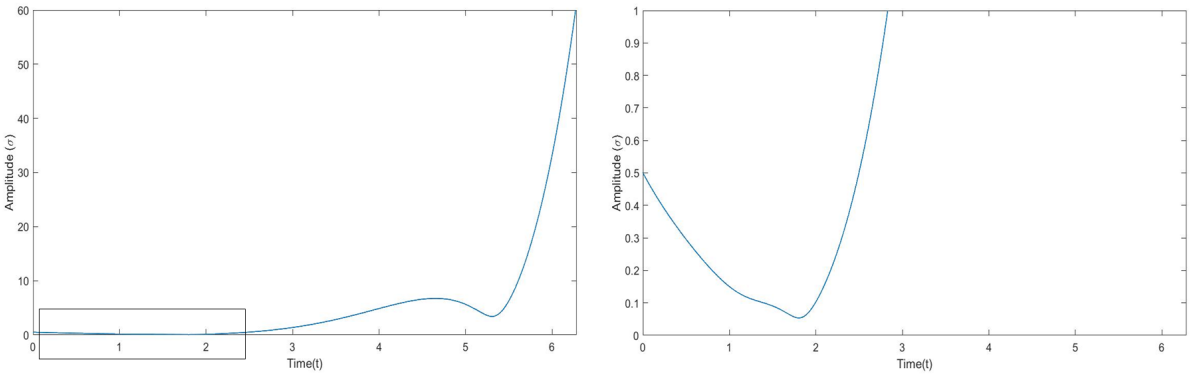

Figure 16: On the left, time tracking of the amplitude evolution of an intermediate orbit in our shooting method for $\mu = 1.05$. On the right, detail of the region where it reaches its minimum amplitude $\sigma = 0.053$.

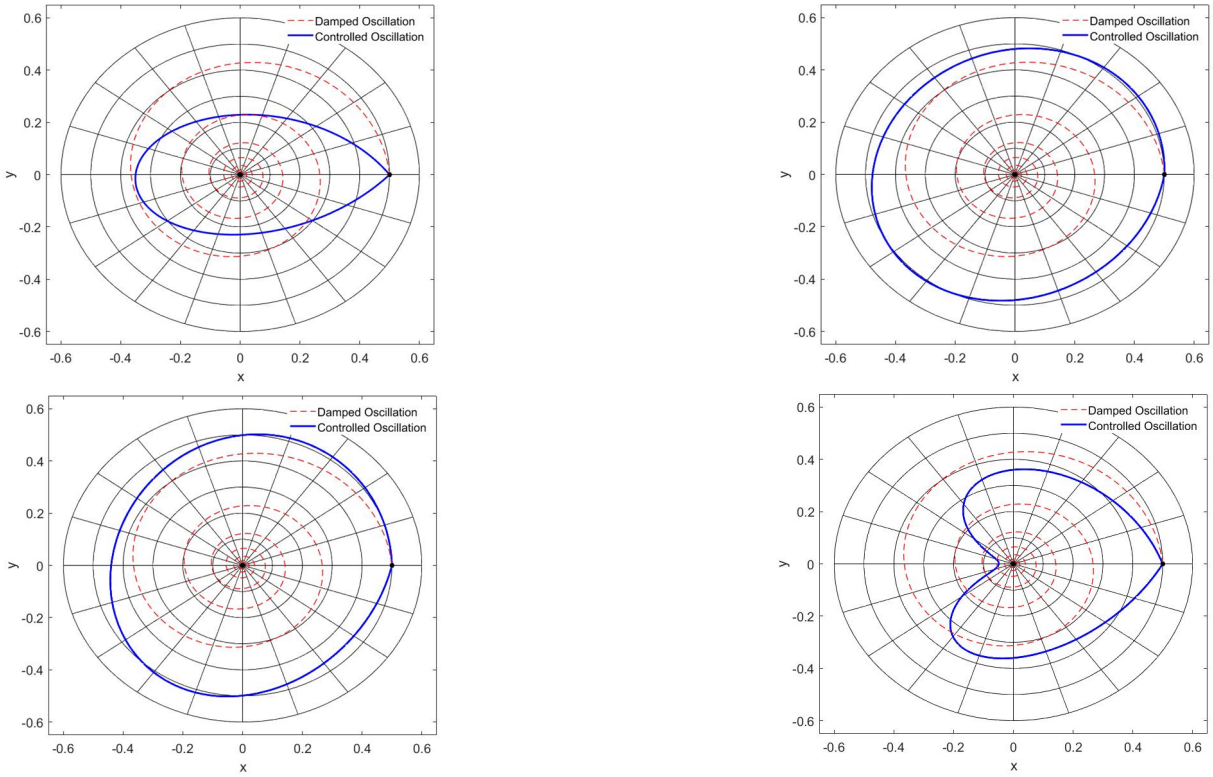

Figure 17: From top left to bottom right, induced periodic orbits around a strong focus with $\alpha = -1$ and $\beta = 10$ and starting at a point $(\theta_0, \sigma_0) = (0, 0.5)$ for choices of parameter $\tau = 0.6$, 1, 1.1 and 1.4.

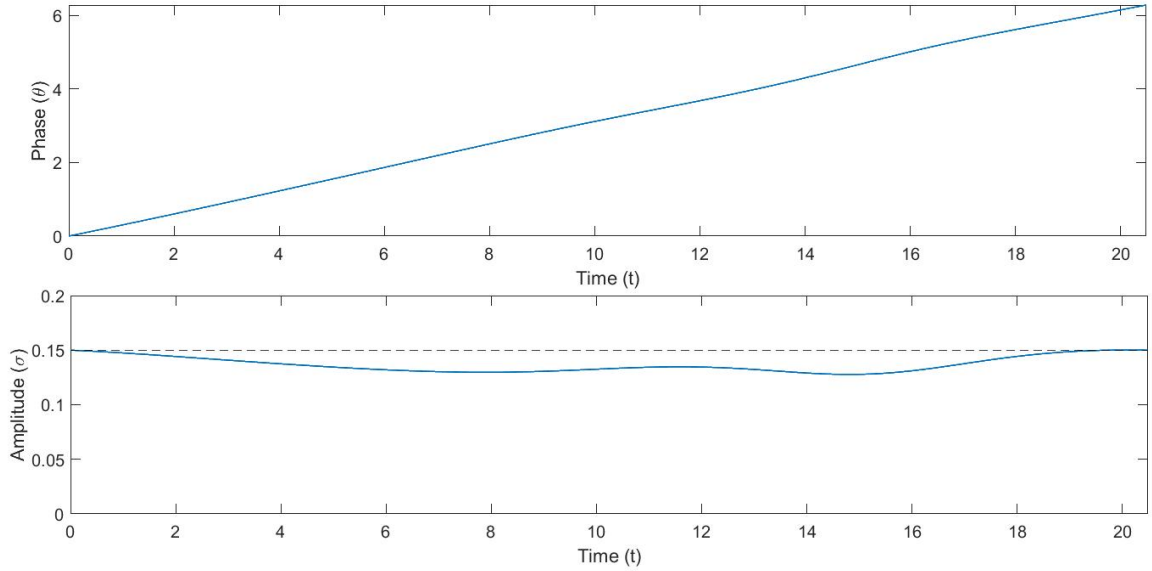

Figure 18: Time tracking of the phase and amplitude variables for the induced oscillation in Figure 13. The dashed line represents the isostable with the objective amplitude $\sigma \equiv 0.15$

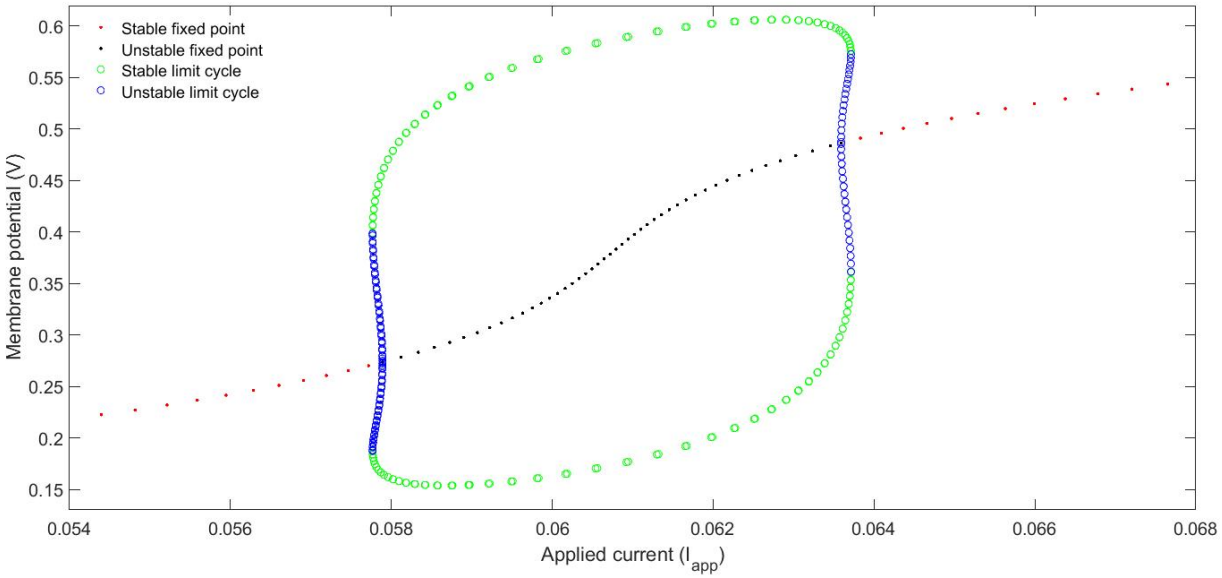

Figure 19: Bifurcation diagram of the Fitzhugh-Nagumo along the I_{app} parameter for $a = 0.14$, $\gamma = 3.24$ and $\varepsilon = 0.08$. Two double limit cycle bifurcations are produced at $I_{app} = 0.0578$ and $I_{app} = 0.0637$ when both limit cycles collide, and two Hopf bifurcations at $I_{app} = 0.0579$ and $I_{app} = 0.0636$ when the fixed point and the unstable limit cycle merge together exchanging their stability character.

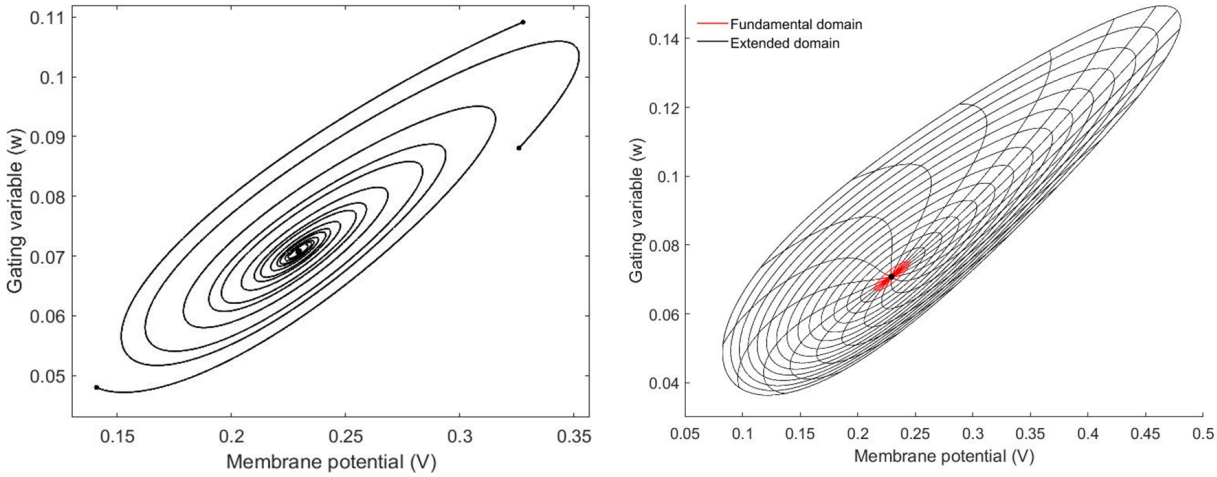

Figure 20: On the left, trajectories of three different points spireling inwards around the strong focus of the Fitzhugh-Nagumo model for the parametric choice (155) with $I_{app} = 0.055$. On the right, some representative isochrones (radial sets) and isostables (closed curves) of such focus. The region in red is the fundamental domain for $tol = 10^{-9}$ and, in black, its extension up to $\sigma_{max} = 0.2$.

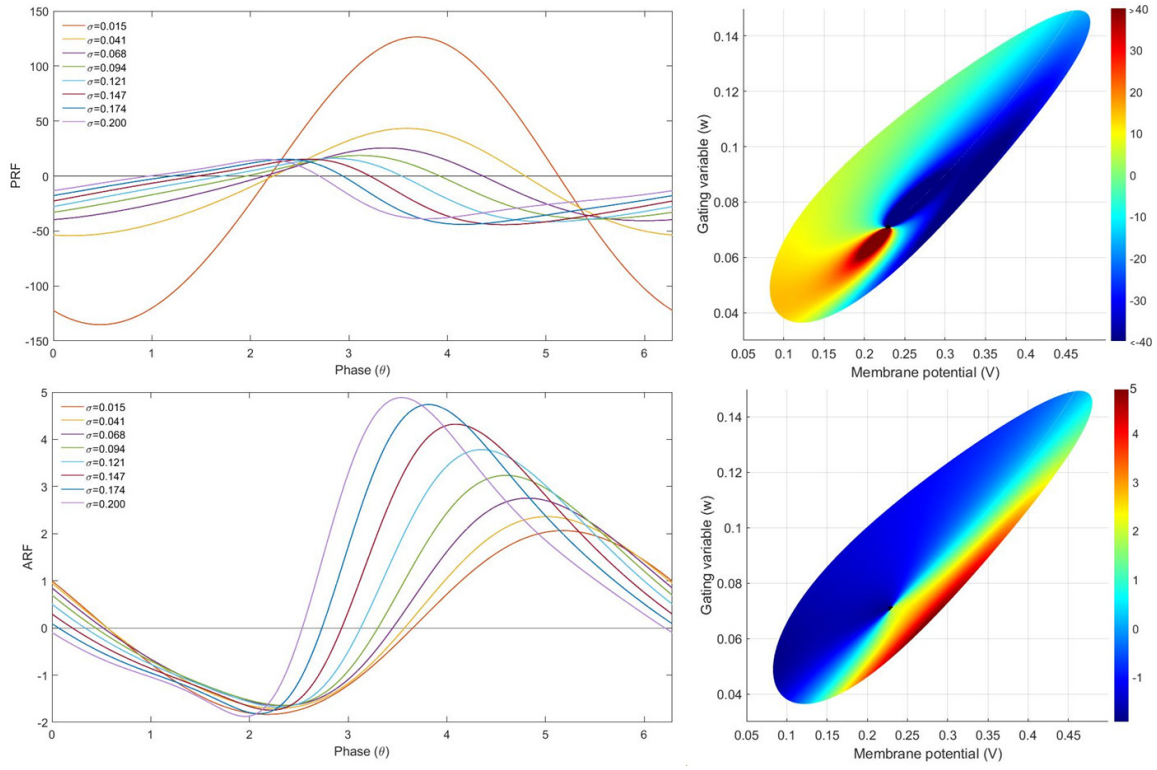

Figure 21: On the left, sections of the PRF (up) and the ARF (down) for eight of the sixteen isostables of the FN model in Figure 20. On the right, color maps depicting the PRF (up) and ARF (down) around the point $\mathcal{P}$. As usual, the darker areas correspond to those regions on the plane that are more sensible to changes in the phase and amplitude of the orbits, respectively.